

2009

Amyloid Aggregation-Mitigating Peptides As Potential Alzheimer's Drugs

Cyrus Kipkurui Bett

Louisiana State University and Agricultural and Mechanical College, cbett1@tigers.lsu.edu

Follow this and additional works at: https://digitalcommons.lsu.edu/gradschool_dissertations



Part of the [Chemistry Commons](#)

Recommended Citation

Bett, Cyrus Kipkurui, "Amyloid Aggregation-Mitigating Peptides As Potential Alzheimer's Drugs" (2009). *LSU Doctoral Dissertations*. 1865.
https://digitalcommons.lsu.edu/gradschool_dissertations/1865

**AMYLOID AGGREGATION-MITIGATING PEPTIDES AS POTENTIAL
ALZHEIMER'S DRUGS**

**A Dissertation
Submitted to the Graduate Faculty of the
Louisiana State University and
Agricultural and Mechanical College
in partial fulfillment of the
requirements for the degree of
Doctor of Philosophy
in
The Department of Chemistry**

**By
Cyrus Kipkurui Bett
B.S., Moi University, 1999
M.S., Moi University, 2005
December, 2009**

DEDICATION

This dissertation is dedicated to my daughter

Tracy Bett

2001-2002

ACKNOWLEDGMENTS

I wish to express my appreciation to a number of people who have contributed immensely to this work in one way or another.

I would like to thank my advisor Dr. Robert Hammer who gave me support, guidance, and help that I needed during this work. I am greatly indebted to Dr. Jayne Garno especially for editing all my papers and my dissertation, and her students Wilson Serem and Johnpeter Ngunjiri for the collaboration on AFM work.

I am especially grateful to Dr. Jayne Garno, Dr. Robin McCarley, Dr. David Spivak, and Dr. Joan King for serving on my advisory committee. I would like also to thank current and former group members especially Maggie Ndinguri, Sibel Erdem, Kristol Fontenot, Amber Scroggs, Marcus Etienne, Gregory McCandless, and Mercy Mudyiwa to name a few for the camaraderie and support you have all given me.

My special thanks also go to facility staff, Dr. Dale Treleaven, Dr. Rafael Cueto, Dr Martha Juban, and collaborators Dr. Jeffery Keller at LSU Pennington Research

Finally yet importantly, I want to extend my outmost appreciation to my wife Caroline Bunei and son Alvin Bett. Thank you for your love, patience, and support you gave me. I know this was not easy on you. Also, I owe great deal to my father Samson Kibet, my mother Sally Kibet, my sisters (Emmy, Doris, Cynthia, Irene, Scholarstica, Jane, Mereline, and Judith) and my brothers (Kenneth, Daniel and Benjamin). Thank you for the love, encouragement, and the support.

TABLE OF CONTENTS

DEDICATION.....	ii
ACKNOWLEDGMENTS.....	iii
LIST OF ABBREVIATIONS.....	vii
ABSTRACT.....	x
CHAPTER 1: GOALS, RESEARCH SYNOPSIS, AND BACKGROUND.....	1
1.1 Research Goals and Aims.....	1
1.2 Research Synopsis.....	1
1.3 Background.....	3
1.3.1 Protein Folding and the Evolution of Diseases.....	3
1.3.2 Alzheimer's Disease.....	4
1.3..2.1 Historical Background.....	4
1.3.2.2 Alzheimer's Disease Prevalence.....	4
1.3.2.3 Etiology of AD Disease; β -Amyloid Hypothesis.....	5
1.3.2.4 A β Aggregation.....	7
1.3.2.5 A β Neurotoxicity.....	9
1.3.6 Strategies for Designing Molecules That Target A β	10
1.3.7 Structures of A β Assemblies.....	12
1.4 Conclusion.....	13
1.5 References.....	13
CHAPTER 2: SYNTHESIS OF ALPHA, ALPHA-DISUBSTITUTED AMINO ACIDS ($\alpha\alpha$ AAS) AND THEN INCORPORATION INTO SHORT PEPTIDES.....	23
2.1 Introduction.....	23
2.2 Experimental Section.....	24
2.2.1 Materials and Instruments.....	24
2.2.1.1 Materials.....	24
2.2.1.2 Instruments.....	24
2.2.2 Synthesis of $\alpha\alpha$ AAs.....	26
2.2.2.1 Synthesis of N $^{\alpha}$ Protected Dipropylglycine(Dpg).....	26
2.2.2.1.1 5, 5-Dipropylhydantoin (1a).....	26
2.2.2.1.2 2, 2-Dipropylglycine (2a).....	27
2.2.2.1.3 9-Fluorenylmethoxycarbonyl-2, 2-Dipropylglycine (3a).....	27
2.2.2.2 Synthesis of N $^{\alpha}$ -Protected Dibenzylglycine.....	28
2.2.2.2.1 Ethyl 2-Benzyl-2-Nitro-3-Phenylpropionate (1b).....	28
2.2.2.2.2 Ethyl 2, 2-Dibenzylglycine ester (2b).....	28
2.2.2.2.3 2, 2-Dibenzylglycine (3b).....	29
2.2.2.2.4 N $^{\alpha}$ -(9-Fluorenylmethoxycarbonyl)-2, 2-Dibenzylglycine (4b).....	29
2.2.2.3 Synthesis of N $^{\alpha}$ -Protected Diisobutylglycine.....	30
2.2.2.3.1 Ethyl 2, 2 – Bis (2-methylallyl)-2-nitroacetate (1c).....	30
2.2.2.3.2 Ethyl 2, 2-Diisobutylglycine Ester (2c).....	30

2.2.2.3.3 2, 2-Diisobutylglycine(3c).....	31
2.2.2.3.4 N-(9-Fluorenylmethoxycarbonyl)-2, 2-Diisobutylglycine(4c).....	31
2.2.3 Peptide Synthesis.....	32
2.2.3.1 General.....	32
2.2.3.2 Attachment of the First Residue on the Resin.....	32
2.2.3.3 Removal of the Fmoc Protective Group.....	32
2.2.3.4 Amino Acid Coupling.....	32
2.2.3.5 N-Acylation of $\alpha\alpha$ AAs Using Symmetrical Anhydrides.....	33
2.2.3.6 Capping of Unreacted Sites.....	33
2.2.3.7 Peptide Cleavage.....	33
2.2.3.8 Fmoc Analysis.....	34
2.2.3.9 Circular Dichroism Measurements.....	34
2.3 Results and Discussion.....	34
2.3.1 Synthesis of $\alpha\alpha$ AAs.....	34
2.3.2 Peptides Synthesis.....	38
2.3.3 Conformational Studies of Mitigators.....	48
2.4 Conclusion.....	51
2.5 References.....	51

CHAPTER 3: STRUCTURE-ACTIVITY RELATIONSHIPS IN PEPTIDE MODULATORS OF AMYLOID β-PROTEIN AGGREGATION.....	54
3.1 Introduction.....	54
3.2 Materials and Methods.....	57
3.2.1 Peptide Synthesis.....	57
3.2.2 Peptide Monomerization.....	57
3.2.3 Thioflavin T Aggregation Assays.....	58
3.2.4 Circular Dichroism.....	58
3.2.5 Atomic Force Microscopy.....	58
3.2.6 Transmission Electron Microscopy.....	59
3.3 Results and Discussion.....	59
3.3.1 Design of Amyloid Aggregation Mitigating Peptide.....	59
3.3.2 Assembly of $A\beta_{1-40}$ and with the Various AAMPs.....	61
3.3.2.1 Effect of AAMPs on $A\beta_{1-40}$ ThT Fluorescence.....	61
3.3.2.2 Effect of $\alpha\alpha$ AA-AAMPs on the Secondary Structure of $A\beta_{1-40}$ Using Circular Dichroism (CD).....	63
3.3.2.3 Size and Morphology of the Various Structures as Determined Using AFM.....	65
3.3.2.4 Morphology of Structures Formed from $A\beta_{1-40}$ Aggregation Mitigation by the Various AAMPs as Observed by TEM.....	76
3.3.3 $A\beta_{1-40}$ Fibril Disassembly.....	78
3.3.3.1 Thioflavin T Fluorescence.....	78
3.3.3.2 Size and Morphology of Structures formed from Disassembly of Preformed Fibrils by various AAMPs as determined using AFM.....	79
3.3.3.3 Morphology of Structures Formed from Disassembly of Preformed Fibrils by Various AAMPs as Determined Using TEM.....	85
3.4 Conclusion.....	87
3.5 References.....	89

CHAPTER 4: EFFECTS OF TERMINAL MODIFICATIONS OF PEPTIDES DERIVED FROM A β CENTRAL HYDROPHOBIC CORE ON A β_{1-40} -PEPTIDE AGGREGATE SIZE AND MORPHOLOGY.....	95
4.1 Introduction.....	95
4.2 Materials and Methods.....	98
4.3 Results and Discussion.....	98
4.3.1 Design of Peptides for Mitigating A β Aggregation.....	98
4.3.2 Effects of AAMPs on A β_{1-40} ThT Fluorescence.....	101
4.3.3 Effect of Various AAMPs on A β_{1-40} CD Spectra.....	104
4.3.4 Assembly of A β_{1-40} Alone and with the Various AAMPs Analyzed Using AFM.....	105
4.3.4.1 Effect of <i>N</i> - and <i>C</i> -Terminal Modifications of AAMPs on A β_{1-40} Fibrillization.....	109
4.3.4.2 Effect of <i>C</i> -Terminal Modifications of AAMPs on A β_{1-40} Fibrillization.....	113
4.3.4.3 Effect of <i>N</i> - or <i>C</i> -Terminal Modifications of AAMPs on A β_{1-40} Fibrillization.....	117
4.3.5 Morphology of Structures Formed from A β_{1-40} Aggregation Mitigation by the Various AAMPs as Observed by TEM.....	121
4.3.6 A β_{1-40} Fibril Disassembly.....	122
4.3.6.1 Size and Morphology of Structures Formed from A β_{1-40} Disassembly by AAMPs.....	123
4.3.6.2 Size and Morphology of Structures Formed from Fibril Disassembly by $\alpha\alpha\text{AA}$ -AAMPs.....	127
4.3.6.3 Morphology of Structures Formed from A β_{1-40} Disassembly by the Various AAMPs as Observed by TEM.....	128
4.4 Conclusions.....	131
4.5 References.....	134
CHAPTER 5: SUMMARY.....	139
5.1 Discussion.....	139
5.2 References.....	141
VITA.....	143

LIST OF ABBREVIATIONS

Arg	arginine
DBU	1, 8-diazobicyclo[4.5.0] undec-7-ene
DIPEA	diisopropylethylamine
DMF	dimethylformamide
Et ₂ O	diethyl ether
EtOH	ethanol
Fmoc	9-fluorenylmethoxycarbonyl
Gly	glycine
HPLC	High performance liquid chromatography
NMR	Nuclear magnetic resonance
MiniPEG	9-Fluorenylmethoxycarbonyl-8-Amino-3,6-Dioxaoctanoic Acid
PYAOP	7-azabenzotriazolyoxytris(pyrrolidino) phosphonium hexafluorophosphate.
TFA	trifluoroacetic acid
MALDI	Matrix assisted laser desorption ionization
min	minute
µM	micromolar
mM	millimolar
mmol	millimole
NaOH	sodium hydroxide
MeCN	acetonitrile
Pip	piperidine

PyAOP	(7-azabenzotriazol-1-yloxy)trypyrrolidinophosphonium hexafluorophosphate
TIPS	triisopropylsilane
TMS	tetramethylsilane
$\alpha\alpha$ AAs	$C^{\alpha,\alpha}$ -disubstituted amino acids
AD	Alzheimer's disease
$A\beta$	β -amyloid peptide
Abs	absorbance
AFM	Atomic force microscopy
APP	Amyloid precursor protein
Bop-Cl	Bis(2-oxo-3-oxslydanyl)phoshinic chloride
$C\alpha$	alpha carbon
CD	Circular dichroism
Dbg	Dibenylglycine
DCC	Dicyclohexylcarbodiimide
Dibg	Diisobutylglycine
Dpg	Dipropylglycine
TEM	Transmission electron microscope
ESI	Electrospray ionization
HATU	(2-(7-Aza-1H-benzotriazole-1-yl)-1,1,3,3-tetramethyluronium hexafluorophosphate
HOAt	1-hydroxy-7-azabenzotriazole
HPLC	High-performance liquid chromatography

PEG	Polyethylene glycol
ThT	Thioflavin T
TBAB	tetrabutylammonium bromide
α	alpha
β	beta

ABSTRACT

Neuronal cytotoxicity observed in Alzheimer's disease (AD) is linked to the aggregation of β -amyloid peptide ($A\beta$) into toxic forms. Increasing evidence points to oligomeric species as the neurotoxic species compared to fibrils; disruption or inhibition of $A\beta$ self-assembly into oligomeric or fibrillar forms remains a viable therapeutic strategy to reduce $A\beta$ neurotoxicity. Amyloid aggregation mitigating peptides (AAMPs) were designed based on the $A\beta$ "hydrophobic core" $A\beta_{17-20}$, with $C^{\alpha,\alpha}$ -disubstituted amino acids ($\alpha\alpha$ AAs) added into this core as disrupting agents. The number, distribution, and side chain functionality of $\alpha\alpha$ AAs incorporated into the mitigator sequence was found influences the resultant aggregate morphology as indicated by ex-situ experiments using AFM and TEM. For instance, AAMP-5 incorporating the sterically hindered diisobutyl side chain to its core sequence disrupted fibril formation. However, AAMP-6 with a dipropyl side chain incorporated into its core sequence only altered fibril morphology, forming shorter and larger sized fibrils compared to those of $A\beta_{1-40}$. Interestingly, $\alpha\alpha$ AA-AAMPs also disassembled preformed fibrils to produce either amorphous aggregates or protofibrillar structures, suggesting the existence of equilibrium between fibrils and prefibrillar structures. Also, AAMPs aged alone did slowly aggregate to form spherical structures, which is inconsistent with circular dichroism spectra showing an unchanged random coil structure.

Several potent mitigators of $A\beta$ fibrillization were derived from *N*- or *C*- terminus modification of KLVFF with various polar groups. The number of $\alpha\alpha$ AAs and polar groups were reduced without affecting the overall disruptive properties of the original mitigator.

CHAPTER 1

GOALS, RESEARCH SYNOPSIS, AND BACKGROUND

1.1 Research Goals and Aims

The predominant hypothesis for the causative agents for neuronal toxicity and cell death observed in Alzheimer's disease (AD) are oligomeric assemblies.¹⁻⁸ One therapeutic approach is to target changes in the A β assembly process into toxic forms. The goal of this research involves the design and synthesis of amyloid aggregation mitigating peptides (AAMPs) that incorporate $\alpha\alpha$ AAs. The use of $\alpha\alpha$ AAs is of particular interest because they have been shown to induce extended conformations⁹ required for model peptides to interact and disrupt the A β assembly process.

The specific aim of this research was to investigate the role of specific changes for one or two $\alpha\alpha$ AAs on the A β assembly and disassembly process as compared to the original designs. The role of polar residues was also investigated with the view of reducing the overall charge of the peptide. The goals were to identify which structural elements of the AAMPs are essential for disruption of A β fibrillization process or fibril dissolution.

1.2 Research Synopsis

Model peptides derived only from natural L- α -amino acids often yield an unordered or unstable secondary structure, which limits their use in potential drug candidates, biological probes, and functionalized-device molecules.^{10, 11} Thus, to increase their stability one of the ways is to replace the α -hydrogen of L- α -amino acid with an alkyl substituent, which results in $\alpha\alpha$ AAs. $\alpha\alpha$ AAs are known to induce extended peptide conformations, which are ideal for design peptides that will interact with A β and disrupt its assembly process. The first aim was to

improve the yields of $\alpha\alpha$ AAs through modification of the existing routes or development of new synthetic routes. This will enable us to carry out a large-scale synthesis of $\alpha\alpha$ AAs because large quantities are required for synthesis of peptide mitigators. Coupling of Fmoc- $\alpha\alpha$ AA-OH onto N-terminal resin and their N-terminal acylation were found to be difficult. Thus, various coupling conditions and methods were evaluated after which a library of $\alpha\alpha$ AA-containing AAMPs was synthesized.

Mitigators containing $\alpha\alpha$ AAs was previously shown to disrupt $A\beta$ fibrillilization forming nonfibrillar assemblies that were stable after 4.5 months. In Chapter 3 we show that the number and position of $\alpha\alpha$ AAs in the recognition element of the original mitigator AAMP-1 (AMY-1)¹² is important in determining the effectiveness of the interaction of our AAMPs with $A\beta$. Also, we further examine the aggregate inhibition role of each $\alpha\alpha$ AA in AAMP-1 by examination of synthetically derived AAMP-1 analogs having $\alpha\alpha$ AAs replaced by their natural amino acid analog (Leu for Dibg, etc). Furthermore, a major finding is that AAMPs that disrupted fibril formation also led to disassembly of preformed (*existing*) $A\beta_{1-40}$ fibrils.

Also our two AAMPs (previously denoted as AMY-1 and AMY-2 and having a hydrophilic Lys tail on the *C*- or *N*-termini, respectively) mitigated $A\beta_{1-40}$ fibril formation in a way such that ill-defined $A\beta_{1-40}$ aggregates of different size were produced. Thus, in chapter 4 we investigate the effect of modifications of the KLVFF hydrophobic core of $A\beta$ by replacing N- and C- terminal groups with various polar moieties. Several of these terminal modifications were found to disrupt the formation of amyloid fibrils, and in some cases induced disassembly of pre-formed fibrils. Significantly, mitigators that incorporate MiniPEG polar groups were found to be effective against $A\beta_{1-40}$ fibrilligonesis. In addition, we further disclose that the number of

polar residues (six) and $\alpha\alpha$ AAs (three) in the original mitigator can be reduced without dramatically changing the ability to disrupt $\text{A}\beta_{1-40}$ fibrillization in vitro.

1.3 Background

1.3.1 Protein Folding and the Evolution of Diseases

Protein folding is crucial for sustaining cellular functions.^{13, 14} Amino acid sequence, mutations and environmental conditions such as temperature, oxidative agents and pH determine whether proteins misfold. When proteins fail to fold, they are degraded by proteasome yielding unfolded nonfunctional proteins (non-native protein). The unfolded proteins are thermodynamically unstable and tend to aggregate to regain stability. The protein aggregates formed are deposited either in the body system or on organs leading to amyloidosis diseases (Table 1.1).

Table 1.1. Examples of protein misfolding diseases.

Disease	Precursor protein	Deposition location
Alzheimer's disease	β -Amyloid, Tau	Brain
Parkinson's disease	α -synuclein	Brain
Huntington's disease	Huntington	Brain
Creutzfeldt-Jakob disease (mad cow)	Prion protein	Brain
Amyotrophic lateral sclerosis	Superoxide dismutase	Brain
Diabetes mellitus	Amylin, IAPP	Pancreas
Atherosclerosis	Lipoprotein	Arteries
Sickle cell anemia	Hemoglobin	Erythrocytes
Renal amyloidosis	Fibrinogen	Kidney
Cataract	Crystallinm	Eye
Senile systemic amyloidosis	Transthyretin	Microvasculature
Injection-localized amyloidosis	Insulin	Skin, muscles

Deposits localized in the regions of the brain, including the central nervous system, have been linked to a number of neurodegenerative diseases that cause dementia. Alzheimer's disease (AD), Prion diseases, Huntington's disease, and Parkinson's disease,¹⁴⁻¹⁷ are all linked to a particular protein (Table 1). The most prevalent and most studied neurodegenerative disease is AD.

1.3.2 Alzheimer's Disease

1.3.2.1 Historical Background

Alzheimer's disease is the most prevalent cause of dementia in elderly humans worldwide. The disease is named after the German neurologist, Alois Alzheimer (1864–1915)¹⁸⁻²⁰ who studied a 51-year-old woman who had developed memory, language and behavioral problems from 1901–1906. Upon her death, he examined her brain during autopsy, and noted unusual thick bundles of nerve fibers and the destruction of nerve cells. He concluded that the changes that occurred in her brain indicated a new disease.²¹ It was not until 1910 when the disease was named after the German neurologist. The symptoms Alois Alzheimer described are still being diagnosed in most patients with the disease today.²²

1.3.2.2 Alzheimer Disease Prevalence

Alzheimer's disease is a permanent, progressive neurodegenerative disease that gradually decimates memory and cognitive functions. It is the most common cause of dementia, accounting for more than half of all such cases, and the sixth leading cause of death in the United States. This year approximately 5.3 million people in the US have AD disease, out of which 5.1 million people are over 65 years in age.²³ New cases of the disease are expected to double by the year 2050. The health care costs associated with the disease have tripled to more than \$148 billion per year, stretching Medicare and Medicaid programs.²³ Worldwide, AD affects more

than 24 million people, with 4.6 million new cases each year. The major risk factor for AD is age, with the disease prevalence increasing from 1 in 10 people for those over age of 65 to almost half of those over 85.²⁴

1.3.2.3 Etiology of AD Disease; β -Amyloid Hypothesis

Amyloid deposits which consist of neurofibrillar tangles and senile plaques characterize the development of AD in the brain.²⁵ A Large body of evidence associates the density of senile plaques with the severity of dementia.^{25, 26} Also, there is significant evidence that shows involvement of Tau protein, the major component of neurofibrillar tangles in etiology of AD. The principal component of these plaques is β -amyloid peptide (A β), which is derived from proteolytic cleavage of the transmembrane protein, amyloid precursor protein (APP), by β -and γ -secretases. Apart from playing a central role as a precursor to A β , APP have a number of additional functions such as autocrine and paracrine functions in growth regulation, neurite growth stimulation, stem cell regulation, and promotion of cell adhesion. Mounting evidence implies that perturbation of some of these functions may play a part in the etiology of AD.²⁷⁻³⁰ Cleavage of APP can occur at three different sites by α , β , or γ secretases as shown in Figure 1.1. The larger extracellular segment of APP peptide is cleaved first by β - or α -secretase, producing membrane bound β - or α - C-terminal fragments. Subsequent cleavage of the β - and α -C-terminal fragments within the membrane by γ -secretase releases A β and p3 peptides respectively into the extracellular domain. Two isoforms of A β are often produced depending on γ -secretase cleavage site; A β_{1-40} (between 40 and 41) and A β_{1-42} (between 42 and 43). The other by-product of γ -cleavage is the cytoplasmic polypeptide, AICD that so far has not been investigated for any role in the etiology of AD.

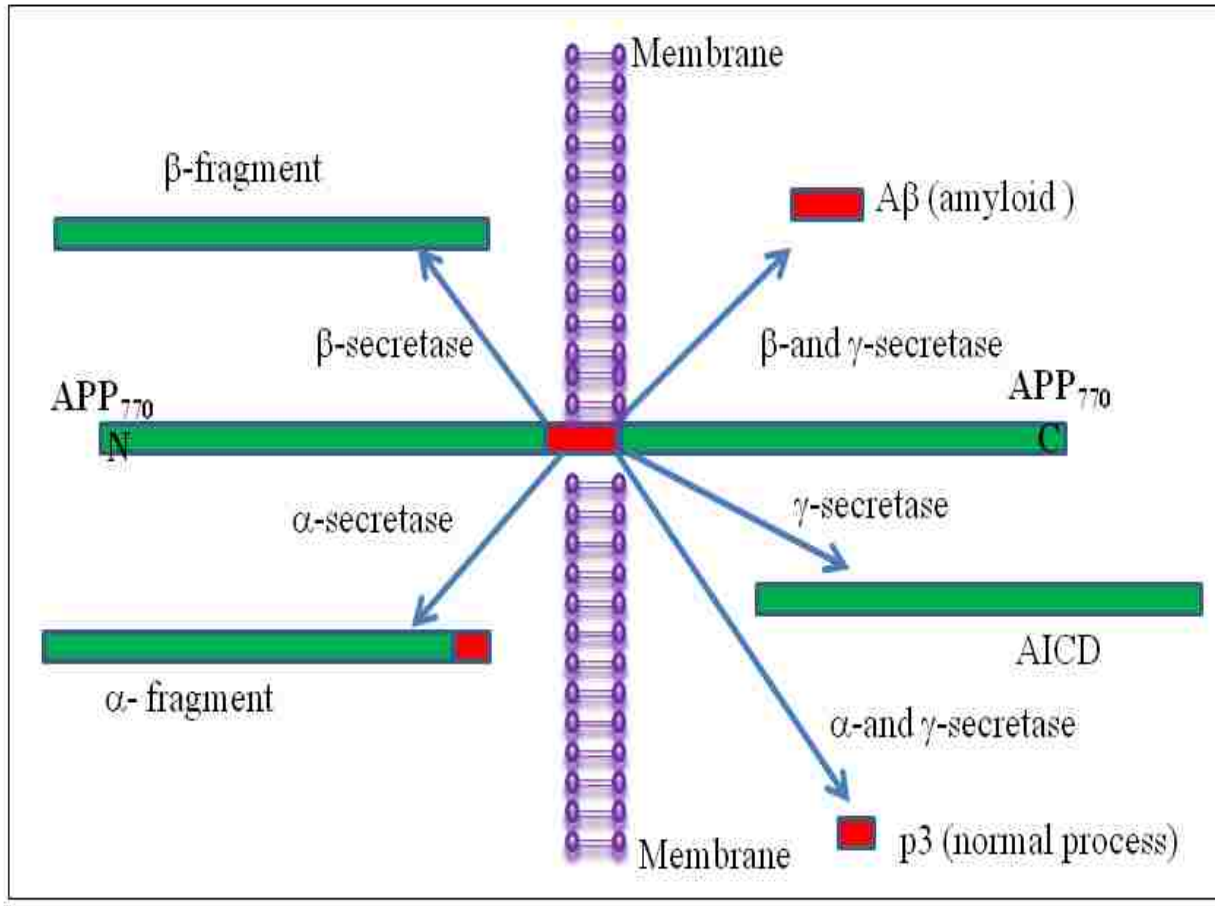


Figure 1.1. Cleavage of APP molecule by aspartyl proteases

It is widely accepted that Aβ plays a central role in the etiology of AD, although the mechanism of neurotoxicity has not been fully established.^{13, 20, 31-33} Several human, transgenic animal, and in vitro studies have supported the central role of Aβ in etiology of AD. For instance, synthetic Aβ has been shown to be toxic to neurons both in vivo³⁴ and in vitro experiments.³⁵⁻³⁸ Also, there was an increase in tau hyperphosphorylation when transgenic mice were injected with synthetic Aβ, leading to formation of tangles.^{39, 40} Monomeric Aβ is nontoxic until it aggregates to form an array of oligomeric and fibrillar structures. Therefore identifying and characterizing the toxic Aβ species is crucial so that compounds that target them can be developed.

1.3.2.4 A β Aggregation

The peptide A β is a normal, soluble component of human plasma and cerebrospinal fluid.^{41, 42} It is toxic only after it undergoes aggregation and/or conformation change to higher ordered species such as oligomers or fibrils.^{35, 43-45} The most common isoforms of A β are A β 40 and A β 42, which differ only by the length of the C terminus. The concentration of secreted A β 42 is about 10% that of A β 40, and yet the predominant component of senile plaques is A β 42.⁴⁶⁻⁴⁹ Biochemical studies have shown that A β 42 aggregates and forms fibrils more quickly than A β 40.⁵⁰⁻⁵² Monomers, dimers, trimers, and tetramers, in rapid equilibrium are the major early aggregation products of A β 40.^{3, 5, 53} In contrast, A β 42 preferentially form pentamer and hexamer units (paranuclei) that assemble further to form beaded superstructures, similar to early protofibrils.⁵⁴ This could explain why assemblies formed by A β 42 are more toxic as compared to those formed by A β 40 during early stages of oligomerization. Also, over expression of the two isoforms in transgenic mice demonstrated that A β 42 is involved in amyloid pathology.⁵⁵

In vitro, synthetic A β has been shown to aggregate via various intermediate species including soluble oligomers, protofibrils, and insoluble fibrils.⁵⁶ This process depends on a number of aggregation conditions, such as acidic pH, metal ions, osmolytes, and interaction with lipid membranes.⁵⁷⁻⁶¹ The mechanism of A β aggregation into the toxic species has been shown to proceed via two distinct pathways. In the presence of preformed fibrils or plaques, A β aggregates by consecutive association onto the ends of existing fibrils.^{62, 63} However, in the absence of seeding, A β monomers aggregate into fibrils by a two step-polymerization process; nucleation and elongation, in which nucleation is the rate determining step.^{7, 43, 64-66} The nucleation phase is a result of an energy barrier that must be overcome in order for A β monomers

to fold into nuclei.⁶⁷ Once the nuclei have been generated, rapid elongation of fibrils occurs in the linear phase.

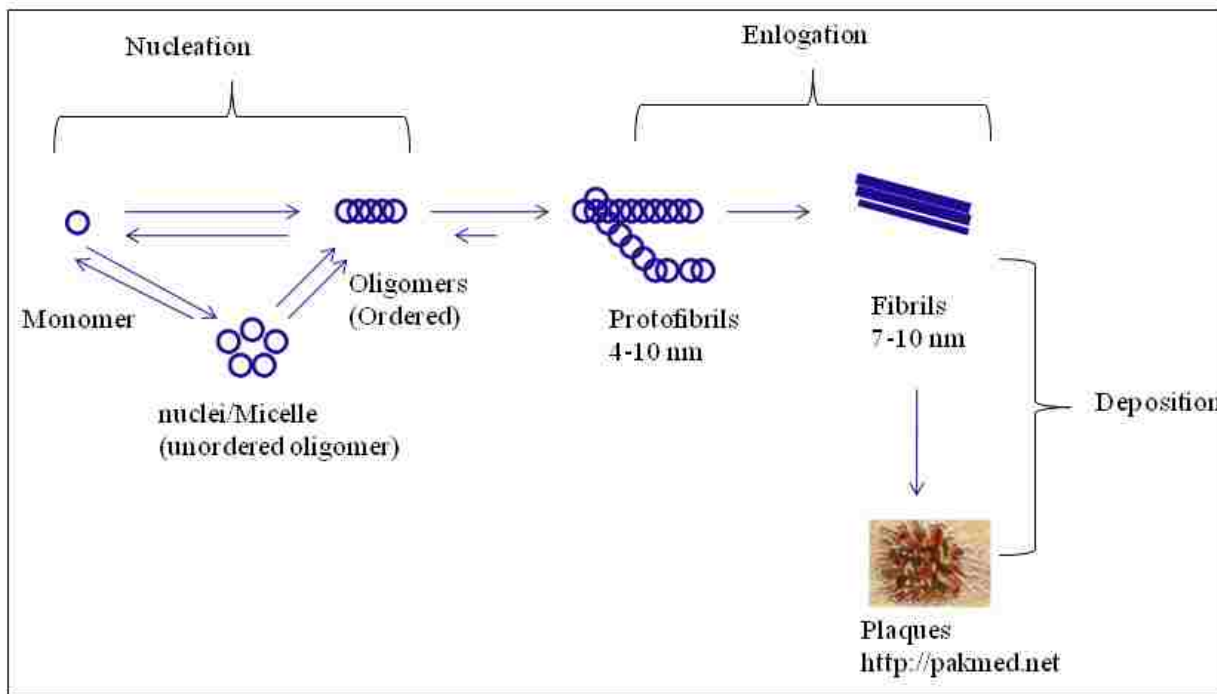


Figure 1.2. The nucleation process of fibrillogenesis.

Computer simulation experiments have also shown that monomeric A β peptides undergo a two-step process that is reliant on the degree of hydrophobicity. In the first step, due to strong interactions between hydrophobic residues monomers coalesce quickly into disordered oligomers. The disordered assemblies reorganize (conformational change) slowly through formation of interchain hydrogen bonds into ordered oligomers rich in β -sheets. Because of conformational change, the hydrophobic residues buried inside the oligomers are exposed to interaction with cellular components such as membranes. This could explain the toxic nature of oligomers. When hydrophobicity is inadequate to drive coalescence to disordered oligomers, peptides form ordered oligomers directly as a result of interchain hydrogen bonds. Temperature and concentration are other factors that affect formation of disordered assemblies.

The morphology of amyloid fibrils formed by various amyloidal proteins such as A β , α -synuclei, amylin, and β -microglobulin has been studied using atomic force microscopy (AFM).⁶⁶ A hierarchical assembly model (HAM) has been proposed to describe the assembly process of amyloid proteins into fibrils.^{68, 69} The HAM model predicts that a monomeric amyloid protein aggregates via a nucleated polymerization mechanism into protofilaments, which elongate by addition of monomers at the ends of protofilaments. Two or three protofilaments can associate to form protofibrils that intertwine to form fibrils. In general, the HAM model predicts that fibrils and protofibrils will exhibit clumping, periodicity, variations in height, and branching.

1.3.2.5 Neurotoxicity of A β

The original “amyloid cascade” hypothesis linked the deposition of fibrillar A β in the brain to neuronal cell death.^{1, 70-72} However, some key observations including poor correlation between deposition of plaques and severity of dementia contradicts this hypothesis. Therefore, the amyloid cascade hypothesis was amended to include soluble oligomeric assemblies rather than fibrils as the main neurotoxic species. This was because a number of studies have shown a stronger correlation between soluble oligomers and severity of AD than fibrils. In addition, transgenic mice APP models exhibited memory and synaptic dysfunction long before plaques (fibrils) were detected.⁷³⁻⁷⁵

The solubility and small sizes of oligomeric species is believed to be a crucial factor as to why oligomers are more toxic than fibrils. In addition, the higher surface area to volume ratio exhibited by oligomers as compared to fibrils ensures maximum interaction with neurons, hence increased neurotoxicity. The interaction between oligomers and neurons has been shown to occur by either insertion of oligomers between membrane layers to generate cytotoxic pores, or binding of oligomers specifically to neuron surfaces as ligands.^{76, 77}

Oligomeric assemblies consist of curvilinear structures (protofibrils) that normally appear as beaded strings and globular particles with heights ranging from 2-5 nm. Protoprofibrils were identified several years ago as intermediates that form during the A β assembly process into fibrils,^{37, 78} and protofibrils have been shown to kill neurons.^{1, 79} More recently, globular oligomers were renamed amyloid- β -derived diffusible ligands (ADDLs) to emphasize their globular nature but also to differentiate from the general “oligomers” that include nontoxic assemblies. The ADDLs were initially discovered from aging A β_{1-42} in the presence of clusterin when no fibrils were formed and yet a dramatic increase in toxicity was observed.^{6, 80} Only nanomolar concentrations of A β_{1-42} are needed to make stable ADDLs that have units ranging from trimers to 24-mers. The hypothesis that ADDLs play a crucial role in AD is gaining momentum. This is specifically because ADDLs bind neuronal receptors inducing synaptic dysfunction rather than the neuronal death caused by fibrils and plaques. Other general consequences caused by A β aggregates include alteration of the physiological properties of membranes, membrane-mediated triggering of neuronal cell death, lipid peroxidation, and calcium-permeable membrane ion-channels. Although increasing evidence points to oligomeric species as the more toxic species, a general strategy to prevent AD may be to interrupt the assembly of A β into these toxic forms.

1.3.2.6 Strategies for Designing Molecules That Target A β

Considerable research effort has focused on discovery of inhibitor compounds that block the toxicity of A β , by targeting a specific step involved in A β aggregation.⁸¹⁻⁸³ Given the hypothesis that aggregation intermediates are responsible for A β toxicity, such compounds could theoretically prevent all aggregation, or alternatively cause further association of toxic oligomers into larger nontoxic aggregates.

Several approaches are under development against production of A β and related aggregates. These include inhibition of proteases involved in cleavage of A β from APP,⁸⁴ antibody therapy through passive immunizations using anti-A β antibodies,⁸⁹⁻⁹² non-antibody based natural mechanism,⁹³⁻⁹⁵ small molecules,⁹⁶⁻¹⁰⁰ and peptides.¹⁰⁰ Peptide-based A β interacting molecules are the focus of this dissertation. Interest in peptides has intensified because they are generally more potent, and show higher specificity and fewer toxicology problems than smaller molecules. Peptide-based drugs approved by the FDA include natural peptides, such as insulin, vancomycin, oxytocin, and cyclosporine and synthetically produced ones, such as Fuzeon (enfuvirtide) and Integritin (eptifibatide). The development of new non-oral drug delivery methods such as subcutaneous and intranasal implants has increased the interest in peptide-based drugs.

One approach is to exploit the self-recognition features of A β to generate compounds that can interact specifically with A β .^{101, 102} Tjenberg et al. identified residues 16-20 (KLVFF) to be essential for fibril formation.^{62, 103} Pentapeptide KLVFF was also found to be the minimum sequence required to bind A β 40/42.^{102, 104} Several groups have developed amyloid aggregation mitigating peptides (AAMPs) based on the KLVFF motif that alter aggregation kinetics or aggregate morphologies of A β . The common design of these AAMPs is to use the KLVFF core as a recognition element, since the initial assembly of A β into oligomeric assemblies is controlled by hydrophobic interactions through side chains. Several modifications of the KLVFF motif reported include amino acid substitutions with regular amino acids, α -carbon modification of some amino acid residues, KLVFF terminal modification using polar groups, peptide backbone atoms modification with ester, isostructural double bond, N-methylation, peptide cyclization with cystines, and insertion of D-amino acids.¹⁰⁵⁻¹⁰⁷ The design strategy

employed both α -carbon and C- or N-terminal modifications to yield AAMPs that we show to be potent mitigators of A β fibrillization.¹²

1.3.2.7 Structures of A β Assemblies

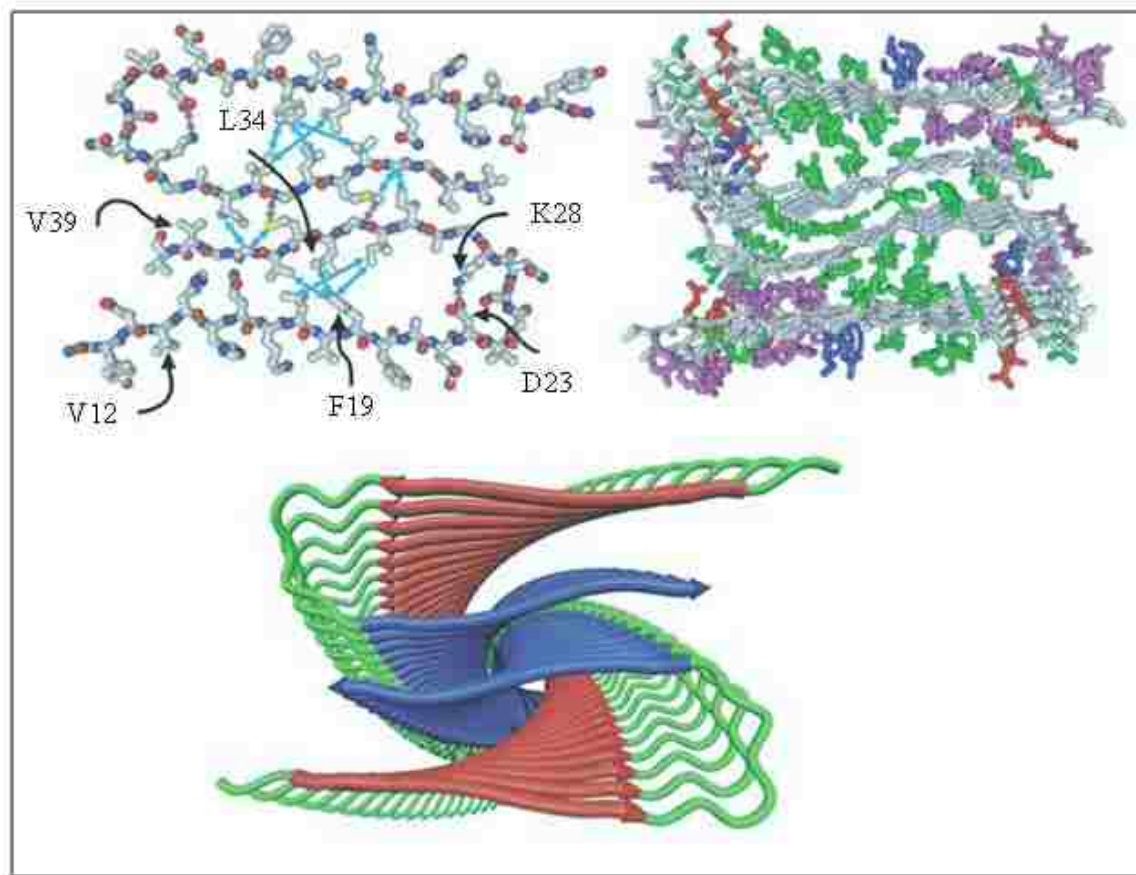


Figure 1.3. Structural model of the protofilament in A β ₁₋₁₄₀ fibril derived from Tycko et al. *Quarterly Reviews of Biophysics* **2006**, 39, (1), 1-55.

Recent experiments have identified different types of A β oligomers that include SDS stable dimers and trimers, protofibrils, annular assemblies, amylospheroids, A β -derived diffusible ligands, and A β *56, all of which have different sizes and morphologies.⁴⁰ This suggests that several oligomeric species may be involved in the A β fibrilization process and neurotoxicity. The structural characterization of oligomers has not been reported because of their noncrystalline nature. Unlike oligomers, fibrils have a well-defined structure. Tycko

through solid-state NMR studies has shown that A β fibrils favor C₂ symmetry.^{108, 109} The symmetry is stabilized by hydrophobic interactions between the two parallel sheets adopted by single A β molecules and between two separate A β molecules. A salt bridge between Asp23 and Lys28 also contributes to the stability of the fibril structure.¹¹⁰ Fibrils formed by longer forms of A β (A β ₁₋₄₀ and A β ₁₀₋₃₅) were more likely to consist of parallel β -sheets as compared to antiparallel β -sheets for fibrils formed by shorter peptide segments, A β ₁₆₋₂₂, A β ₁₁₋₂₅, and A β ₃₄.

¹¹⁰
42.

1.4 Conclusion

Alzheimer's disease AD is a neurodegenerative disease that affects nearly 5.3 million people in the US and new cases of the disease are expected to double by the year 2050. There is still no cure for the disease, but drugs in the market act only to slow down progression of the disease. Current approaches to the development of possible therapeutic involve targeting of secretases responsible for secretion of A β as well as the toxic structures formed during A β assembly into fibrils. Oligomeric and protofibrillar assemblies have been shown to be more toxic to neurons than fibrils. Unlike fibrils, no structural data has been reported for oligomeric structures. Structural determination of oligomers is urgently needed in order to find ways of stabilizing or disrupting their formation. Peptide-based drugs offer great potential because of their specificity and limited side effects as compared to small molecules, especially with the development of non-oral methods of drug delivery. The lethality of AD and the excessive financial and social cost associated with it require that all possible leads be pursued.

1.5 References

1. Hartley, D. M.; Walsh, D. M.; Ye, C. P.; Diehl, T.; Vasquez, S.; Vassilev, P. M.; Teplow, D. B.; Selkoe, D. J., Prototibrillar intermediates of amyloid beta-protein induce acute electrophysiological changes and progressive neurotoxicity in cortical neurons. *J Neurosci* **1999**, *19* (20), 8876-84.

2. Baglioni, S.; Casamenti, F.; Bucciantini, M.; Luheshi, L. M.; Taddei, N.; Chiti, F.; Dobson, C. M.; Stefani, M., Prefibrillar amyloid aggregates could be generic toxins in higher organisms. *J. Neurosci.* **2006**, *26* (31), 8160-8167.
3. Bitan, G.; Lomakin, A.; Teplow, D. B., Amyloid beta -Protein Oligomerization. Prenucleation interactions revealed by photo-induced cross-linking of unmodified proteins *J. Biol. Chem.* **2001**, *276* (37), 35176-35184.
4. Favrin, G.; Irback, A.; Mohanty, S., Oligomerization of amyloid A beta(16-22) peptides using hydrogen bonds and hydrophobicity forces. *Biophys. J.* **2004**, *87* (6), 3657-3664.
5. GarzonRodriguez, W.; SepulvedaBecerra, M.; Milton, S.; Glabe, C. G., Soluble amyloid A beta-(1-40) exists as a stable dimer at low concentrations. *J. Biol. Chem.* **1997**, *272* (34), 21037-21044.
6. Klein, W. L., A beta toxicity in Alzheimer's disease: globular oligomers (ADDLs) as new vaccine and drug targets. *Neurochem. Int.* **2002**, *41* (5), 345-352.
7. Lomakin, A.; Chung, D. S.; Benedek, G. B.; Kirschner, D. A.; Teplow, D. B., On the nucleation and growth of amyloid beta-protein fibrils: Detection of nuclei and quantitation of rate constants. *Proc. Natl. Acad. Sci. U. S. A.* **1996**, *93* (3), 1125-1129.
8. Walsh, D. M.; Selkoe, D. J., Oligomers in the brain: The emerging role of soluble protein aggregates in neurodegeneration. *Protein Peptide Lett.* **2004**, *11* (3), 213-228.
9. Toniolo, C.; Crisma, M.; Formaggio, F.; Peggion, C., Control of peptide conformation by the Thorpe-Ingold effect (C-alpha-tetrasubstitution). *Biopolymers* **2001**, *60* (6), 396-419.
10. Tanaka, M., Design and synthesis of non-proteinogenic amino acids and secondary structures of their peptides. *Yakugaku Zasshi* **2006**, *126* (10), 931-944.
11. Tanaka, M., Design and synthesis of chiral alpha ,alpha -disubstituted amino acids and conformational study of their oligopeptides. *Chem. Pharm. Bull. (Tokyo)* **2007**, *55* (3), 349-358.
12. Etienne, M. A.; Aucoin, J. P.; Fu, Y. W.; McCarley, R. L.; Hammer, R. P., Stoichiometric inhibition of amyloid beta-protein aggregation with peptides containing alternating alpha,alpha-disubstituted amino acids. *J. Am. Chem. Soc.* **2006**, *128* (11), 3522-3523.
13. Selkoe, D. J., Folding proteins in fatal ways. *Nature* **2003**, *426* (6968), 900-904.
14. Cohen, F. E.; Kelly, J. W., Therapeutic approaches to protein-misfolding diseases. *Nature* **2003**, *426* (6968), 905-909.
15. Maurer, K., Historical background of Alzheimer's research done 100 years ago. *J. Neural Transm.* **2006**, *113* (11), 1597-1601.
16. Jellinger, K. A., Alzheimer 100 - highlights in the history of Alzheimer research. *J. Neural Transm.* **2006**, *113* (11), 1603-1623.

17. Agorogiannis, E. I.; Agorogiannis, G. I.; Papadimitriou, A.; Hadjigeorgiou, G. M., Protein misfolding in neurodegenerative diseases. *Neuropathol. Appl. Neurobiol.* **2004**, *30* (3), 215-224.
18. Selkoe, D. J., Amyloid protein and Alzheimers-Disease. *Sci. Am.* **1991**, *265* (5), 40-47.
19. Selkoe, D. J., Alzheimers-Disease- in the Beginning. *Nature* **1991**, *354* (6353), 432-433.
20. Selkoe, D. J., The molecular pathology of Alzheimers-Disease. *Neuron* **1991**, *6* (4), 487-498.
21. Chen, M., Was Alois Alzheimer right or wrong.? *Scientist* **2007**, *21* (6), 23-23.
22. Derouesne, C., Alzheimer and Alzheimer's disease: the present enlightened by the past. An historical approach. *Psychologie & Neuropsychiatrie Du Vieillissement* **2008**, *6* (2), 115-128.
23. Alzheimer's Disease Facts and Figures. *Alzheimer's & Dementia* **2009**, *5* (3), 234-270.
24. Irvine, G. B.; El-Agnaf, O. M.; Shankar, G. M.; Walsh, D. M., Protein aggregation in the brain: The molecular basis for Alzheimer's and Parkinson's diseases. *Molecular Medicine* **2008**, *14* (7-8), 451-464.
25. Selkoe, D. J., The molecular pathology of Alzheimer's disease. *Neuron* **1991**, *6* (4), 487-498.
26. Iversen, L. L.; Mortishire-Smith, R. J.; Pollack, S. J.; Shearman, M. S., The toxicity in vitro of b-amyloid protein. *Biochemical Journal* **1995**, *311* (1), 1-16.
27. Chen, J. X.; Yan, S. D., Amyloid-beta-induced mitochondrial dysfunction. *J. Alzheimer's Dis.* **2007**, *12* (2), 177-184.
28. Ferreiro, E.; Oliveira, C. R.; Pereira, C. M. F., The release of calcium from the endoplasmic reticulum induced by amyloid-beta and prion peptides activates the mitochondrial apoptotic pathway. *Neurobiology of Disease* **2008**, *30* (3), 331-342.
29. Nizri, E.; Wirguin, I.; Brenner, T., The role of cholinergic balance perturbation in neurological diseases. *Drug News & Perspectives* **2007**, *20* (7), 421-429.
30. de Planque, M. R. R.; Raussens, V.; Contera, S. A.; Rijkers, D. T. S.; Liskamp, R. M. J.; Ruysschaert, J. M.; Ryan, J. F.; Separovic, F.; Watts, A., beta-sheet structured beta-amyloid(1-40) perturbs phosphatidylcholine model membranes. *J. Mol. Biol.* **2007**, *368* (4), 982-997.
31. Selkoe, D. J., Alzheimer's disease: Genes, proteins, and therapy. *Physiol. Rev.* **2001**, *81* (2), 741-766.
32. Selkoe, D. J., Alzheimer's disease is a synaptic failure. *Science* **2002**, *298* (5594), 789-791.

33. Joachim, C. L.; Selkoe, D. J., The Seminal Role of Beta-amyloid in the Pathogenesis of Alzheimer disease. *Alzheimer Disease & Associated Disorders* **1992**, *6* (1), 7-34.
34. Walsh, D. M.; Klyubin, I.; Fadeeva, J. V.; Cullen, W. K.; Anwyl, R.; Wolfe, M. S.; Rowan, M. J.; Selkoe, D. J., Naturally secreted oligomers of amyloid beta protein potently inhibit hippocampal long-term potentiation in vivo. *Nature* **2002**, *416* (6880), 535-539.
35. Pike, C. J.; Walencewicz, A. J.; Glabe, C. G.; Cotman, C. W., Invitro aging of beta-amyloid protein causes peptide aggregation and neurotoxicity. *Brain Res.* **1991**, *563* (1-2), 311-314.
36. Pike, C. J.; Walencewicz, A. J.; Kosmoski, J.; Cribbs, D. H.; Glabe, C. G.; Cotman, C. W., structure-activity analyses of beta-amyloid peptides - contributions of the beta-25-35 region to aggregation and neurotoxicity. *J. Neurochem.* **1995**, *64* (1), 253-265.
37. Walsh, D. M.; Lomakin, A.; Benedek, G. B.; Condron, M. M.; Teplow, D. B., Amyloid beta-protein fibrillogenesis - Detection of a protofibrillar intermediate. *J. Biol. Chem.* **1997**, *272* (35), 22364-22372.
38. Walsh, D. M.; Selkoe, D. J., A beta Oligomers - a decade of discovery. *J. Neurochem.* **2007**, *101* (5), 1172-1184.
39. Gotz, J.; Chen, F.; van Dorpe, J.; Nitsch, R. M., Formation of neurofibrillary tangles in P301L tau transgenic mice induced by Abeta 42 fibrils. *Science (New York, N.Y.)* **2001**, *293* (5534), 1491-5.
40. De Felice, F. G.; Wu, D.; Lambert, M. P.; Fernandez, S. J.; Velasco, P. T.; Lacor, P. N.; Bigio, E. H.; Jerecic, J.; Acton, P. J.; Shughrue, P. J.; Chen-Dodson, E.; Kinney, G. G.; Klein, W. L., Alzheimer's disease-type neuronal tau hyperphosphorylation induced by A[beta] oligomers. *Neurobiol. Aging* **2008**, *29* (9), 1334-1347.
41. Seubert, P.; Vigo-Pelfrey, C.; Esch, F.; Lee, M.; Dovey, H.; Davis, D.; Sinha, S.; Schlossmacher, M.; Whaley, J.; et al., Isolation and quantification of soluble Alzheimer's b-peptide from biological fluids. *Nature (London, United Kingdom)* **1992**, *359* (6393), 325-7.
42. Pitschke, M.; Prior, R.; Haupt, M.; Riesner, D., Detection of single amyloid beta-protein aggregates in the cerebrospinal fluid of Alzheimer's patients by fluorescence correlation spectroscopy. *Nat. Med.* **1998**, *4* (7), 832-834.
43. Ghanta, J.; Shen, C.-L.; Kiessling, L. L.; Murphy, R. M., A strategy for designing inhibitors of b-amyloid toxicity. *J. Biol. Chem.* **1996**, *271* (47), 29525-29528.
44. Pike, C. J.; Burdick, D.; Walencewicz, A. J.; Glabe, C. G.; Cotman, C. W., Neurodegeneration induced by b-amyloid peptides in vitro: the role of peptide assembly state. *J. Neurosci.* **1993**, *13* (4), 1676-87.

45. Simmons, L. K.; May, P. C.; Tomaselli, K. J.; Rydel, R. E.; Fuson, K. S.; Brigham, E. F.; Wright, S.; Lieberburg, I.; Becker, G. W.; Brems, D. N.; Li, W. Y., Secondary structure of amyloid beta-peptide correlates with neurotoxic activity in-vitro
Mol. Pharmacol. **1994**, *45* (3), 373-379.
46. Iwatsubo, T.; Odaka, A.; Suzuki, N.; Mizusawa, H.; Nukina, N.; Ihara, Y., Visualization of α -beta-42(43) and α -beta-40 in senile plaques with end-specific α -beta monoclonals - evidence that an initially deposited species is α -beta-42(43)
Neuron **1994**, *13* (1), 45-53.
47. Miller, D. L.; Papayannopoulos, I. A.; Styles, J.; Bobin, S. A.; Lin, Y. Y.; Biemann, K.; Iqbal, K., Peptide compositions of the cerebrovascular and senile plaque core amyloid deposits of alzheimers-disease
Arch. Biochem. Biophys. **1993**, *301* (1), 41-52.
48. Bayer, T. A.; Wirths, O.; Majtenyi, K.; Hartmann, T.; Multhaup, G.; Beyreuther, K.; Czech, C., Key factors in Alzheimer's disease: beta-amyloid precursor protein processing, metabolism and intraneuronal transport.
Brain Pathology **2001**, *11* (1), 1-11.
49. Turner, P. R.; O'Connor, K.; Tate, W. P.; Abraham, W. C., Roles of amyloid precursor protein and its fragments in regulating neural activity, plasticity and memory.
Prog. Neurobiol. **2003**, *70* (1), 1-32.
50. Jarrett, J. T.; Berger, E. P.; Lansbury, P. T., The carboxy terminus of the beta-amyloid protein is critical for the seeding of amyloid formation - implications for the pathogenesis of alzheimers-disease
Biochemistry **1993**, *32* (18), 4693-4697.
51. Lansbury, P., Hot papers - Neurochemistry - the carboxy-terminus of the beta-amyloid protein is critical for the seeding of amyloid formation - implications for the pathogenesis of alzheimers-disease
Scientist **1995**, *9* (12), 15-15.
52. Teplow, D. B., Structural and kinetic features of amyloid beta-protein fibrillogenesis.
Amyloid the international journal of experimental and clinical investigation the official journal of the International Society of Amyloidosis **1998**, *5* (2), 121-42.
53. Tseng, B. P.; Esler, W. P.; Clish, C. B.; Stimson, E. R.; Ghilardi, J. R.; Vinters, H. V.; Mantyh, P. W.; Lee, J. P.; Maggio, J. E., Deposition of monomeric, not oligomeric, A beta mediates growth of Alzheimer's disease amyloid plaques in human brain preparations.
Biochemistry **1999**, *38* (32), 10424-10431.
54. Bitan, G.; Kirkitaadze, M. D.; Lomakin, A.; Vollers, S. S.; Benedek, G. B.; Teplow, D. B., Amyloid beta-protein (A beta) assembly: A beta 40 and A beta 42 oligomerize through distinct pathways.
Proc. Natl. Acad. Sci. U. S. A. **2003**, *100* (1), 330-335.
55. McGowan, E.; Pickford, F.; Kim, J.; Onstead, L.; Eriksen, J.; Yu, C.; Skipper, L.; Murphy, M. P.; Beard, J.; Das, P.; Jansen, K.; DeLucia, M.; Lin, W. L.; Dolios, G.; Wang, R.;

Eckman, C. B.; Dickson, D. W.; Hutton, M.; Hardy, J.; Golde, T., A beta 42 is essential for parenchymal and vascular amyloid deposition in mice. *Neuron* **2005**, *47* (2), 191-199.

56. Mastrangelo Iris, A.; Ahmed, M.; Sato, T.; Liu, W.; Wang, C.; Hough, P.; Smith Steven, O., High-resolution atomic force microscopy of soluble Abeta42 oligomers. *J. Mol. Biol.* **2006**, *358* (1), 106-19.

57. Barrow, C. J.; Zagorski, M. G., Solution structures of beta peptide and its constituent fragments: relation to amyloid deposition. *Science* **1991**, *253* (5016), 179-82.

58. Hilbich, C.; Kisters-Woike, B.; Reed, J.; Masters, C. L.; Beyreuther, K., Aggregation and secondary structure of synthetic amyloid beta A4 peptides of Alzheimer's disease. *J. Mol. Biol.* **1991**, *218* (1), 149-63.

59. Yang, D. S.; Yip, C. M.; Huang, T. H.; Chakrabartty, A.; Fraser, P. E., Manipulating the amyloid-beta aggregation pathway with chemical chaperones. *J. Biol. Chem.* **1999**, *274* (46), 32970-4.

60. Lee, S.; Fernandez, E. J.; Good, T. A., Role of aggregation conditions in structure, stability, and toxicity of intermediates in the A beta fibril formation pathway. *Protein Sci.* **2007**, *16* (4), 723-732.

61. Yip Christopher, M.; Darabie Audrey, A.; McLaurin, J., Abeta42-peptide assembly on lipid bilayers. *J. Mol. Biol.* **2002**, *318* (1), 97-107.

62. Esler, W. P.; Stimson, E. R.; Ghilardi, J. R.; Vinters, H. V.; Lee, J. P.; Mantyh, P. W.; Maggio, J. E., In vitro growth of Alzheimer's disease beta-amyloid plaques displays first-order kinetics. *Biochemistry* **1996**, *35* (3), 749-57.

63. Maggio, J. E.; Stimson, E. R.; Ghilardi, J. R.; Allen, C. J.; Dahl, C. E.; Whitcomb, D. C.; Vigna, S. R.; Vinters, H. V.; Labenski, M. E.; Mantyh, P. W., Reversible in vitro growth of Alzheimer disease beta-amyloid plaques by deposition of labeled amyloid peptide. *Proc. Natl. Acad. Sci. U. S. A.* **1992**, *89* (12), 5462-6.

64. Jarrett, J. T.; Berger, E. P.; Lansbury, P. T., Jr., The carboxy terminus of the b amyloid protein is critical for the seeding of amyloid formation: Implications for the pathogenesis of Alzheimer's disease. *Biochemistry* **1993**, *32* (18), 4693-7.

65. Harper, J. D.; Lansbury, P. T., Jr., Models of amyloid seeding in Alzheimer's disease and scrapie: mechanistic truths and physiological consequences of the time-dependent solubility of amyloid proteins. *Annu. Rev. Biochem.* **1997**, *66*, 385-407.

66. Harper, J. D.; Lieber, C. M.; Lansbury, P. T., Atomic force microscopic imaging of seeded fibril formation and fibril branching by the Alzheimer's disease amyloid-beta protein. *Chemistry & Biology* **1997**, *4* (12), 951-959.

67. Kusumoto, Y.; Lomakin, A.; Teplow, D. B.; Benedek, G. B., Temperature dependence of amyloid beta-protein fibrillization. *Proc. Natl. Acad. Sci. U. S. A.* **1998**, *95* (21), 12277-12282.

68. Kad, N. M.; Myers, S. L.; Smith, D. P.; Smith, D. A.; Radford, S. E.; Thomson, N. H., Hierarchical assembly of beta(2)-microglobulin amyloid in vitro revealed by atomic force microscopy. *J. Mol. Biol.* **2003**, *330* (4), 785-797.
69. Khurana, R.; Ionescu-Zanetti, C.; Pope, M.; Li, J.; Nielson, L.; Ramirez-Alvarado, M.; Regan, L.; Fink, A. L.; Carter, S. A., A general model for amyloid fibril assembly based on morphological studies using atomic force microscopy. *Biophys. J.* **2003**, *85* (2), 1135-1144.
70. Hardy, J. A.; Higgins, G. A., Alzheimer's disease: the amyloid cascade hypothesis. *Science* **1992**, *256* (5054), 184-5.
71. Higgins, G. A., Etiology of Alzheimer's disease: The 'amyloid cascade' hypothesis. *Proc. Int. Conf. Alum. Health, 2nd* **1992**, 71-2.
72. Hardy, J. A.; Higgins, G. A., Alzheimers-Disease- The Amyloid Cascade Hypothesis *Science* **1992**, *256* (5054), 184-185.
73. Lamber, M. P.; Barlow, A. K.; Chromy, B. A.; Edwards, C.; Freed, R.; Liosatos, M.; Morgan, T. E.; Rozovsky, I.; Trommer, B.; Viola, K. L.; Wals, P.; Zhang, C.; Finch, C. E.; Krafft, G. A.; Klein, W. L., Diffusible, nonfibrillar ligands derived from Ab1-42 are potent central nervous system neurotoxins. *Proc. Natl. Acad. Sci. U. S. A.* **1998**, *95* (11), 6448-6453.
74. Hartley, D. M.; Walsh, D. M.; Ye, C. P.; Diehl, T.; Vasquez, S.; Vassilev, P. M.; Teplow, D. B.; Selkoe, D. J., Prototibrillar intermediates of amyloid b-protein induce acute electrophysiological changes and progressive neurotoxicity in cortical neurons. *J. Neurosci.* **1999**, *19* (20), 8876-8884.
75. Kirkitadze, M. D.; Bitan, G.; Teplow, D. B., Paradigm shifts in Alzheimer's disease and other neurodegenerative disorders: the emerging role of oligomeric assemblies. *J. Neurosci. Res.* **2002**, *69* (5), 567-577.
76. Haass, C.; Selkoe, D. J., Soluble protein oligomers in neurodegeneration: lessons from the Alzheimer's amyloid beta -peptide. *Nat. Rev. Mol. Cell Biol.* **2007**, *8* (2), 101-112.
77. Caughey, B.; Lansbury, P. T., Prototibrils, pores, fibrils, and neurodegeneration: Separating the responsible protein aggregates from the innocent bystanders. *Annu. Rev. Neurosci.* **2003**, *26*, 267-298.
78. Harper, J. D.; Wong, S. S.; Lieber, C. M.; Lansbury, P. T., Observation of metastable A beta amyloid prototibrils by atomic force microscopy. *Chem. Biol.* **1997**, *4* (2), 119-125.
79. Walsh, D. M.; Hartley, D. M.; Kusumoto, Y.; Fezoui, Y.; Condron, M. M.; Lomakin, A.; Benedek, G. B.; Selkoe, D. J.; Teplow, D. B., Amyloid beta-protein fibrillogenesis - Structure and biological activity of prototibrillar intermediates. *J. Biol. Chem.* **1999**, *274* (36), 25945-25952.
80. Lambert, M. P.; Barlow, A. K.; Chromy, B. A.; Edwards, C.; Freed, R.; Liosatos, M.; Morgan, T. E.; Rozovsky, I.; Trommer, B.; Viola, K. L.; Wals, P.; Zhang, C.; Finch, C. E.;

Krafft, G. A.; Klein, W. L., Diffusible, nonfibrillar ligands derived from A beta(1-42) are potent central nervous system neurotoxins. *Proc. Natl. Acad. Sci. U. S. A.* **1998**, *95* (11), 6448-6453.

81. Hughes, E.; Burke, R. M.; Doig, A. J., Inhibition of toxicity in the b-amyloid peptide fragment b-(25-35) using N-methylated derivatives: a general strategy to prevent amyloid formation. *J. Biol. Chem.* **2000**, *275* (33), 25109-25115.

82. Camilleri, P.; Haskins, N. J.; Howlett, D. R., beta-Cyclodextrin interacts with the Alzheimer amyloid beta-A4 peptide. *FEBS Lett.* **1994**, *341* (2-3), 256-8.

83. Tomiyama, T.; Shoji, A.; Kataoka, K.; Suwa, Y.; Asano, S.; Kaneko, H.; Endo, N., Inhibition of amyloid beta protein aggregation and neurotoxicity by rifampicin. Its possible function as a hydroxyl radical scavenger. *J. Biol. Chem.* **1996**, *271* (12), 6839-44.

84. Kornilova, A. Y.; Wolfe, M. S., Secretase inhibitors for Alzheimer's disease. In *Annu. Rep. Med. Chem.*, 2003; Vol. 38, pp 41-50.

85. Estrada, L. D.; Soto, C., Disrupting beta -amyloid aggregation for Alzheimer disease treatment. *Curr. Top. Med. Chem. (Sharjah, United Arab Emirates)* **2007**, *7* (1), 115-126.

86. Kreft, A. F.; Martone, R.; Porte, A., Recent Advances in the Identification of gamma -Secretase Inhibitors To Clinically Test the Abeta Oligomer Hypothesis of Alzheimer's Disease. *J. Med. Chem.*, ACS ASAP.

87. Olson, R. E.; Albright, C. F., Recent progress in the medicinal chemistry of gamma -secretase inhibitors. *Curr. Top. Med. Chem. (Sharjah, United Arab Emirates)* **2008**, *8* (1), 17-33.

88. Tomita, T., Secretase inhibitors and modulators for Alzheimer's disease treatment. *Expert Rev. Neurother.* **2009**, *9* (5), 661-679.

89. Bard, F.; Barbour, R.; Cannon, C.; Carreto, R.; Fox, M.; Games, D.; Guido, T.; Hoenow, K.; Hu, K.; Johnson-Wood, K.; Khan, K.; Kholodenko, D.; Lee, C.; Lee, M.; Motter, R.; Nguyen, M.; Reed, A.; Schenk, D.; Tang, P.; Vasquez, N.; Seubert, P.; Yednock, T., Epitope and isotype specificities of antibodies to beta-amyloid peptide for protection against Alzheimer's disease-like neuropathology. *Proc. Natl. Acad. Sci. U. S. A.* **2003**, *100* (4), 2023-2028.

90. Bard, F.; Cannon, C.; Barbour, R.; Burke, R. L.; Games, D.; Grajeda, H.; Guido, T.; Hu, K.; Huang, J. P.; Johnson-Wood, K.; Khan, K.; Kholodenko, D.; Lee, M.; Lieberburg, I.; Motter, R.; Nguyen, M.; Soriano, F.; Vasquez, N.; Weiss, K.; Welch, B.; Seubert, P.; Schenk, D.; Yednock, T., Peripherally administered antibodies against amyloid beta-peptide enter the central nervous system and reduce pathology in a mouse model of Alzheimer disease. *Nat. Med.* **2000**, *6* (8), 916-919.

91. Citron, M., beta -Secretase inhibition for the treatment of Alzheimer's disease - promise and challenge. *Trends Pharmacol. Sci.* **2004**, *25* (2), 92-97.

92. Dodart, J. C.; Bales, K. R.; Gannon, K. S.; Greene, S. J.; DeMattos, R. B.; Mathis, C.; DeLong, C. A.; Wu, S.; Wu, X.; Holtzman, D. M.; Paul, S. M., Immunization reverses memory

deficits without reducing brain A beta burden in Alzheimer's disease model. *Nat. Neurosci.* **2002**, 5 (5), 452-457.

93. Kotilinek, L. A.; Bacskai, B.; Westerman, M.; Kawarabayashi, T.; Younkin, L.; Hyman, B. T.; Younkin, S.; Ashe, K. H., Reversible memory loss in a mouse transgenic model of Alzheimer's disease. *J. Neurosci.* **2002**, 22 (15), 6331-6335.

94. Banks, W. A.; Farr, S. A.; Morley, J. E.; Wolf, K. M.; Geylis, V.; Steinitz, M., Anti-amyloid beta protein antibody passage across the blood-brain barrier in the SAMP8 mouse model of Alzheimer's disease: an age-related selective uptake with reversal of learning impairment. *Exp. Neurol.* **2007**, 206 (2), 248-256.

95. Banks, W. A.; Terrell, B.; Farr, S. A.; Robinson, S. M.; Nonaka, N.; Morley, J. E., Passage of amyloid beta protein antibody across the blood-brain barrier in a mouse model of Alzheimer's disease. *Peptides (N. Y., NY, U. S.)* **2002**, 23 (12), 2223-2226.

96. Amijee, H.; Scopes David, I. C., The quest for small molecules as amyloid inhibiting therapies for Alzheimer's disease. *J Alzheimers Dis* **2009**, 17 (1), 33-47.

97. Blanchard Barbara, J.; Chen, A.; Rozeboom Leslie, M.; Stafford Kate, A.; Weigle, P.; Ingram Vernon, M., Efficient reversal of Alzheimer's disease fibril formation and elimination of neurotoxicity by a small molecule. *Proc. Natl. Acad. Sci. U. S. A.* **2004**, 101 (40), 14326-32.

98. Gestwicki Jason, E.; Crabtree Gerald, R.; Graef Isabella, A., Harnessing chaperones to generate small-molecule inhibitors of amyloid beta aggregation. *Science (New York, N.Y.)* **2004**, 306 (5697), 865-9.

99. Necula, M.; Breydo, L.; Milton, S.; Kayed, R.; van der Veer Wytze, E.; Tone, P.; Glabe Charles, G., Methylene blue inhibits amyloid Abeta oligomerization by promoting fibrillization. *Biochemistry* **2007**, 46 (30), 8850-60.

100. Findeis, M. A., Approaches to discovery and characterization of inhibitors of amyloid beta -peptide polymerization. *Biochim. Biophys. Acta, Mol. Basis Dis.* **2000**, 1502 (1), 76-84.

101. Tjernberg, L. O.; Lilliehook, C.; Callaway, D. J. E.; Naslund, J.; Hahne, S.; Thyberg, J.; Terenius, L.; Nordstedt, C., Controlling amyloid beta-peptide fibril formation with protease-stable ligands. *J. Biol. Chem.* **1997**, 272 (19), 12601-12605.

102. Tjernberg, L. O.; Naslund, J.; Lindqvist, F.; Johansson, J.; Karlstrom, A. R.; Thyberg, J.; Terenius, L.; Nordstedt, C., Arrest of beta-amyloid fibril formation by a pentapeptide ligand. *J. Biol. Chem.* **1996**, 271 (15), 8545-8.

103. Hilbich, C.; Kisters-Woike, B.; Reed, J.; Masters, C. L.; Beyreuther, K., Substitutions of hydrophobic amino acids reduce the amyloidogenicity of Alzheimer's disease bA4 peptides. *J. Mol. Biol.* **1992**, 228 (2), 460-73.

104. Tjernberg, L. O.; Lilliehook, C.; Callaway, D. J.; Naslund, J.; Hahne, S.; Thyberg, J.; Terenius, L.; Nordstedt, C., Controlling amyloid beta-peptide fibril formation with protease-stable ligands. *J. Biol. Chem.* **1997**, 272 (19), 12601-5.
105. Sciarretta, K. L.; Gordon, D. J.; Meredith, S. C., Peptide-based inhibitors of amyloid assembly. In *Amyloid, Prions, and Other Protein Aggregates, Pt C*, 2006; Vol. 413, pp 273-312.
106. Takahashi, T.; Mihara, H., Peptide and Protein Mimetics Inhibiting Amyloid beta-Peptide Aggregation. *Acc. Chem. Res.* **2008**, 41 (10), 1309-1318.
107. Stains, C. I.; Mondal, K.; Ghosh, I., Molecules that target beta-amyloid. *Chemmedchem* **2007**, 2 (12), 1675-1692.
108. Petkova, A. T.; Yau, W. M.; Tycko, R., Experimental constraints on quaternary structure in Alzheimer's beta-amyloid fibrils. *Biochemistry* **2006**, 45 (2), 498-512.
109. Tycko, R., Solid-state NMR as a probe of amyloid structure. *Protein Peptide Lett.* **2006**, 13 (3), 229-234.
110. Tycko, R., Molecular structure of amyloid fibrils: insights from solid-state NMR. *Q. Rev. Biophys.* **2006**, 39 (1), 1-55.

CHAPTER 2

SYNTHESIS OF ALPHA, ALPHA-DISUBSTITUTED AMINO ACIDS ($\alpha\alpha$ AAS) AND THEN INCORPORATION INTO SHORT PEPTIDES

2.1 Introduction

Peptide-protein or protein-protein interactions play an important role in many cellular processes, hence what is an increasingly popular source for the design of inhibitors. One approach involves designing short model inhibitor peptides that will interact with specific residues in the target molecule.¹ Such model peptides allow elucidation of the roles of the target molecules in cellular function as potential targets for development of new therapeutic agents. Tjernberg et al. identified residues KLVFF as critical for self recognition and fibril formation.¹ Effective mitigators of A β assembly are reported to incorporate this region in their core sequence. For a mitigator to interact with A β , it has to adopt an extended conformation similar to A β . C $^{\alpha,\alpha}$ -disubstituted glycine residues ($\alpha\alpha$ AAs) have been shown to promote helical or extended conformation depending on substituent's at the α -carbon. Thus, short peptides incorporating one or more $\alpha\alpha$ AAs adopt an extended conformation with two faces where one face containing $\alpha\alpha$ AAs blocks the necessary hydrogen bonds required for β -sheet extension and the other face is available for interaction with A β . In addition, $\alpha\alpha$ AAs increase the stability of $\alpha\alpha$ AAs-containing peptides from proteolytic degradation, enhancing their potential as therapeutic agents. This dissertation will focus mainly on synthesis of the $\alpha\alpha$ AAs dibenzylglycine (Dbg), dipropylglycine (Dpg) and diisobutylglycine (Dibg) and their incorporation into model peptides as possible mitigators of A β assembly. We hypothesize that these $\alpha\alpha$ AAs that have larger side chains than methyl groups when incorporated into a model peptide will induce extended peptide conformations. Thus, peptides containing $\alpha\alpha$ AAs would have strong affinity for β -sheet assemblies and block one putative face from hydrogen bonding with another β -sheet moiety.

The inhibitor peptides consist of hydrophobic core of A β 16-20 where $\alpha\alpha$ AAs are substituted into hydrophobic core of A β at key positions.

2.2 Experimental Section

2.2.1. Materials and Instruments

2.2.1.1 Materials

Fmoc-protected amino acids and Fmoc-PAL-PEG-PS support (initial loading 0.16-0.22 mmol/g) were purchased from Applied Biosystems (Foster, CA), Novabiochem (Darmstadt, Germany), or Peptide international (Louisville, KE). N-[(dimethylamino)-1H-1, 2, 3-triazolo[4, 5-b]pyridino-1-ylmethylene]-N-methylmethanaminium hexafluorophosphate N-oxide (HATU), 7-azabenzotriazol-1-yloxy-tris-(pyrrolidino) phosphonium hexafluorophosphate (PyAOP), N-hydroxybenzotriazole (HOBr), 1-Hydroxy-7-Azabenzotriazole (HOAt), O-Benzotriazole-N,N,N',N'-tetramethyl-uronium-hexafluoro-phosphate (HBTU), and O-(Benzotriazol-1-yl)-N,N,N',N'-tetramethyluronium tetrafluoroborate were obtained from Applied Biosystems (Foster CA) or GL Biochem Ltd (Shanghai, China). N,N'-dicyclohexylcarbodiimide (DCC), N,N'-diisopropylcarbodiimide (DIC), bis(2-oxo-3-oxazolidinyl)phosphonic chloride (BOP-Cl), triisopropylsilane (TIPS), trifluoroacetic acid (TFA), benzyl bromide, ethylnitroacetate, Diisopropylethylamine (redistilled), liquefied phenol and solvents (drum) were purchased from Sigma-Aldrich (Milwaukee, WI). Diisopropylethylamine (DIEA), piperidine (4-methypiperidine) and collidine were obtained from Fisher Scientific. TLC plates and silica gel were purchased from sorbent technologies

2.2.1.2 Instruments

- GC/MS: Varian Saturn 2200 GC/MS

- Mass Spectrometry: Bruker ProFLEX III MALDI-TOF mass spectrometer and Agilent 6210 time-of-flight MS
- **2.2.1.2.3** Microwave: MARS System with XP-1500 PlusT vessels, the ESP-1500 Plus and RTP-300

Table 2.1 microwave-coupling conditions

Amino acid	Power (watts)	Coupling time	Hold temperature
$\alpha\alpha$ As	400	10	95
Symmetrical anhydride	400	20	75
Natural amino acid	400	5	75

- Peptide Synthesizer: MilliGen 9050 PepSynthesizer
- NMR: Bruker DPX-250 and Bruker AV-400
- Amino Acid Analysis: Dionex AAA-Direct instrumentation
- Circular dichroism (CD): Aviv Circular Dicroism Spectrometer Model 62DS
- HPLC: Waters
 - Software: Empower
 - Controller: Waters 600E (multisolvent delivery system)
 - Pump: Waters 625
 - Detector: Waters 486 UV detector set at 220 nm
 - Columns: Waters Delta-Pak C₄ (15 μ m, 100 \AA), 8 \times 100 mm for analytical HPLC
Waters Delta-Pak C₄ (15 μ m, 100 \AA), 25 \times 10 mm for preparative HPLC
 - Buffer A: H₂O, 0.1 % TFA (v/v)
 - Buffer B: ACN, 0.1 % TFA (v/v)

Table 2.2. Standard method for analytical HPLC

Time (min)	Buffer A (%)	Buffer B (%)	Flow (ml/min)	UV (nm)
0	90	10	1	220 nm
60	30	70	1	
65	30	70	1	
70	90	10	1	

Table 2.3 Standard method for preparative HPLC

Time (min)	Buffer A (%)	Buffer B (%)	Flow (ml/min)	UV (nm)
0	90	10	10	220 nm
60	60	40	10	
65	30	70	10	
70	30	70	10	
75	90	10	10	

2.2.2 Synthesis of $\alpha\alpha$ AAs

Facile synthetic routes for $\alpha\alpha$ AAs are required to obtain enough amino acid for solid phase peptide synthesis of designed inhibitor peptides. Syntheses followed previously published procedures with some slight modifications. Fmoc reactions were carried out following Bolin procedure.²

2.2.2.1 Synthesis of N^α- Protected Dipropylglycine(Dpg)

2.2.2.1.1 5, 5-Dipropylhydantoin (1a)

Previously synthesized following bucherer-Bergs protocol for aldehydes or ketones.^{3, 4} A solution of 4-heptanone (20 g, 175.2 mmol), potassium cyanide (24 g, 367.6 mmol), and ammonium carbonate (37.2 g, 385.2 mmol) in methanol (100 mL) and water (100 mL) was heated at 50 °C in a capped vessel for 36 h. The precipitated solid was filtered and washed with a +small portion of water and dried in air to yield the hydantoinhydantoin **1a** as an off-white powder (25.0 g, 80% yield). ¹H NMR (250 MHz, CD₃SOCD₃) δ: 10.55 (s, 1H), 7.81 (s, 1H), 1.69 -1.57 (m, 4H), 1.43 -1.38 (m, 2H), 1.22 -1.19 (m, 2H), 0.88 - 0.85 (t, 6H). ¹³C NMR (75 MHz, DMSO-d₆) δ: 178.89, 157.71, 76.07, 66.49, 17.11, 14.77.

2.2.2.1.2 2, 2-Dipropylglycine (2a)

The hydantoin **1a** (18 g, 97.8 mmol) was suspended in 5 N NaOH (272 mL, 1.36 mol), and refluxed for 40 h. The mixture was then cooled and acidified to pH 6.5 with concentrated HCL. The precipitate that formed was then filtered, concentrated *in vacuo*, and further washed with a small portion of acetone to remove the unreacted hydantoin. Both the filtrate residue and the solid that precipitated out upon acidification were extracted with warm ethanol several times. Dipropylglycine (Dpg) was obtained as a white solid upon removal of ethanol *in vacuo*. The free amino acid **2a** was purified using Dowex 50X8-400 ion exchange resin, packed tightly in a büchner funnel connected to suction pressure. The resin was activated by rinsing with 2N HCl and then with water until the eluent was neutral. Dipropylglycine was dissolved in 2 N HCl, added to the activated resin, and rinsed with water (3 L) to remove all inorganic salts that were formed during acidification. The amino acid bound to the resin was washed off the resin with 2 N NH₄OH (2 L) and solvent removed *in vacuo* to yield **2a** (15.6 g, 75%). Anal. Calcd. for C₁₀H₂₁NO₂: C, 60.35; H, 10.76; N, 8.80; Found: C, 60.14; N, 10.73; N, 8.73. ¹HNMR (250 MHz, CD₃SOCD₃) δ: 7.34(s, 2H), 1.51-1.10 (m, 8H), 0.87-0.78 (t, 6H).

2.2.2.1.3 9-Fluorenylmethoxycarbonyl-2, 2-dipropylglycine (3a)

Trimethylsilylchloride (7.27 mL, 57.26 mmol) was added in one portion to a suspension of **2a** (4.52 g, 28.63 mmol) in 45 mL of anhydrous CH₂CL₂, and refluxed for 8 h. The mixture was cooled in an ice bath then, N, N-diisopropylethylamine (9.85 mL, 57.26 mmol) and Fmoc chloride (6.73 g, 26.02 mmol) were added. The solution was stirred at 0°C for 30 min before the reaction was allowed to warm up to room temperature and stirred further for 24 h. The resulting mixture was concentrated *in vacuo* to provide an oil that was dissolved in DI water (60 mL), acidified to pH 2 with 12 N HCl, and then extracted with ethyl acetate (3×60 mL). The

combined organic layers were dried over anhydrous MgSO₄ and concentrated in *vacuo* to provide a yellow solid which was triturated in hexanes to afford a white solid product **3a** (8.51 g, 86%). ¹H NMR (250 MHz, CD₃SOCD₃) δ: 10.68 (s, 1H), 7.91-7.88 (d, 2H), 7.71 - 7.69 (d, 2H), 7.44-7.29 (m, 4H), 6.95 (s, 1H), 4.28 - 4.21 (m, 3H), 1.76 - 1.74 (m, 4H), 1.20 - 1.10 (m, 2H), 0.86 - 0.82 (m, 6H). Anal. Calcd. for C₂₅H₃₁NO₄: C, 74.42; H, 7.13; N, 3.67. Found: C, 72.57; H, 7.30; N, 3.80.

2.2.2.2 Synthesis of *N*^α-Protected Dibenzylglycine

Dibenzylglycine was synthesized following previously reported protocol from ethyl nitro acetate.³

2.2.2.2.1 Ethyl 2-benzyl-2-nitro-3-phenylpropanoate (**1b**)

To a solution of ethyl nitroacetate (1.0 g, 7.51 mmol) in dry DMF (5 mL) was added DIEA (2.0 g, 15.4 mmol) and Bu₄N⁺Br⁻ (0.24 g, 0.75 mmol). To this clear yellow solution, benzyl bromide (2.6 g, 15.4 mmol) was added and the reaction spontaneously warmed to 60 °C over 5 min. After 20 min., DIEA•HBr precipitated out of solution. After 1 h, DIEA•HBr was filtered, washed with ether (100 mL), and the combined filtrate washed with H₂O (5 x 50 mL). The organic layer was dried (Na₂SO₄) and ether removed under *vacuo* to provide a yellow oil, which was of sufficient purity to be used in further reactions or could be purified by silica gel chromatography using pentane : ether (90:10) to provide a white solid **1b**, yield 0.55 g (55%).

2.2.2.2.2 Ethyl 2, 2-dibenzylglycine ester (**2b**)

To a solution of nitro ester **1b** (0.51 g, 1.80 mmol) in glacial AcOH (1mL) and absolute ethanol (10 mL), a catalytic amount of Raney Nickey 50 % (w/v) was added. The resulting mixture was reduced over hydrogen gas; pressure (50 psi) for 24 h. Raney Nickel was filtered over Celite cake and washed with 30 mL of ethanol. Ethanol was removed in *vacuo* and the

crude product dissolved in 30 mL diethyl ether, washed with 10 mL (3X) saturated sodium carbonate, and then with 10 mL (3X) brine. The resulting organic fraction was dried over anhydrous sodium sulfate for 45 min and ether removed under *vacuo* to give the crude product (0.32 g) which was purified via silica gel column chromatography using ethyl acetate: hexane (70:30).

2.2.2.3 2, 2-Dibenzylglycine (3b)

A suspension of dibenzylglycine ester **2b** (0.90 mg, 0.35 mmol) in 2 M KOH (50 mL) and ethanol (25 mL) was refluxed under argon for 24 h. The resulting mixture was concentrated to 20 mL *in vacuo* and acidified to pH 6.5 using 12 N HCl. The white precipitate formed was filtered, washed with cold water (5 mL), and air dried to provide the free amino acid which was purified via ion exchange chromatography using cationic exchange Dowex 50X8-400 resin to afford **3b** (430 mg, 1.68 mmol). ¹HNMR (250MHZ, CD₃OD) σ : 7.26 - 7.3 (10H), 3.45 (d, 2H) 2.87 (d, 2H), 1.27 (s, 2H), Anal. Calcd for C₁₆H₁₇NO₂: C, 75.27; H, 6.71; N, 5.48. Found: C, 75.12; H, 6.66; N, 5.59.

2.2.2.4 N^a-(9-Fluorenylmethoxycarbonyl)-2, 2-dibenzylglycine (4b)

To a suspension of **3b** (430 mg, 1.68 mmol) in dry DCM (6.45 mL) was added Trimethylsilyl chloride (108.64 mg, 3.36 mmol) and refluxed under argon for 8 h. The mixture was cooled to 0°C in an ice bath and DIEA (129.25 mg, 1.68 mmol) and Fmoc-Cl (390 mg, 1.51 mmol) were added. The reaction was allowed to warm to 25 °C and stirred for 30 h. The resulting mixture was concentrated *in vacuo* to provide a yellow solid, which was dissolved in water (30 mL), acidified to pH 2.0 with 12 N HCl, and extracted with ethyl acetate (3 x 35 mL). The combined ethyl acetate fractions were dried over anhydrous magnesium sulfate and concentrated *in vacuo* to provide a light yellow solid. The crude product was triturated in hexanes to afford a white

solid **4b** in 75 % yield. ^1H NMR (250MHz, CDCl₃) σ : 7.82-7.12 (m, 18H), 5.51 (s, 1H), 4.50 (d, J = 7 Hz, 2H), 4.30 (t, J = 7.0Hz, 1H), 3.93 (d, J = 13.6Hz, 2H), 3.25 (d, J = 13.6Hz, 2H). ^{13}C NMR (75 MHz, CDCl₃) σ : 177.49, 155.03, 144.21, 141.74, 136.17, 130.13, 128.86, 128.17, 127.53, 125.60, 124.48, 120.42, 67.08, 66.94, 47.67, and 42.17. Anal.Calcd. for C₃₁H₂₇NO₄: C, 77.96; H, 5.70; N, 2.93. Found: C, 78.06; H, 5.63; N 2.47.

2.2.2.3 Synthesis of N^α -Protected Diisobutylglycine

Diisobutylglycine was synthesized following previously reported protocol⁵

2.2.2.3.1 Ethyl 2, 2 – Bis (2-methylallyl)-2-nitroacetate (**1c**).

To a solution of ethyl nitro acetate (10.0 g, 75.1 mmol) in dry THF (110 mL) were added 2-methylallyl acetate (18.0 g, 157.1 mmol) and Pd(PPh₃)₄ (4.5 g, 3.9 mmol). After 15 min, DIEA (20.1 g, 157.1 mmol) was added, and the reaction stirred under argon for 8 h at 50 °C. The resulting solution was filtered over Celite while washing with THF (2 × 120 mL). The filtrate was concentrated, dissolved in 75 mL of EtOAc, and washed with 10% K₂CO₃ (50 mL). To the organic layer was added 6 g of PS-PPh₃ (1.3 mmol/g) Argonaut resin and the mixture was shaken for 25 min. The resin was filtered and the filtrate purified via column chromatography using hexane : EtOAc (80:20) to provide a light yellow oil **1c** (7.65g, yield 97%). ^1H NMR (250 MHz, CDCl₃) σ : 4.94 - 4.92 (m, 2H), 4.78 - 4.77 (m, 2H), 4.26 - 4.18 (q, 2H), 3.0-2.99 (m, 4H), 1.69 (m, 6H), 1.29 - 1.23 (t, 3H).

2.2.2.3.2 Ethyl 2, 2-Diisobutylglycine Ester (**2c**).

To a solution of **1c** (17.64g, 72.9 mmol) in absolute ethanol (30 mL) were added glacial acetic acid (4 mL) and a 50 % (w/w) slurry of Raney nickel in water (6.0 g). The reaction was hydrogenated over H₂ gas (50 psi) for 24 h. The resulting solution was filtered carefully over Celite while washing with EtOH (2 x 50 mL). The solvent was removed *in vacuo* and the crude

dissolved in diethyl ether (80 mL), washed with saturated sodium carbonate (60 mL), and brine (60 ml). The resulting organic fraction was dried over anhydrous sodium sulfate and reduced under *vacuo* to afford **2c** (14.2g, 90% yield). ^1H NMR (250 MHz, CDCl_3) δ : 4.08 - 4.0 (q, 2H), 1.67 - 1.59 (m, 6H), 1.40 - 1.35 (m, 2H), 1.21-1.16 (t, 3H), 0.85 - 0.82 (m, 6H), 0.73 - 0.71 (m, 6H).

2.2.2.3.3 2, 2-Diisobutylglycine(3c).

A suspension of **2c** (14.2 g, 65.7 mmol) in 3 M KOH (200 mL) and ethanol (100 mL) was refluxed under N_2 for 24 h. The resulting mixture was concentrated to 100 mL and acidified to pH 6.5 with 12 N HCl. The solvent was evaporated and the residue re-dissolved in a minimum amount of water (~50 mL). The mixture was added to an activated Dowex 50X8-400 ion-exchange resin (600 g) washed with 2 L of water and then eluted with methanol (300 mL) and 2 N NH_4OH (2 L). The collected 2 N NH_4OH fractions were evaporated in *vacuo* to give the free amino acid **3c** (9.5g, yield 83%) as a white powder. mp 224 - 227 °C; ^1H NMR (250 MHz, DMSO-d₆) δ 7.3 (s, 2H), 1.76-1.70 (m, 2H), 1.62-1.43 (m, 4H), 0.86-0.83 (m, 12 H); ^{13}C NMR (75 MHz, DMSO-d₆) δ : 172.2, 62.7, 45.9, 25.0, 23.3, 23.0; Anal. Calcd. for $\text{C}_{10}\text{H}_{21}\text{NO}_2$: C 64.13; H, 11.30; N, 7.48. Found; C, 64.39; H, 11.84; N 7.60.

2.2.2.3.4 Synthesis of N^α -Protected Dibg. *N*-(9-Fluorenylmethoxycarbonyl)-2, 2-diisobutylglycine(4c)

Trimethylsilylchloride (8.8 g, 81.0 mmol) was added to a suspension of the amino acid **3c** (7.4 g, 39.6 mmol) in dry CH_2Cl_2 (80 mL) and refluxed under N_2 for 8 h. The mixture was cooled to 0°C, and DIEA (10.5 g, 81.0 mmol) and Fmoc-Cl (10.0 g, 38.6 mmol) were added. The reaction was allowed to warm to 25 °C and stirred for 20 h. The resulting mixture was concentrated in *vacuo* to provide a yellow solid that was then dissolved in EtOAc (80 mL). To this mixture, water was added (40 mL), and the solution acidified to pH 2.0 with 2 N HCl. The

separated organic layer was dried over magnesium sulfate and concentrated in vacuo to provide a light yellow solid. The crude product was triturated in hexanes to afford a white solid **4c** (13.7 g, 88% yield): mp 132-133 °C; ¹H NMR (250MHz, DMSO-*d*6) δ: 7.90-7.28 (m, 8H), 6.48 (s, 1H), 4.33 (d, *J*) 6.7 Hz, 2H), 4.20 (t, *J*) 6.7 Hz, 1H), 2.03-1.97 (m, 2H), 1.63-1.48 (m, 4H), 0.80-0.76 (m, 12 H); ¹³C NMR (75 MHz, DMSO-*d*6) δ: 175.7, 153.4, 143.7, 140.7, 127.6, 127.0, 125.0, 120.1, 64.9, 61.5, 46.7, 43.6, 23.8, 23.7, 23.1. Anal. Calcd for C₂₅H₃₁NO₄: C, 73.32; H, 7.63; N, 3.42. Found: C, 73.50; H, 7.76; N 3.52.

2.2.3 Peptide Synthesis.

2.2.3.1 General

All peptides were synthesized by solid phase peptide synthesis (SPSS) on PAL-PEG-PS resin (0.16-0.22 mmol/g) or Rink amide resin (0.52 mmol/g) either manually or on automated pioneer peptide synthesizer.

2.2.3.2 Attachment of the First Residue on the Resin.

The resin is swollen in DMF or DCM for 20 min and drained before use. The first amino acid residue attached to the resin linker is always coupled twice to increase the overall peptide yield and prevent formation of C-terminally related truncated peptides.

2.2.3.3 Removal of the Fmoc Protective Group

A solution of 5 % piperidine and 2 % DBU in DMF (4 ml/g resin) is added to resin. The mixture is shaken for 2 min at room temperature and drained. This is repeated for 5 and 10 min before the resin is washed with DMF (5×1 mL) and DCE (5×1mL).

2.2.3.4 Amino Acid Coupling

Amino acid (4 equiv) and HBTU/HOBt (4 equiv each) is dissolved in 0.5 M DIEA and added to the unprotected resin (1 equiv) for 1 hr while shaking. The coupling mixture is drained and resin

washed with DMF (5×1 mL), and DCM (5×1 mL). For difficult couplings especially $\alpha\alpha$ AAs, the stronger activating agents such as PyAOP/HOAt or HATU/HOAt were used and couplings carried out using DCE: DMF (2:1) as solvent and at elevated temperature (50°C). Small quantities of resin are tested for un-reacted amine with bromophenol blue test. If the test is positive, the coupling reaction is repeated

2.2.3.5 N-acylation of $\alpha\alpha$ AAs Using Symmetrical Anhydrides.

10.0 equiv of amino acid (relative to resin) is dissolved in dry DCM under argon (drops of DMF may be needed for complete dissolution) and cooled to 0°C . 5.0 equiv of DIC (relative to resin) are slowly added. The mixture is stirred for 30 min before DCM is evaporated and residue dissolved in a minimum amount of DCE: DMF (9:1). The mixture is added to the resin for 8 hr at 50°C while shaking. Resin is filtered, washed with (5×1 mL), (5×1 mL) and small quantities of resin are tested for un-reacted amine with bromophenol blue test. If the test is positive, the coupling reaction is repeated

2.2.3.6 Capping of Unreacted Sites

Resin is capped specifically after difficult couplings using 0.2 M acetic acid and 0.28 M DIEA (24 mL) for 2 hr to terminate deletion sequences arising from unreacted sites. Capping solution is removed and resin washed with DMF (10×1 mL).

2.2.3.7 Peptide Cleavage

Resins were treated with standard cleavage solution (trifluoroacetic acid: triisopropylsilane: water: phenol (8.8:0.2:0.5:0.5) at room temperature for 2 h to cleave the peptide from the solid support. After filtration, the filtrate is diluted in cold ethyl ether and allowed to co-precipitate overnight. The precipitate was centrifuged at 40,000 rpm, washed with

cold ethyl ether, and centrifuged for ten minutes (3x). The supernatant was filtered and the resulting pellet allowed to dry overnight yielding the crude product.

2.2.3.8 Fmoc Analysis

Coupling yields for each step were determined by detection of Fmoc-piperidine conjugate using a UV spectrophotometer at 300 nm and the absorbance reading was used to calculate the yield based on the new resin substitution as compared to the original. Also bromophenol blue (10% in acetonitrile) was used to monitor the presence of free amine; blue color, positive test while yellow color is a negative test.

2.2.3.9 Circular Dichroism Measurements

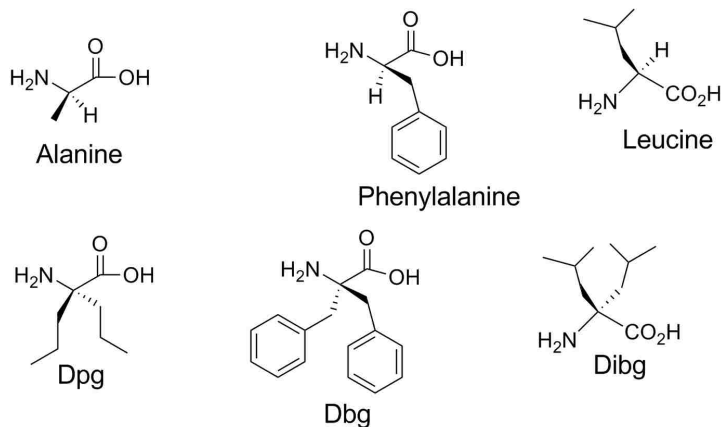
All measurements were carried out using an Aviv Circular Dichroism Spectrometer Model 62DS with Igor plotting software. The CD spectra are averages of three scans made at 1.00 nm intervals acquired from 250 nm to 190 nm (UV Abs range) recorded at 25⁰C.

2.3 Results and Discussion

2.3.1 Synthesis of $\alpha\alpha$ AAs

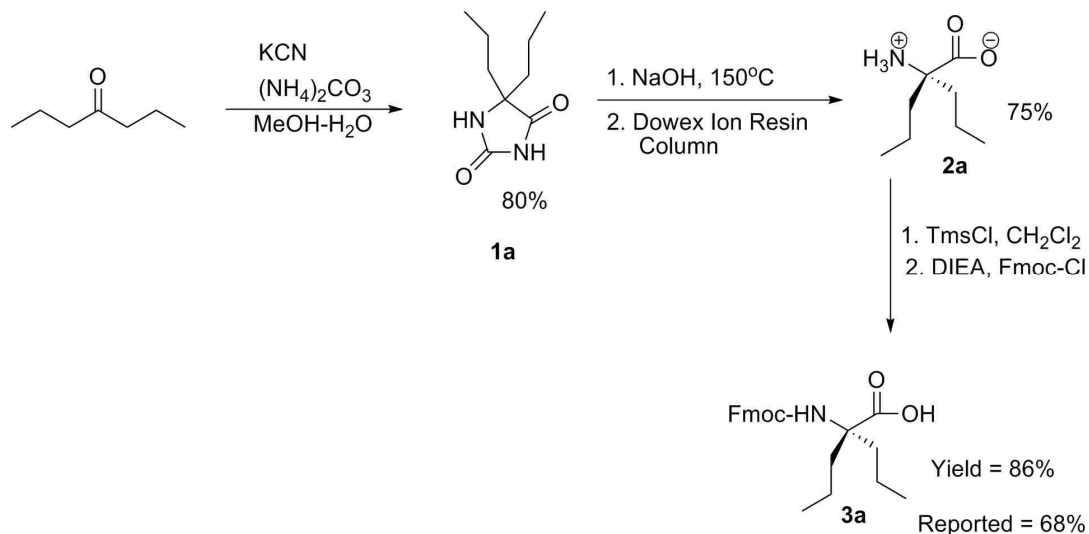
The $\alpha\alpha$ AAs, Dibg, Dbg, and Dpg are achiral analogues of the natural amino acids leucine, phenylalanine, and alanine respectively (Scheme 1). The most common method of synthesizing $\alpha\alpha$ AAs is via Bucherer-Bergs or Strecker syntheses,⁶ yet only Dpg was successfully synthesized using this method (Scheme 2). The only modification to this procedure was the longer reaction time, and improved work up procedures during the Fmoc reaction of **2a** which resulted in dramatic increase in yield of **3a** (68%) to 86%. The other amino acids, Dbg, and Dibg failed because they form sterically hindered hydantoins, which are extremely difficult to hydrolyze to free amino acids even under extremely harsh conditions.

Scheme 1



This prompted development of other alternative synthetic routes to $\alpha\alpha$ AAs such as glycine anion and cation equivalents.⁷ Nitroacetate esters have long been recognized as potentially useful synthetic intermediates for the preparation of amino acids as well as other biologically significant compounds.⁸

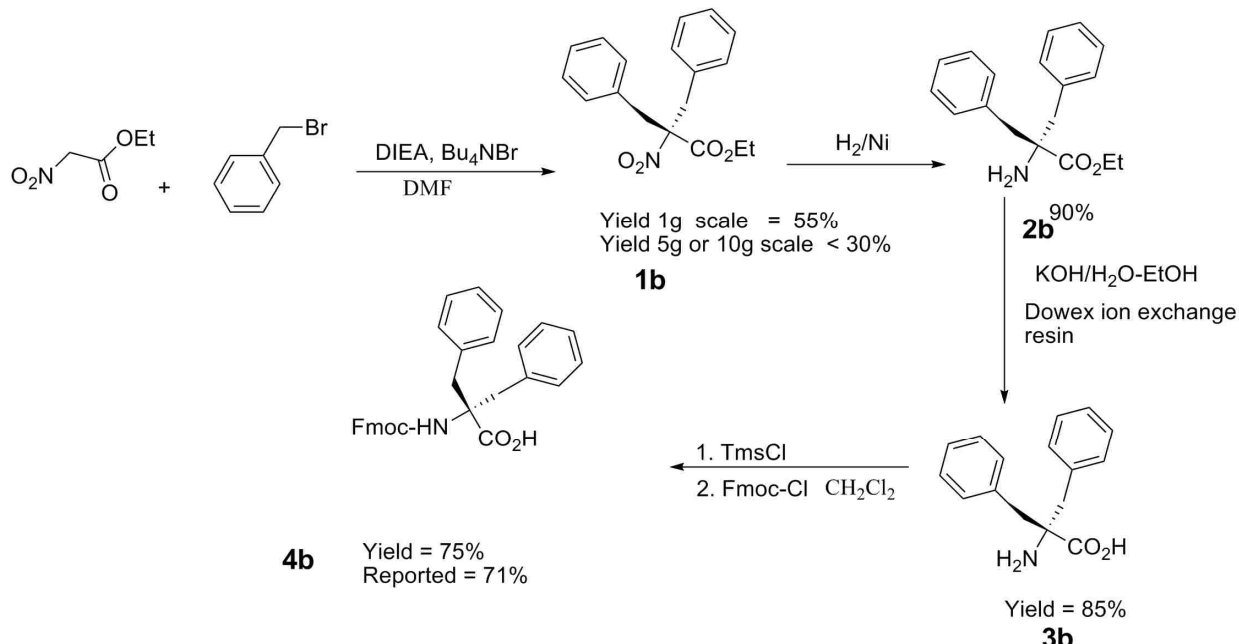
Scheme 2



Fu et al, devised a strategy that uses commercially available ethyl nitro acetate, tertiary base, and a catalyst to synthesize the dialkylated nitro esters such as ethyl 2, 2-dibenzylglycine ester **1b** (Scheme 2). The nitro ester was then reduced to the free amine **2b** using hydrogen gas in

presence of Raney nickel, followed by hydrolysis of the ester using KOH/EtOH to afford the free amino acid **3b**. The N-terminal of **3b** was protected with Fmoc protecting group to yield **4b**, which was suitable for SPPS.

Scheme 3



The overall yields were consistent with those reported by Fu (Scheme 3). The only modification to this method was the workup procedure for extracting **4b** from the reaction mixture. We found that some of the product was washed off during ether washings. To solve this, the crude product was directly dissolved in water, acidified to pH 2 (if necessary), and extracted with ethyl acetate to yield Fmoc protected dibenzyl glycine **4b** in an improved yield of 75 %. Most of the intermediate synthetic steps were high yielding except the initial dialkylation of ethyl nitroacetate. The low yields dropped further to 30% when the reaction was scaled up (30 %). The reaction conditions, change of base, and order of addition were optimized in an effort to improve the yields, and results are presented in Table 2.4. The overall strategy is to have a

synthetic route that is simple, reproducible, and has the ability to be scaled up in order to synthesize enough amino acid for peptide synthesis.

Table 2.4. Alkylation of ethyl nitroacetate.

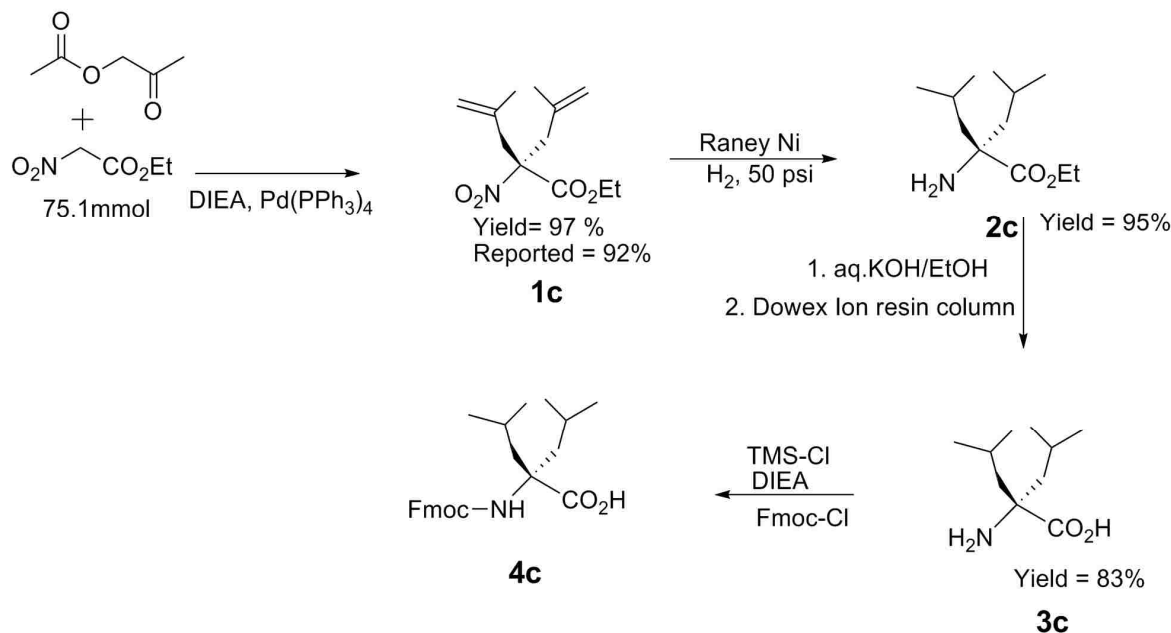
Ester	Bromide	Base	Scale of Ester (mmoles)	Order of addition	%Yield	Temp° C
O ₂ NCH ₂ CO ₂ Et	PhCH ₂ Br	DIEA	7.51	Base first	50	Room temp
O ₂ NCH ₂ CO ₂ E	PhCH ₂ Br	DIEA	7.51	Base first	55	0
O ₂ NCH ₂ CO ₂ E	PhCH ₂ Br	DIEA	7.51	Base last	44	Room temp
O ₂ NCH ₂ CO ₂ E	PhCH ₂ Br	DIEA	7.51	Base first Excess solvent	57	0
O ₂ NCH ₂ CO ₂ Et	PhCH ₂ Br	DIEA	37.5	Base first	30	Room temp
O ₂ NCH ₂ CO ₂ Et	PhCH ₂ Br	t-BuO-K+	7.51	Base first	52.2	Room temp

The yields were slightly improved when the reaction was carried out at 0° C as compared to room temperature (Table 2.4). Alkylation of ethyl nitroacetate is an exothermic reaction, and explains why higher yields are observed at 0° C as compared to room temperature. Changing the order of addition between the base and benzyl bromide showed no significant effect on the yield of dialkylated product. Further investigations of the extraction procedure, reveals that some of the product was detected in solvent waste during rotary evaporation, bringing into question the stability of **1b**. This is supported by the improved yields obtained when benzyl bromides having electron withdrawing groups were used. Microwave irradiation technology has been introduced to organic synthesis, and in particular has been successfully employed to hydrolyze sterically hindered hydantoins.⁴ Thus Dbg, which previously failed because of hydantoin hydrolysis problems, can now be synthesized via Bucherer-Bergs or Strecker syntheses, the most common method of synthesizing $\alpha\alpha$ AAs.

Synthesis of Dibg was accomplished via Palladium mediated dialylation of ethyl nitro acetate to obtain the dialkylated nitro ester **1c** in 97% yield (Scheme 4).⁹ The other synthetic steps were the same as for Dbg (scheme 3). This synthetic route is facile and efficient

as depicted by the high yields in all the reaction steps. The only modification to this procedure was the amount of palladium catalyst used, which was reduced to 1% without affecting the yield of **1c**. This also helps to reduce the amount of polystyrene bound triphenyl phosphine needed to scavenge the palladium catalyst. This leads to a more facile separation in addition to cost reduction.

Scheme 4



2.3.2 Peptides Synthesis

Incorporation of $\alpha\alpha$ AAs is a recognized way of inducing secondary structure in peptides.¹⁰ Peptides without $\alpha\alpha$ AAs were easily synthesized using HBTU or TBTU/HOBt coupling chemistry in good yields and purity at room temperature. Peptides incorporating $\alpha\alpha$ AAs were coupled using various coupling chemistries. All natural amino acids before any $\alpha\alpha$ AAs were coupled using HBTU or TBTU/HOBt, but those incorporated after $\alpha\alpha$ AAs were generally difficult to couple, hence coupled using PyAOP/HOAt activating agent. The less sterically hindered Dpg has been incorporated into peptides via conventional coupling methods in good

yields.¹¹ Coupling of Dpg were accomplished using PyAOP/HOAt chemistry at 50° C and were re-coupled. Incorporation of the more sterically hindered $\alpha\alpha$ AAs such as Dbg and Dibg into peptides was more problematic. Fu et al⁹ reported optimal coupling techniques necessary for the incorporation of sterically hindered Dbg and Dibg into peptide sequences. Coupling of Dbg was achieved using PyAOP/HOAt chemistry while Dibg was coupled via HATU/HOAt chemistry at elevated temperature and were re-coupled.

The real difficulty mainly stems from the inefficient acylation of the $\alpha\alpha$ AAs N-termini. Fu also reported that acylation of the N-terminus of these $\alpha\alpha$ AAs is possible via the symmetrical anhydride method in the absence of a base.¹² However, we continue to have a lower coupling yields for acylation of N-terminus of $\alpha\alpha$ AAs especially Dbg. Design of peptides incorporating $\alpha\alpha$ AAs, places valine after Dbg, which has an isopropyl side chain that we suspect is responsible for the lower yields. Lysine was easily coupled to Dibg via symmetrical anhydrides. Lysine has n-side chain as compared to sterically hindered valine.

The low coupling could be because of poor yields of valine (30 %) as compared to lysine (60%) symmetrical anhydrides. Coupling yields for each coupling step were determined by Fmoc analysis using a UV spectrometer at 300 nm. Also, bromophenol blue was used to monitor any unreacted sites. Blue color is a positive test for presence of free amine and yellow is negative test. All the reaction conditions, equivalents, solvents, ratios, and bases for coupling of each amino acid are listed in Table 2.5. The peptide was cleaved from the resin using trifluoroacetic acid, precipitated out using cold ether, dried, and analyzed using analytical HPLC and MALDI-MS or ESI. The various AAMPs were synthesized following a general synthetic route (Figure 2.1). Peptides without $\alpha\alpha$ AAs were generally synthesized in good yields and purity as analyzed by analytical HPLC.

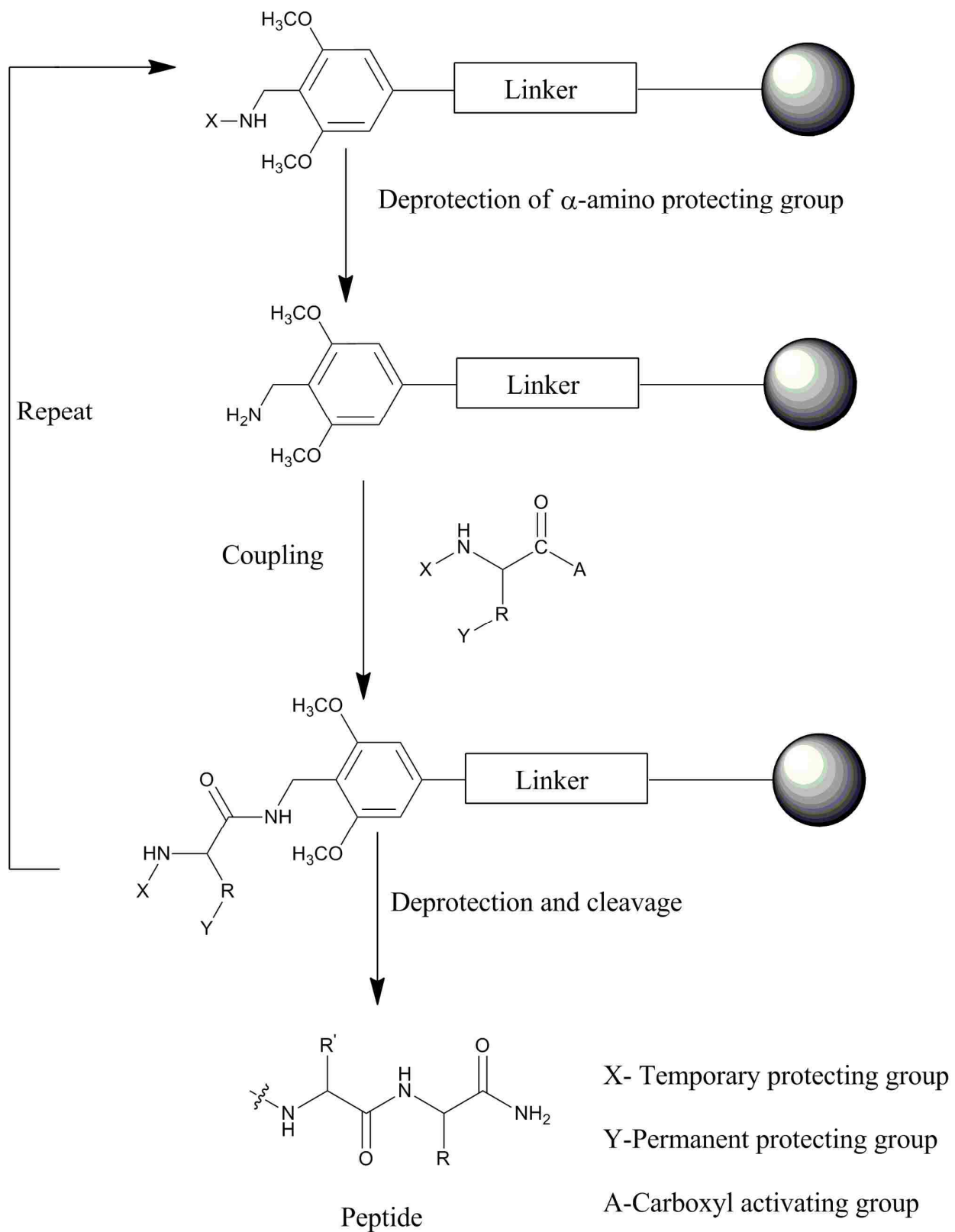


Figure 2.1. General synthetic route for the synthesis of AAMPs

Table 2.5. General reagents and conditions for coupling of various amino acids to a peptide sequence

Amino acid	Resin equiv.	Amino acid equiv.	Activator	Activator equiv.	base	Base equiv.	Solvent	Time (min)	Temp °C
Natural amino acids	1	4	HBTU/HOBt	4.0	DIEA	8.0	DMF	3	25
Dpg, Dbg	1	4	PyAOP/HOAt	4.0	DIEA	8.0	DMF	3	50
Dbg	1	4	PyAOP/HOAt	4.0	DIEA	8.0	DCE:DMF (2:1)	8	50
Dibg	1	4	HATU/ HOAt	4.0	DIEA	8.0	DCE:DMF (2:1)	8	50
acylation of $\alpha\alpha$ AAs	1	2	DCC, DIC, BOP-Cl	1.0	No base	-	DCE:DMF (9:1)	8	50

Peptide AAMP-19 is presented as an example to show clean synthesis for peptides without $\alpha\alpha$ AAs incorporated in their sequence. The chromatogram for AAMP-19 (Figure 2.2) shows a single peak with $R_t = 26.5$ min, and was confirmed by ESI-MS as the expected mass ion peak (837.1 mass units). Purification and mass spectrometry data for various AAMPs are presented in Table 2.6.

Synthesis of peptides incorporating $\alpha\alpha$ AAs amino acids were more challenging. For example, our first attempt to synthesize AAMP-2 failed as no peaks from analytical HPLC crude (Figure 2.3A) matched the calculated mass ion peak of 1652 mass units for AAMP-2. The major peak at $R_t = 32.67$ corresponded to the peptide (DbgPheDpgK6) with Val, Leu, and Lys deleted. This shows the difficulty of acylating the C-terminus of $\alpha\alpha$ AAs. One major reason for the failed synthesis was the low concentration of the coupling reagents (0.08M). The peptide was re-synthesized using 0.3M concentrations of coupling reagents. Analytical crude HPLC spectrum (Figure 2.3B) for the re-synthesized peptide showed a peak at $R_t = 36.5$ which corresponded with the expected molecular ion peak of 1652 mass units.

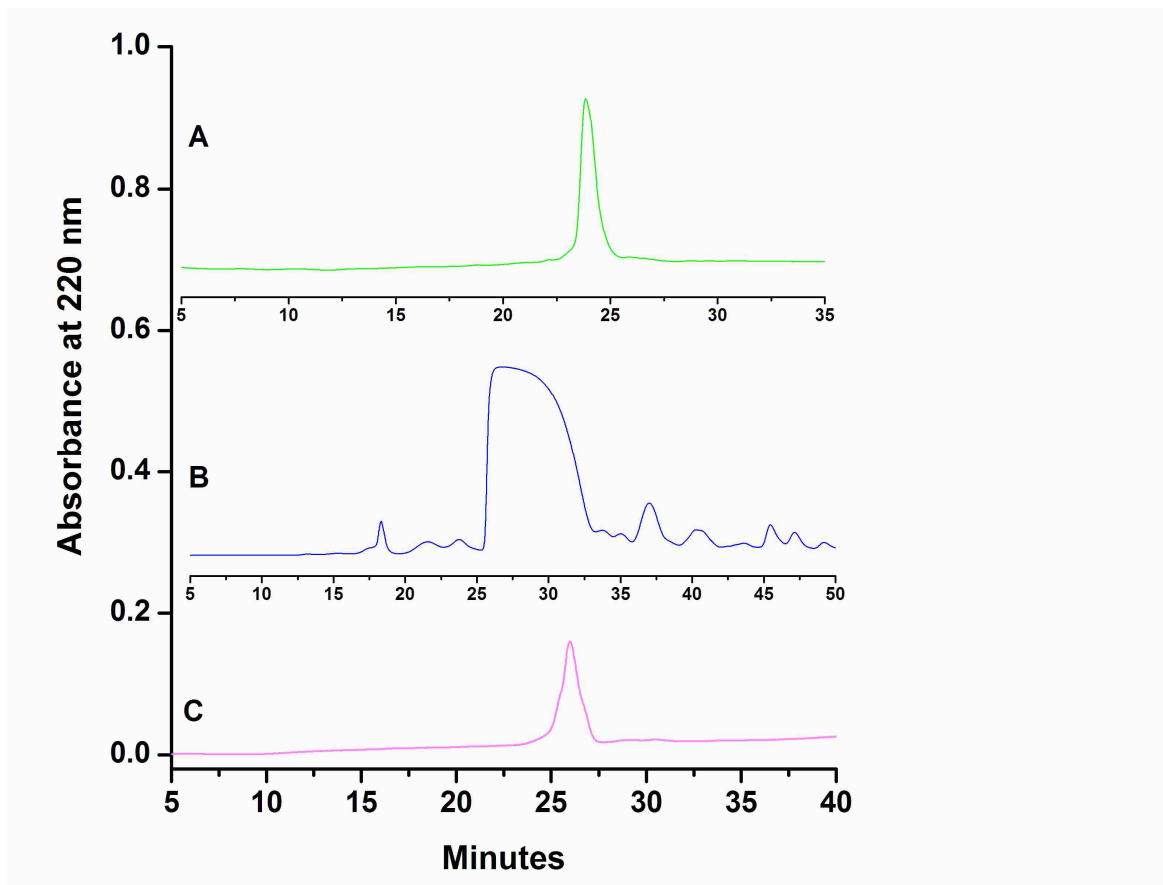


Figure 2.2. HPLC chromatograms of AAMP-19 [A] Analytical HPLC for pure peptide; [B] Analytical HPLC for peptide synthesized using microwave irradiation; [C] Analytical HPLC for peptide synthesized using conventional heating method. HPLC conditions for A: 20-40% B in 30 min, 10-70 % B in 80 min for B and 10-70% B in 60 min.

However, the major peak at $R_t = 43.5$ matched the molecular ion peak for deletion peptide detected earlier. Further improvements in coupling conditions such as change of coupling solvents, coupling reagents, were unsuccessful. The real problem with the coupling arises from poor acylation of the sterically hindered $\alpha\alpha$ AAs, and especially with valine. Coupling yields showed were slightly increased when valine was replaced with less sterically hindered alanine as measured by UV Fmoc analysis. To improve the yields microwave irradiation shown recently to exponentially increase rate of reactions resulting in higher yields in a short time was employed for difficult couplings.

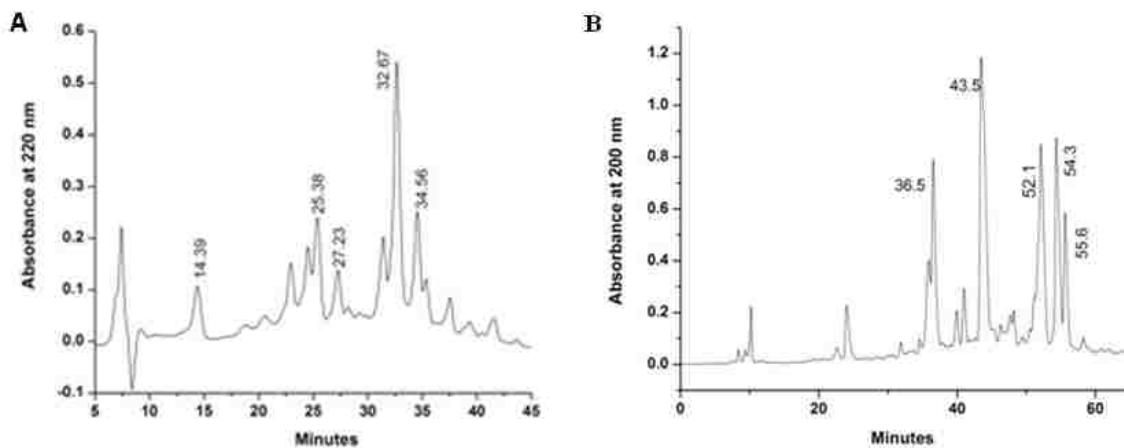


Figure 2.3. HPLC chromatograms of AAMP-2, [A] Analytical HPLC 1st trial. [B] Analytical spectrum 2nd trial after coupling steps was optimized. HPLC conditions for 1st trial: 10-70% B in 60 min and 10-50 % B in 60 min for 2nd trial.

Microwave technology has been used in organic chemistry since early 1980 for various chemical reactions that require heating.¹³⁻¹⁷ The first application of microwave technology to peptide synthesis was reported in 1992.¹⁸ Microwave irradiation takes advantage of certain solvents to convert electromagnetic radiation into heat. Growing peptide chains during conventional synthesis have a propensity to aggregate. However, during microwave irradiation, the peptide chains are in constant random motion breaking up any aggregation. Microwave heating is increasingly used in peptide synthesis because coupling yields are significantly increased in a shorter time. Microwave heating was applied to coupling of sterically hindered amino acids and its acylation on the N-terminus. We found increased yields for Dbg coupling and Val using microwave irradiation, and various coupling methods were investigated to optimize efficient synthesis of AAMPs. Microwave irradiation technology was used to synthesize AAMPs with $\alpha\alpha$ AAs incorporated into their sequences. Synthesis of AAMP-8 (KLVDbgFAK₆) with Dbg involved coupling the first 8 natural amino acids at room temperature.

Table 2.6. MALDI-MS results of inhibitor peptides analogs.

Entry	AAMPs	Sequence	Exact mass	Observed (M+H) ⁺	t _R (min)	% Peptide content
1	AAMP-0	KLVFFK ₆	1419.98	1420.99	20.1	67
2	AAMP-1	KDibgVDbgFDpgK ₆	1707.21	1708.21	24.6	51
3	AAMP-2	KLVDbgFDpgK ₆	1651.14	1652.15	23.8	39
4	AAMP-3	KDibgVFFDpgK ₆	1617.16	1618.16	23.9	50
5	AAMP-4	KDibgVDbgFAK ₆	1637.13	1638.17	25.6	52
6	AAMP-5	KDibgVFFAK ₆	1547.08	1548.09	22.9	72
7	AAMP-6	KLVAFDpgK ₆	1561.10	1562.10	21.9	51
8	AAMP-7	KLVDbgFAK ₆	1581.06	1582.06	25.4	49
9	AAMP-8	KLDpgFFAK ₆	1533.06	1535.07	23.1	49
10	AAMP-9	KLVFDpgK ₆	1414.03	1415.05	19.5	50
11	AAMP-10	DibgVFFAK ₆	1418.99	1419.99	21.2	49
12	AAMP-11	RGKLVFFGR	1077.66	1078.67	27.1	64
13	AAMP-12	KGKLVFFGK	1021.63	1022.65	24.0	100
14	AAMP-13	EGKLVFFGE	1023.54	1024.54	24.5	61
15	AAMP-14	mPEGGKLVFFGmPEG	1055.56	1056.61	24.1	55
16	AAMP-15	RRRGKLVFFGRRR	1702.06	1703.07	20.6	80
17	AAMP-16	KLVFFGR	864.53	865.54	28.1	62
18	AAMP-17	KLVFFGmPEG	853.51	854.52	30.4	83
19	AAMP-18	KLVFFGK	836.53	837.54	23.9	71
20	AAMP-19	RGKLVFF	864.53	865.54	24.6	48
21	AAMP-20	KLVFFDpgGK	977.64	978.65	26.2	60
22	AAMP-21	KGKDibgVFFGK	1077.71	1079.1	24.	58
23	AAMP-22	KDibgVFFDpgGKKK	1289.88	1290.90	27.2	53
24	AAMP-23	KKKGKLVFFDpgGKKK	1676.12	1677.14	21.0	57
25	AAMP-24	KDibgVFFAGGKKK	1120.80	1121.76	27.6	62
26	AAMP-25	KLVFFF DpgGKKK	1233.82	1234.84	23.0	65
27	Aβ16-22m	KL(Me)VF(Me)FA(Me)E	895.84	896.85	22.88	66

The other amino acids were coupled using microwave heating. Conventional synthesis of the AAMP-8 was carried out to compare the two methods. Analysis of their analytical spectrums (Figure 2.4) shows an increase in the peptide peak when microwave heating (Figure 2.4B) was used ($R_t = 34.5$) as compared to the conventional heating (Figure 2.4C) method ($R_t = 36.5$).

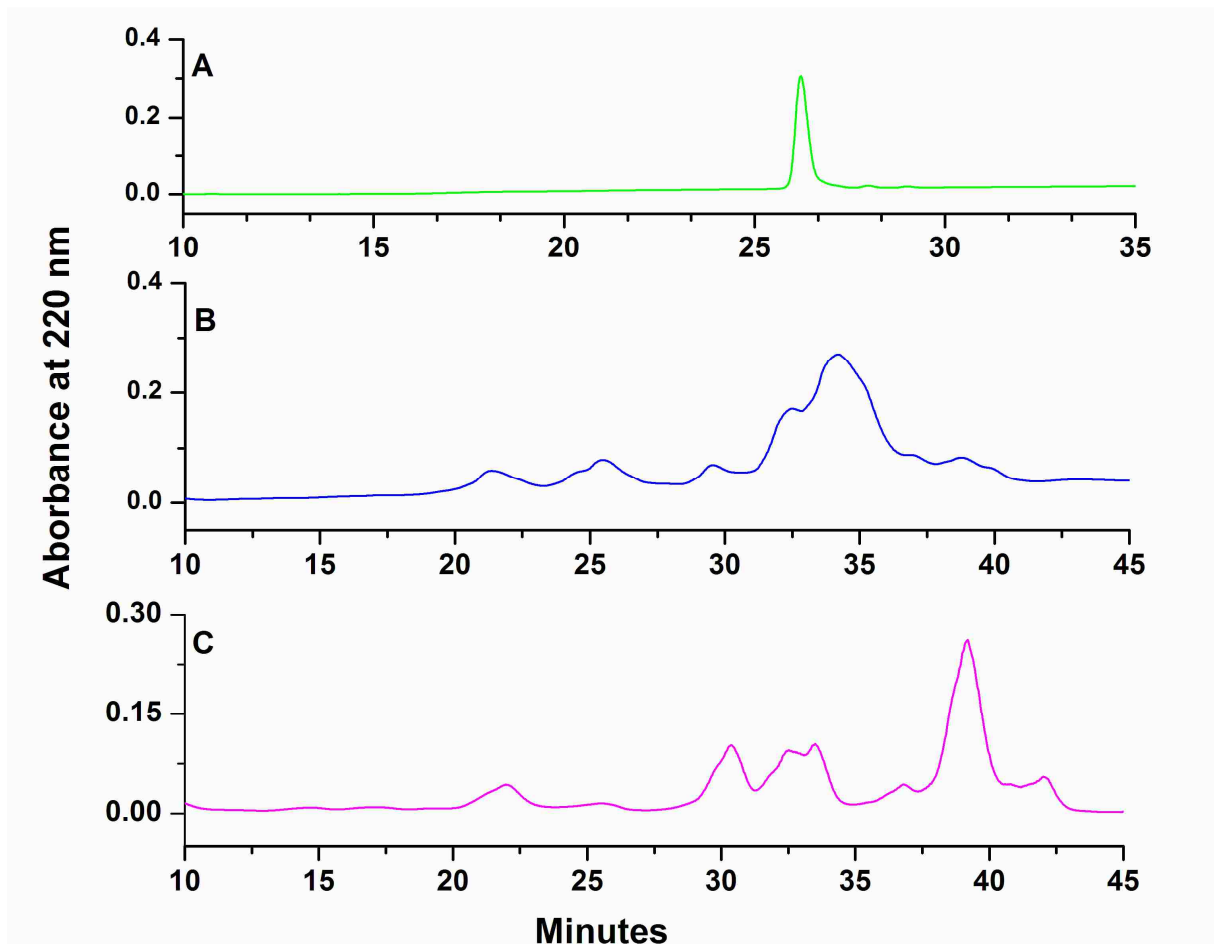


Figure 2.4 HPLC chromatograms of AAMP-7. [A] Analytical HPLC for pure peptide; [B] Analytical HPLC for peptide synthesized using microwave irradiation; [C] Analytical HPLC for peptide synthesized using conventional heating method. HPLC conditions for A: 20-40% B in 30 min, 10-70 % B in 60 min for B and C.

Coupling of the carboxyl group of $\alpha\alpha$ AAs Dbg to a growing peptide chain and acylation of the N-terminal $\alpha\alpha$ AAs was previously shown to be difficult in both solution and solid phase peptide synthesis.⁵ Various coupling methods were investigated for coupling of Dbg and Val

during synthesis of AAMP-7 by determining the yields using UV analysis at 300 nm of Fmoc-deprotection. The first eight amino acids were coupled via automated peptide synthesis and coupling of Dbg and Val, which follows, was then studied using the various coupling methods (Table 2.7).

Table 2.7 Coupling of Dbg and then Val onto Phe-Phe-Ala-(Lys)₆ (AAMP-7)

	Entry	Coupling agent	Base	Solvent	Time	temp	yield	Equiv.	Conc. (M)
Dbg	1	PyAOP/HOAt	DIEA	DMF	20 min	95	90	5	0.3
	2	PyAOP/HOAt	DIEA	DMF	10 min	95	80	5	0.3
	3	PyAOP/HOAt	collidine	DMF	10 min	95	35	5	0.3
	4	PyAOP/HOAt	DIEA	DMF:DCE (3:1)	5 min	110	92	5	0.3
	5	HATU/HOAt	DIEA	DMF:DCE (3:1)	5 min	110	72	5	0.3
	6	PyAOP/HOAt	DIEA	DMF	12 h	50	50	5	0.3
	7	PyAOP/HOAt	DIEA	DMF	12 h	50	30	4	0.3
	8	PyAOP/HOAt	DIEA	DMF	12 h	50	50	8	0.3
	9	PyAOP/HOAt	DIEA	DMF	12 h	50	55	5	0.4
Val	10	DCC		DMF:DCE	1 h	95	61	5	
	11	DCC		DMF:DCE	20 min	95	45	5	
	12	BOP-Cl	DIEA	DMF:DCE	20 min	95	35	5	
	13	DIC		DMF:DCE	20 min	95	45	5	
	14	DCC		DMF:DCE	12 h	50	35	20	
	15	DiC		DMF:DCE	12 h	50	40	20	
	16	BOP-Cl		DMF:DCE	12 h	50	30	20	

Higher yields for Dbg and Val coupling were obtained in a short time when microwave irradiation was used as compared to conventional heating. Coupling of Fmoc-Dbg-OH onto the N-terminus of the Phe on the resin using PyAOP/HOAt was more effective than HATU/HOAt (entry 4 and 5). The strength of the base used affected the coupling yields of Dbg where higher yields were realized when DIEA (entry 2) was used as compared to collidine (entry 3). There was no significant change in yields with longer coupling time (entry 1 and 2), temperature (entry 1 and 4), and solvent mixture (entry 1 and 4). Higher Dbg coupling yields at room temperature were observed with increased concentration of coupling agents/amino acid (entry 8 vs 9) or

equivalents of amino acid (entry 7 vs 8). Acylation of Dbg N-terminus was previously coupled with higher yields using Fmoc-Val symmetric anhydride as compared to PyAOP or HATU coupling methods. Higher yields were observed for Val coupled earlier (second) in the peptide sequence as compared to the lower yields we report for Val coupled later in the synthesis (tenth). Yields for Val were increased when microwave irradiation (entry 10-13) was used as compared to conventional heating (entry 14-16). Fmoc-Val-OH symmetrical anhydrides obtained from DCC (entry 10, 11) or DIC (13) used to acylate Dbg N-terminus gave higher yields as compared to BOP-Cl (entry 12). Similarly, higher yields for coupling Val using Fmoc-Val symmetrical anhydrides were observed when microwave irradiation was used as compared to conventional heating.

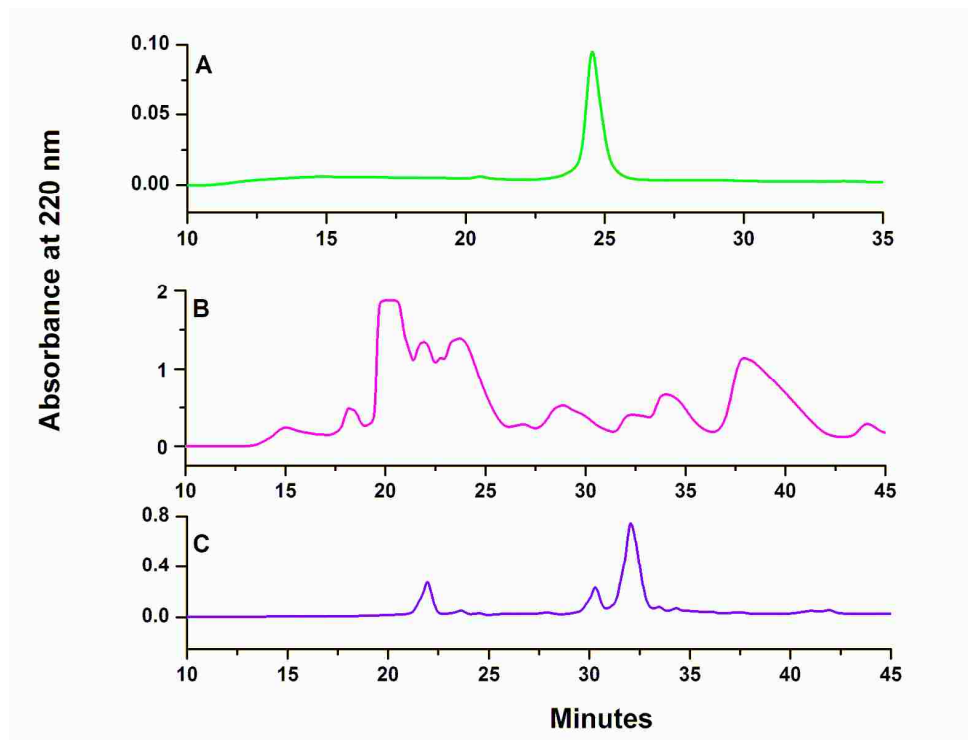


Figure 2.5. HPLC chromatograms of AAMP-21. [A] Analytical HPLC for pure peptide; [B] Analytical HPLC for peptide synthesized using microwave irradiation; [C] Analytical HPLC for peptide synthesized using conventional heating method. HPLC conditions for A: 20-40% B in 30 min, 10-50 % B in 60 min for B and10-70 % B in 60 min for C.

Another example to show the success of microwave technology was synthesis of AAMP-21 (KDibgVFFGK) containing Dibg. The HPLC spectrum from peptides synthesized by conventional synthesis showed two closely related peaks (Figure 2.5C). The peak with Rt = 30.5 matched the expected mass ion peak. The other taller peak Rt = 33.8 corresponded to deletion of Lys, consistent with the problem in acylating the N-terminus of $\alpha\alpha$ AAs. However, using microwave irradiation method, the deletion peptide observed in conventional heating disappeared (Figure 2.5B) and a peak (37.8 min) that corresponded to the expected molecular ion increased.

2.3.3 Conformational Studies of Mitigators

Circular dichroism studies of sample of peptides were carried out to determine their aggregation behavior. The effect of the various AAMPs on A β assembly into β -sheet structures will be discussed later in chapters 3 and 4. The CD spectra for all AAMPs showed a characteristic random coil structure as shown by a large negative band near 200 nm and small positive band near 220 nm. There was no transition from random coil to β -sheet observed for all the AAMPs synthesized with varying concentrations. This suggests that the propensity for the AAMPs to aggregate is minimal, and that they do not misfold or unfold at higher concentrations through a multistep folding process. There was no significant difference observed in the CD signal of mitigators containing $\alpha\alpha$ AAs (Figures 2.6, 2.7 and 2.11) as compared to those without (Figures 2.8-2.10). Also, mitigators with different terminal modifications (*C*-, *N*- and *C*-, and *N*-) displayed similar CD signals (Figures 2.8-2.10).

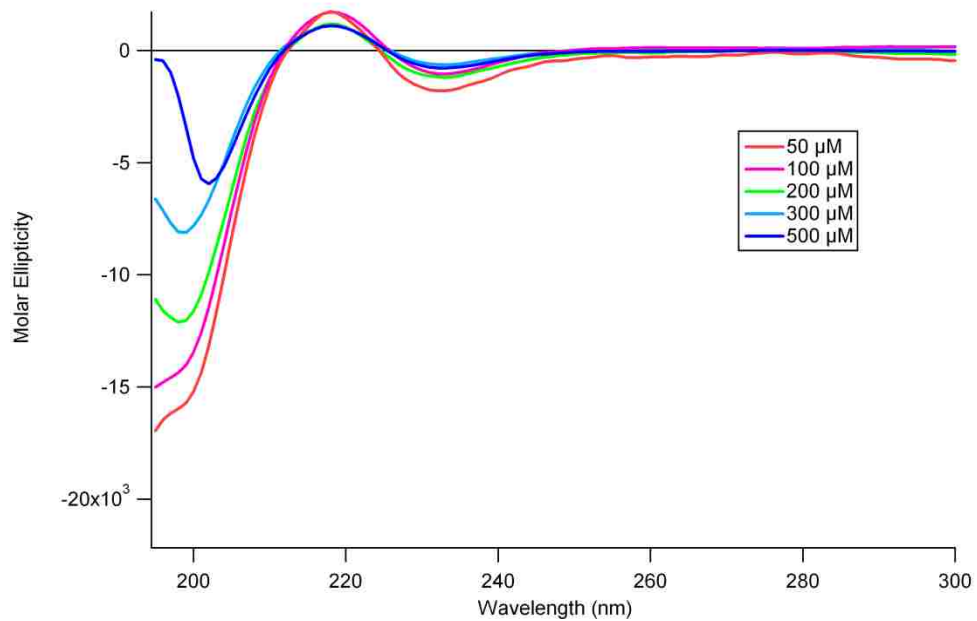


Figure 2.6 Concentration studies of AAMP-5. CD spectra taken in 50 mM PBS (150mm NaCl); pH 7.4. Molar ellipticity- [θ] units- degcm²dmol⁻¹.

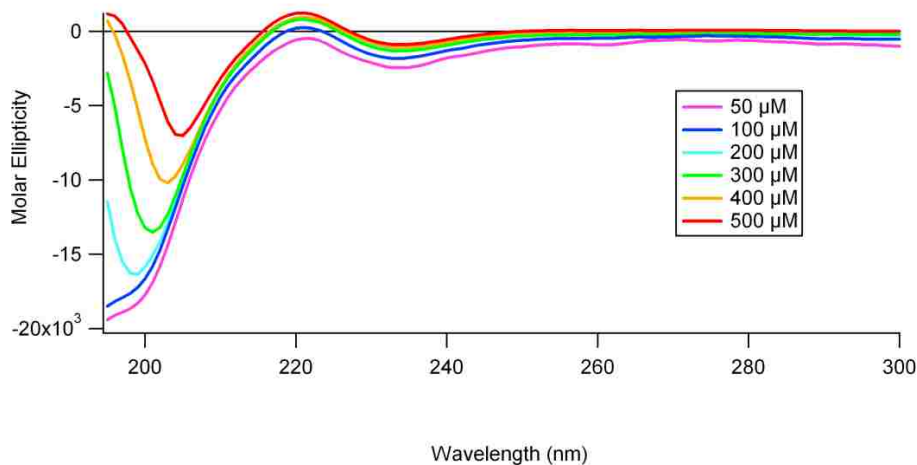


Figure 2.7 Concentration studies of AAMP-6. CD spectra taken in 50 mM PBS (150mm NaCl); pH 7.4. Molar ellipticity- [θ] units- degcm²dmol⁻¹.

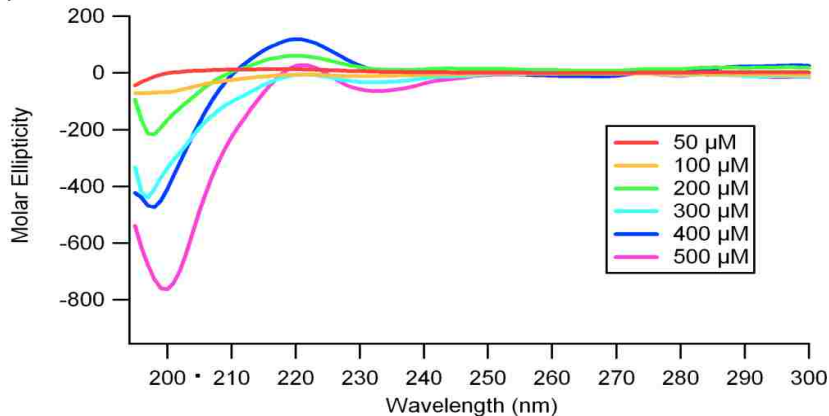


Figure 2.8 Concentration studies of AAMP-11. CD spectra taken in 50 mM PBS (150mm NaCl); pH 7.4. Molar ellipticity- $[\theta]$ units- $\text{degcm}^2\text{dmol}^{-1}$.

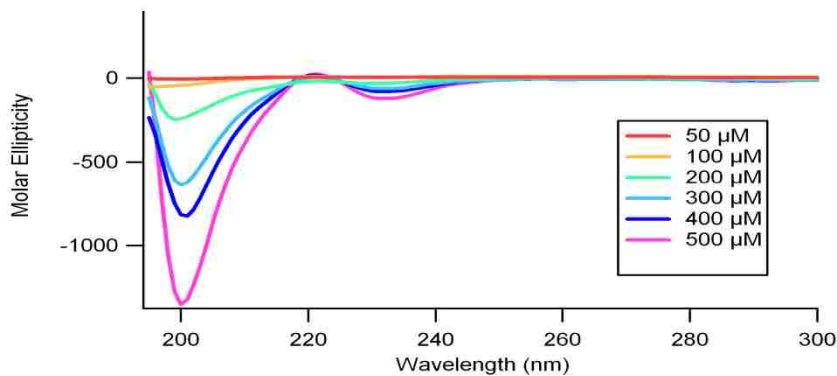


Figure 2.9 Concentration studies of AAMP-16. CD spectra taken in 50 mM PBS (150mm NaCl); pH 7.4. Molar ellipticity- $[\theta]$ units- $\text{degcm}^2\text{dmol}^{-1}$.

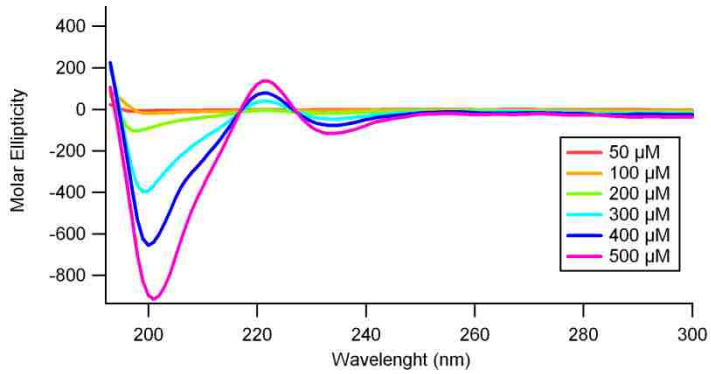


Figure 2.10 Concentration studies of AAMP-19. CD spectra taken in 50 mM PBS (150mm NaCl); pH 7.4. Molar ellipticity- $[\theta]$ units- $\text{degcm}^2\text{dmol}^{-1}$.

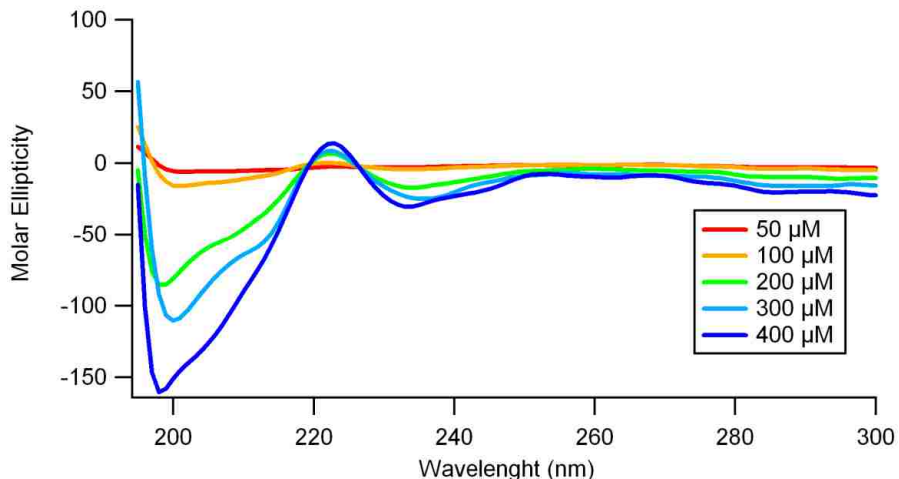


Figure 2.11 Concentration studies of AAMP-20. CD spectra taken in 50 mM PBS (150 mM NaCl); pH 7.4. Molar ellipticity- [θ] units- degcm²dmol⁻¹.

2.4 Conclusion

The various synthetic methods for $\alpha\alpha$ AAs were improved by modifying specific steps. We found that ethyl 2-benzyl-2-nitro-3-phenylpropanoate (**1b**) was unstable to rotary evaporation, and the compound was detected in the waste. The focus of future work should be on the possibility of using microwave irradiation to hydrolyze the sterically hindered hydantoin. Solid phase peptide synthesis of AAMPs without $\alpha\alpha$ AAs was achieved with high purity. Microwave technology was successfully used to synthesize AAMPs with $\alpha\alpha$ AAs in higher yields than conventional methods. The CD spectral analysis shows that all AAMPs displayed a characteristic random coil structure that was stable to concentration changes. This is important for use as mitigators of the A β assembly process.

2.5 References

1. Tjernberg, L. O.; Lilliehook, C.; Callaway, D. J.; Naslund, J.; Hahne, S.; Thyberg, J.; Terenius, L.; Nordstedt, C., Controlling amyloid beta-peptide fibril formation with protease-stable ligands. *J. Biol. Chem.* **1997**, 272 (19), 12601-5.
2. Bolin, D. R.; Sytwu, I. I.; Humiec, F.; Meienhofer, J., Preparation of oligomer-free Na-Fmoc and Na-urethane amino acids. *Int. J. Pept. Protein Res.* **1989**, 33 (5), 353-9.

3. Fu, Y.; Hammarstroem, L. G. J.; Miller, T. J.; Fronczek, F. R.; McLaughlin, M. L.; Hammer, R. P., Sterically Hindered C α , α -Disubstituted α -Amino Acids: Synthesis from α -Nitroacetate and Incorporation into Peptides. *J. Org. Chem.* **2001**, *66* (21), 7118-7124.
4. Ware, E., The Chemistry of the Hydantoins. *Chem. Rev.* **1950**, *46* (3), 403-470.
5. Fu, Y. W.; Etienne, M. A.; Hammer, R. P., Facile synthesis of alpha,alpha-diisobutylglycine and anchoring its derivatives onto PAL-PEG-PS resin. *J. Org. Chem.* **2003**, *68* (25), 9854-9857.
6. Dyker, G., Amino Acid Derivatives by Multicomponent Reactions. *Angew. Chem. Int. Ed.* **1997**, *36*, 1700-1702.
7. Shipchandler, M. T.; , The Utility of Nitroacetic Acid and its Esters in Organic Synthesis *synthesis* **1979**, 666-686.
8. Shipchandler, M. T., The utility of nitroacetic acid and its esters in organic synthesis. *Synthesis* **1979**, (9), 666-86.
9. Fu, Y.; Etienne, M. A.; Hammer, R. P., Facile Synthesis of a,a-Diisobutylglycine and Anchoring its Derivatives onto PAL-PEG-PS Resin. *J. Org. Chem.* **2003**, *68* (25), 9854-9857.
10. Vijayalakshmi, S.; Rao, R. B.; Karle, I. L.; Balaram, P., Comparison of helix-stabilizing effects of a,a-dialkyl glycines with linear and cycloalkyl side chains. *Biopolymers* **2000**, *53* (1), 84-98.
11. Humphrey, J. M.; Chamberlin, A. R., Chemical Synthesis of Natural Product Peptides: Coupling Methods for the Incorporation of Noncoded Amino Acids into Peptides. *Chem. Rev.* **1997**, *97* (6), 2243-2266.
12. Fu, Y.; Hammer, R. P., Efficient acylation of the N-terminus of highly hindered C α , α -disubstituted amino acids via amino acid symmetrical anhydrides. *Org. Lett.* **2002**, *4* (2), 237-240.
13. Colacino, E.; Lamaty, F.; Martinez, J.; Parrot, I., Microwave-assisted solid-phase synthesis of hydantoin derivatives. *Tetrahedron Lett.* **2007**, *48* (30), 5317-5320.
14. Petricci, E.; Mugnaini, C.; Radi, M.; Corelli, F.; Botta, M., Microwave-assisted acylation of amines, alcohols, and phenols by the use of solid-supported reagents (SSRs). *J. Org. Chem.* **2004**, *69* (23), 7880-7887.
15. Graebin, C. S.; Eifler-Lima, V. L., The use of microwave ovens in solid-phase organic synthesis. *Quim. Nova* **2005**, *28* (1), 73-76.
16. Strohmeier, G. A.; Kappe, C. O., Rapid parallel synthesis of polymer-bound enones utilizing microwave-assisted solid-phase chemistry. *J. Comb. Chem.* **2002**, *4* (2), 154-161.

17. Grieco, P., The use of microwave irradiation in peptide chemistry. *Chimica Oggi-Chemistry Today* **2004**, 22 (7-8), 18-20.
18. Yu, H. M.; Chen, S. T.; Wang, K. T., Enhance Coupling Efficiency in Solid-Phase Peptide-Synthesis by Microwave irradiation. *J. Org. Chem.* **1992**, 57 (18), 4781-4784.

CHAPTER 3

STRUCTURE-ACTIVITY RELATIONSHIPS IN PEPTIDE MODULATORS OF AMYLOID β -PROTEIN AGGREGATION

3.1 Introduction

Alzheimer's disease is a progressive, neurodegenerative disorder characterized by extracellular plaque deposits and neurofibrillary tangles. The plaque deposits are composed primarily of the 39-42 amino acids, natively unfolded amyloid β -peptide (A β) that is derived from proteolytic cleavage of the extracellular segment of the transmembrane amyloid precursor protein (APP).¹⁻³ The normal physiological concentration of A β in the brain is less than 10 nM. However, the critical concentration for A β to aggregate in vitro into amylogenic forms is 1-10 μ M.^{4,5} Several hypotheses as to how A β aggregates in the brain below the critical concentration include concentration of A β to several orders of magnitude by membranes or organelles, lowering of critical concentration by acidic pH or metal ions, and covalent adducts between A β and oxidative metabolites allowing A β to aggregate at the nanomolar concentrations.⁵⁻⁷

Conversion of monomeric A β peptide into the aggregated products (oligomers, protofibrils and fibrils) in the brain is believed to be the vital event in AD pathology.^{8,9} Fibrils were previously thought to be the species responsible for neuronal toxicity and cell death (amyloid cascade). However, growing evidence suggests that much smaller soluble oligomeric species present in the brain correlates better with severity of AD than plaques (fibrils).^{2, 10-16} Therefore assembly of A β into either oligomeric or fibrillar assemblies remains a rational target to reduce A β neurotoxicity. In addition, fibril dissolution agents could be possible targets for reducing plaque loads in the brain.

Several approaches aimed at reducing A β and its related aggregates in the brain are under development. This include inhibition of proteases involved in the cleavage of A β from the

amyloid precursor protein (APP),¹⁷ antibody therapy through passive immunizations using anti-A β antibodies,¹⁸⁻²⁰ non-antibody based natural mechanism,²¹⁻²³ small molecules²⁴, and peptides.²⁴ Interest in peptide-based aggregation mitigators has intensified because peptides are generally more potent, show higher specificity, and fewer toxicology problems than smaller organic molecules. A number of peptide-based AAMPs that alter A β aggregation kinetics or aggregate morphologies have been developed. All of these peptide based mitigators exploit the self-interacting A β central hydrophobic core (A β_{16-20}) as a recognition element since the assembly of A β oligomers is controlled by initial interaction of hydrophobic side-chains.

Several modifications on the hydrophobic core (A β_{16-20}) aimed at designing AAMPs that enhance the disruption of fibril formation and/or induce fibril disassembly have been reported.^{9, 25-30} Murphy and Kessling added an oligolysine tail to the A β_{16-20} hydrophobic core that enhanced A β aggregation rates resulting in nontoxic fibrillar species.²⁸⁻³⁰ More recently, RG-/-RG polar groups added to N- and C-terminal proved to be effective inhibitors of fibril formation and protected SH-SY5Y from A β toxicity. Amide backbone modifications of A β_{16-20} core with N-methyl amino acids,^{31, 32} ester linkages,^{31, 33} and isostructural E-olefin bond^{34, 35} disrupted fibril formation and induced disassembly of preformed fibrils. Also, Soto and coworkers designed the peptide LPFFD containing a single proline residue in the A β_{16-20} core which disrupt fibril formation, disassemble preformed fibrils, and increased cell viability.³⁶ Although these AAMPs altered the A β fibrillization pathway by inducing different A β aggregate morphologies, the processes often required unusually high inhibitor/A β molar ratios.

Our design of AAMPs is also based on the A β_{16-20} hydrophobic core where some natural amino acids were replaced by the modified analogues ($\alpha\alpha$ AAs). The α -carbon of the natural amino acid was modified by introducing a second similar side chain to form $\alpha\alpha$ AAs. When

$\alpha\alpha$ AAs are incorporated in short peptides, they are known to induce stable extended conformations which are ideal for interacting with A β through hydrogen bonding as well as by side-chain interactions. $\alpha\alpha$ AAs are placed at alternating positions (i, i+2, i+4) which positions them on the same hydrogen bonding face of the extended peptide, sterically blocking it from further hydrogen bonding hence disrupting fibril propagation. Also, $\alpha\alpha$ AAs with larger side chains impose restrictions of peptides that contain them. Thus, peptides incorporating $\alpha\alpha$ AAs could be better disrupters of β -sheets than proline-containing mitigators.³⁶ Peptide mitigators containing $\alpha\alpha$ AAs with methyl side chains have long been known to disrupt β -sheets.³⁷ Thus, we hypothesize that mitigators incorporating $\alpha\alpha$ AAs with side chains larger than methyl groups should be effective disrupters of β -sheets (disassemble preformed fibrils).

We previously communicated that peptides containing $\alpha\alpha$ AAs altered A β assembly pathway at stoichiometric and sub-stoichiometric concentrations resulting in non-fibrillar, non-toxic assemblies.³⁸ The two mitigators (AMY-1 and AMY-2 with hydrophilic Lys tail on C-and N-terminal respectively) mitigated A β_{1-40} fibril formation producing particles with different sizes. Herein, we show that the number and position of $\alpha\alpha$ AAs in the recognition element (A β central hydrophobic core) of the original mitigator AAMP-1³⁸ is important in determining the effectiveness of the interaction of the AAMPs with A β . Also, we further examine the role of each $\alpha\alpha$ AAs in AAMP-1 through the synthesis of AAMP-1 analogs where $\alpha\alpha$ AAs were replaced by their natural amino acid analog (Leu for Dibg, etc). This A β_{1-40} -AAMP interaction nucleates the size and morphology differences of the nanoparticles formed as determined by AFM and TEM. We also show that AAMPs alone do slowly aggregate forming exclusively spherical particles. This might provide insight into the mechanism by which they disrupt A β_{1-40}

fibril formation. A major finding was that mitigators, which disrupted fibril formation, also disassembled preformed fibrils.

3.2 Materials and Methods

3.2.1 Peptide Synthesis

Samples of AAMPs were prepared from *9H*-fluoren-9-ylmethoxycarbonyl (Fmoc) amino acids using solid phase peptide synthesis (SPSS) on PAL-PEG-PS resin or Rink amide ChemMatrix resin. Couplings, Fmoc removal, and resin cleavage were carried out using previously described methods.³⁹⁻⁴¹ The crude peptides were purified by reversed phase HPLC using a 10% to 70% B linear gradient over 60 min [Waters C₄ 100 Å column using Solvent A (water and 0.1% TFA) and solvent B (acetonitrile and 0.1% TFA)]. The purity of the peptides were checked by analytical HPLC, and the masses confirmed by ESI-MS. The percent peptide content was established by amino acid analysis. This was discussed in Chapter 2.

3.2.2 Peptide Monomerization

Lyophilized Aβ₁₋₄₀ (Invitrogen Corporation, Carlsbad, CA, USA.) was pretreated to form monomeric solutions following our previously published protocol.⁴² Briefly, Aβ₁₋₄₀ was dissolved in neat trifluoroacetic acid (TFA) at 1 mg/mL and sonicated for 10-20 min. Removal of TFA using a centrivac yielded a dark yellow oil, which was re-dissolved in 1 mL of hexafluoroisopropanol (HFIP) at 1 mg/mL and incubated at 37 °C for 1 h. Removal of HFIP yielded a white powder, which was re-dissolved in HFIP and split into 0.25 mg fractions based on the assumption that the mass of Aβ₁₋₄₀ was 50 % at this point in the preparation. The fractions were incubated for 1 h upon which HFIP was removed, and the resulting white powder was lyophilized overnight. The lyophilized white powder was dissolved in 2 mM NaOH and PBS (100 mM, 300 mM NaCl, pH 7.4) at 1:1 and centrifuged for 20 min at 13,000 g, which was

then ready for the aggregation assay. The supernatant was subjected to amino acid analysis to determine the net peptide content.

3.2.3 Thioflavin T Aggregation Assays

Monomerized A β ₁₋₄₀ was aged alone and in the presence of AAMPs at 37 °C while shaking in PBS buffer (50 mM, 150 mM NaCl pH 7.4). At various time points, 10 μ L of sample, 10 μ L of 100 μ M ThT stock solution in water, and 180 μ L of PBS were mixed in a low binding 96 well plate with clear bottom (Corning or Falcon). A ThT fluorescence emission spectrum was acquired at 480 nm (excitation at 440 nm) using a fluorescence plate reader (BMG, LABTECH).

3.2.4 Circular Dichroism

Monomeric samples of A β ₁₋₄₀ were aged alone and with equimolar AAMP at 37 °C for several days while shaking. The CD spectrum was recorded at room temperature on an Aviv CD spectrometer.

3.2.5 Atomic Force Microscopy

A sample aliquot of 10 μ L was diluted two-fold and adsorbed onto the surface of freshly cleaved mica (0001) for 5-10 min (Ruby muscovite mica, S&J Trading Co., NY). The remaining excess liquid was absorbed onto a filter paper or lab tissue. Salts and excess unbound peptide were removed by rinsing the surface three times with 40 μ L of deionized water. An Agilent 5500 atomic force microscope (AFM) equipped with Pico Scan v5.3.3 software was used for surface characterizations (Agilent Technologies AFM, Inc. Chandler, AZ). Cantilevers (NSL-20) from Nanoworld Holdings AG (Schaffhausen, Switzerland) were used for imaging samples by tapping mode in air. The cantilever was driven to oscillate at 185± 10 kHz for ambient AFM characterizations.

3.2.6 Transmission Electron Microscopy

Samples for TEM analysis were prepared by placing sample droplet onto a carbon support Cu coated grid (EMS 400-CU) for 1-2 min. Excess sample was absorbed into a filter paper, placed onto a droplet of water, and then stained using 2% uranyl acetate droplet. The grid was cleared of excess uranyl acetate, labeled, and then stored in a Petri dish. Images were recorded using a JEOL 100 CX TEM, 80 kV accelerating voltage.

3.3 Results and Discussion

3.3.1 Design of Amyloid Aggregation Mitigating Peptide

The central hydrophobic region of A β (16-20) is responsible for self-association and aggregation leading to the formation of mature fibrils.²⁵ When incorporated into a peptide, $\alpha\alpha$ AAs are known to induce extended peptide conformations, which are ideal for interaction with A β .^{43, 44} We hypothesize that peptides containing alternating natural amino acids and $\alpha\alpha$ AAs in a β -strand (extended) conformation would have one hydrogen bonding “face” blocked due to the steric hindrance associated with $\alpha\alpha$ AAs, and the other face would remain accessible for additional β -strand hydrogen bonds. This design strategy (Figure 1) does not prevent A β oligomerization but disrupts additional peptides from adding to one face of the growing β -sheet, thus changing the A β fibrilization pathway. Previously, we have shown that no fibrils were observed from AAMP-1/A β ₁₋₄₀ mixture after 4.5 months of incubation at room temperature.³⁸ In this study, we seek to elucidate the relationship between size and morphology of the resulting assemblies with the side chain functionality, as well as the positioning and distribution of $\alpha\alpha$ AAs in the recognition element (KLVFFA) of AAMPs. A library of AAMP-1 analogs was synthesized and evaluated for ability to disrupt A β ₁₋₄₀ fibril formation (Figure 3.1). Mitigator

AAMP-0 (KLVFFK_6) previously described by Murphy and coworkers was used as control peptide due to the similarity in design strategy to our AAMPS but with no $\alpha\alpha$ AAs.^{28,29}

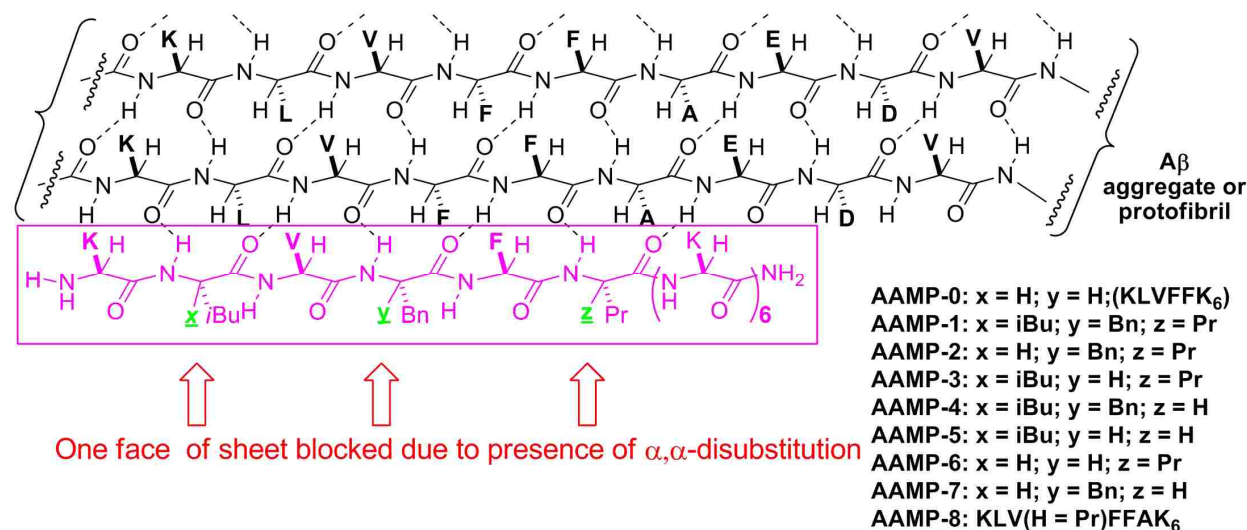


Figure 3.1. Design of mitigators with $\alpha\alpha$ AAs as disrupters of $\text{A}\beta$ assembly.

When bound to amyloid fibrils Thioflavin T dye (ThT) undergoes a red shift of its absorbance maximum from 342 to 442 nm, resulting in a characteristic enhanced fluorescence signal at 482 nm. Binding of the ThT dye to $\text{A}\beta$ fibrils is complete within 1 min and does not interfere with $\text{A}\beta$ aggregation. Thus, ThT fluorescence is commonly used to monitor the presence of $\text{A}\beta$ fibrils and their rates of formation. It has also been shown that ThT can bind to certain amorphous aggregates to produce an increased fluorescence signal.⁴⁵⁻⁴⁷ Therefore, ThT fluorescence cannot be used solely to monitor $\text{A}\beta$ formation or disruption. Other complementary methods such as circular dichroism (CD), AFM, and TEM, which reveals the conformation, size, length, and morphology of aggregates, are needed to probe mitigation of $\text{A}\beta_{1-40}$ fibril formation by designed inhibitors. We shall emphasize high-resolution AFM data because of its unique capability to probe early aggregation products (oligomers) and three-dimensional

characterization of A β assembly products relative to other microscopy techniques such as TEM.

48-52

Aggregation of A β_{1-40} proceeds via a nucleation-dependent polymerization mechanism where a nucleus is first formed before growth by A β_{1-40} monomer addition. This is a rate-limiting step, and the presence of seeds greatly accelerates aggregation, possibly bypassing the nucleation step. Thus it is critical that A β_{1-40} is pretreated to ensure monomeric starting solutions, using a previously published protocol.⁵³

3.3.2 Assembly of A β_{1-40} and with the Various AAMPs

3.3.2.1 Effect of AAMPs on A β_{1-40} ThT Fluorescence

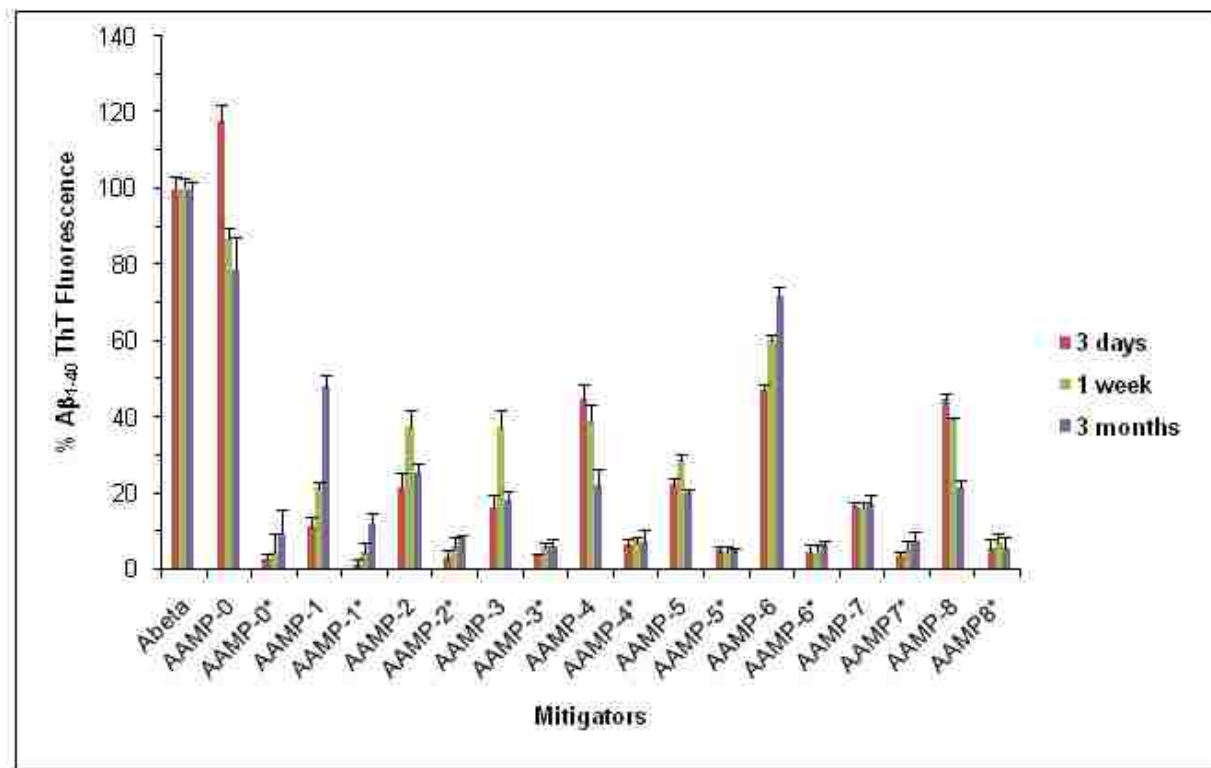


Figure 3.2. Disruption of fibril formation by designed AAMPs. Time dependent ThT fluorescence of A β_{1-40} assembly in the presence or absence of the various AAMPs. Fluorescence (ThT) was set arbitrarily to 100 percent relative to A β_{1-40} . * denotes mitigators aged alone.

Monomeric A β ₁₋₄₀ was aged alone and in the presence of equimolar AAMPs (40 μ M of A β ₁₋₄₀ or A β ₁₋₄₀/AAMPs) in pH 7.4 phosphate buffer, shaking for 10 min during each h at 37 °C. The time course of ThT fluorescence for A β ₁₋₄₀ aged alone or with equimolar mixture of AAMPs is presented as a percent of the fluorescence of A β ₁₋₄₀ alone (Figure 2). Mitigators aged alone or in the presence of equimolar A β ₁₋₄₀ display time dependent increases in ThT fluorescence, consistent with increased aggregation although with variable time rates (Figure 2). Results from ThT fluorescence show minimal fluorescence from mitigators aged alone compared to A β ₁₋₄₀ or AAMP/ A β ₁₋₄₀. These results are indicative of very low aggregation to ThT active species. In some cases, quenching of fluorescent signal was observed after 24 h aging of mitigators alone.

A significant observation was the decrease in total ThT fluorescent signal after 3 months of incubation in most of the AAMP/A β ₁₋₄₀ mixtures. We can speculate that the decreased fluorescence that is observed results from continuous aggregation of these mixtures that leads to the formation of larger assemblies, hence precipitating out of solution. In addition, the decrease also can result from mitigator molecules binding and displacing ThT molecules from mature fibrils/aggregates. The control peptide (AAMP-0) described by Murphy and coworkers to enhance A β ₁₋₄₀ self-assembly forming a network of fibrils²⁸ was compared to our designed mitigators to probe the importance of $\alpha\alpha$ AAs. A mixture of A β ₁₋₄₀/AAMP-0 shows an increase in fluorescence of 120% relative to that of A β ₁₋₄₀ alone after 3 days of incubation, and an 80 % reduction in fluorescence for prolonged aging times. This is consistent with previous reports describing enhanced A β ₁₋₄₀ fibrillogenesis.^{28, 29}

A significant reduction in A β ₁₋₄₀ ThT fluorescence is observed when A β ₁₋₄₀ is aged with an equimolar mixture of $\alpha\alpha$ AA-AAMPs. Mitigators AAMP-1, AAMP-2, AAMP-3, AAMP-4, AAMP-5, AAMP-7, and AAMP-8 exhibit a reduction of ThT fluorescence between 50 and 80%

relative to that of A β ₁₋₄₀ alone, even after 3 months of aging. The only mitigator incorporating $\alpha\alpha$ AA that displayed a reduced ThT fluorescence of 20% relative to A β ₁₋₄₀ was the dipropylglycine (Dpg)-containing AAMP-6, which remained unchanged for even longer incubation times (3 months). Comparison of the sequence of AAMP-6 with other AAMPs that showed reduction in ThT fluorescence between 50-80% relative to the control reveals the importance of steric effects and position of $\alpha\alpha$ AAs relative to the recognition element. Therefore, fibrillar assemblies were observed in AAMP-6, which incorporates the less bulky $\alpha\alpha$ AAs (Dpg) at the C-terminal end of KLVFF recognition core, hence ineffective at blocking one hydrogen bonding face from addition of extended peptides.

3.3.2.2 Effect of $\alpha\alpha$ AA-AAMPs on the Secondary Structure of A β ₁₋₄₀ Using Circular Dichroism (CD)

To examine the effect of $\alpha\alpha$ AA-AAMPs on A β ₁₋₄₀ assemblies, far-UV circular dichroism (CD) was employed. The CD spectra of unstructured monomeric AAMPs and A β ₁₋₄₀ showed a strong minimum and maximum at around 200 nm and 220 nm respectively, which is consistent with a random coil conformation. After a week of aging AAMPs alone at 37 °C with shaking, the random coil conformation observed with monomeric AAMPs remained unchanged with a minimum and maximum around 200 and 217 nm respectively, however with weaker intensities (Table 3.1).

Assembly of A β ₁₋₄₀ reveals that the time course of forming β -sheet conformation is consistent with previously reported β -sheet rich assemblies.^{38, 54} The structure of A β ₁₋₄₀ alone changed from random coil (monomeric) to β -sheet (Figure 3.3) after 7 days of incubation (maxima at 198 nm and 214 nm). In contrast, an equimolar mixture AAMPs and A β ₁₋₄₀ leads to an unusual CD signature with characteristics of both random coil and β -sheets (Figure 4.3),

which is consistent with our previous results of AAMP-1/ A β ₁₋₄₀ mixture.³⁸ The Maxima and minima of CD signals for A β ₁₋₄₀ aged alone and with the various mitigators aged are presented in Table 3.1.

Table 3.1. Wavelength and corresponding minimum and maximum ellipticities of CD analysis of AAMPs alone, A β ₁₋₄₀ alone and for AAMP/ A β ₁₋₄₀ mixtures.

entry	AAMPs	With A β (1:1)							
		3 days aging				7 days aging			
		λ (nm)	Min/Max [θ] × 10 ³	λ (nm)	Min/Max [θ] × 10 ³	λ (nm)	Min/Max [θ] × 10 ³	λ (nm)	Min/Max [θ] × 10 ³
1	A β ₁₋₄₀	206	-4.89	220	-0.275	198	5.03	214	-14.53
2	AAMP-0	204	-31.34	219	-1.821	195 (199)	-14.66 (-39.86)	207 (221)	2.4 (3.98)
3	AAMP-2	202	-20.88	218	21.10	200 (199)	-9.89 -36.271	218 (217)	0.46 15.823
4	AAMP-3	202	-50.18	220	-4.12	206 (195)	0.297 -29.63	220 (213)	-3.25 (15.22)
5	AAMP-4	204	-18.43	221	2.82	203 (202)	-7.93 (-22.47)	213 (215)	-2.95 (11.83)
6	AAMP-6	202	-50.18	218	-4.41	202 (202)	-8.27 (-40.96)	219 (219)	2.35 (14.12)
7	AAMP-7	202	-25.34	222	-5.85	200 202	-11.20 (-22.47)	224 (221)	-0.69 (13.95)

Note: Values in parenthesis are for AAMPs aged alone after 1 week.

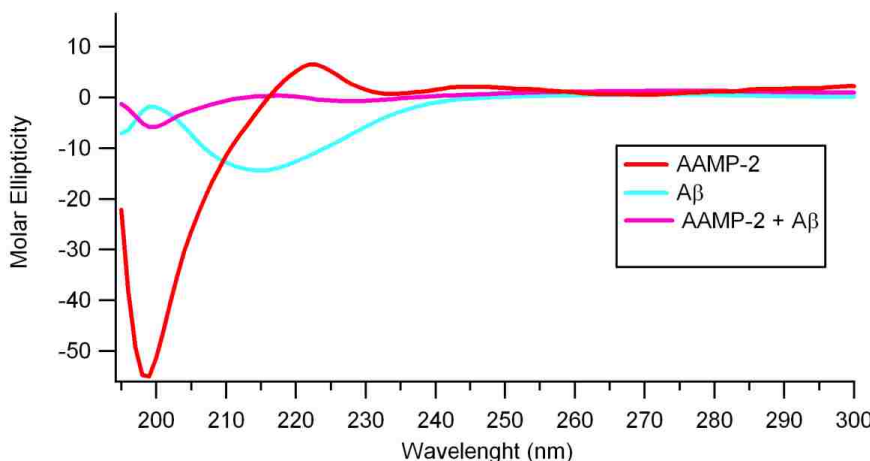


Figure 3.3 Example of CD signature obtained for A β ₁₋₄₀ alone, AAMP alone, and A β ₁₋₄₀/AAMP mixture after 1 week aging.

3.3.2.3 Size and Morphology of the Various Structures as Determined Using AFM

AAMPs aged alone sparsely aggregate forming spherical beads (Figure 3.4) exclusively with mean height range of 4-10 nm (Table 3.2)

Table 3.2. Mean heights of spherical aggregates observed after 3 days and 1-week aging the various AAMPs alone.

Entry	Mitigators	Type/size of nanostructures formed			
		3 days	7 days	90 days	3 days
		aggregate type	mean height (nm)	aggregate type	mean height (nm)
11	AAMP-0	spherical	4.9±3.4	amorphous	5.4±2.2
12	AAMP-1	spherical	1.9±1.1	amorphous	9.6±7.7
13	AAMP-2	spherical	2.1±0.9	amorphous	5.3±4.3
14	AAMP-3	spherical	2.2±1.5	amorphous	5.3±3.2
15	AAMP-4	spherical	2.6±3.6	amorphous	6.3±3.6
16	AAMP-5	spherical	4.3±2.3	amorphous	6.3±3.6
17	AAMP-6	spherical	3.5±2.1	amorphous	4.6±3.4
18	AAMP-7	spherical	3.1±1.3	amorphous	5.1±1.9
19	AAMP-8	spherical	3.2±2.3	amorphous	4.8±2.5

The absence of fibril formation is consistent with CD results, which show little change in the random coil conformation with maxima around 220 nm and minima at 217 nm after 1 week of incubation. Also, the minimal ThT fluorescence observed with AAMPs aged alone relative to A β ₁₋₄₀, suggests that the nanostructures formed are not β -sheet rich. One possible drawback for the observed spherical beads is that they could act as seeds for A β ₁₋₄₀ aggregation, increasing the rate at which fibrils are formed. However, fibrils were not observed suggesting that particles produced by AAMPs alone do act as seeds for A β fibril formation. We speculate that the hydrophobic forces are stronger than hydrogen bonding forces resulting in the observed morphology of aggregates formed. The small-sized spherical aggregates (height ~ 1.6 nm) formed when AAMP-1 was aged alone for 3 days may explain the toxicity to the cells we have reported before.⁵⁵ The various nanostructures formed from aging the various AAMPs alone are presented in Figure 3.4

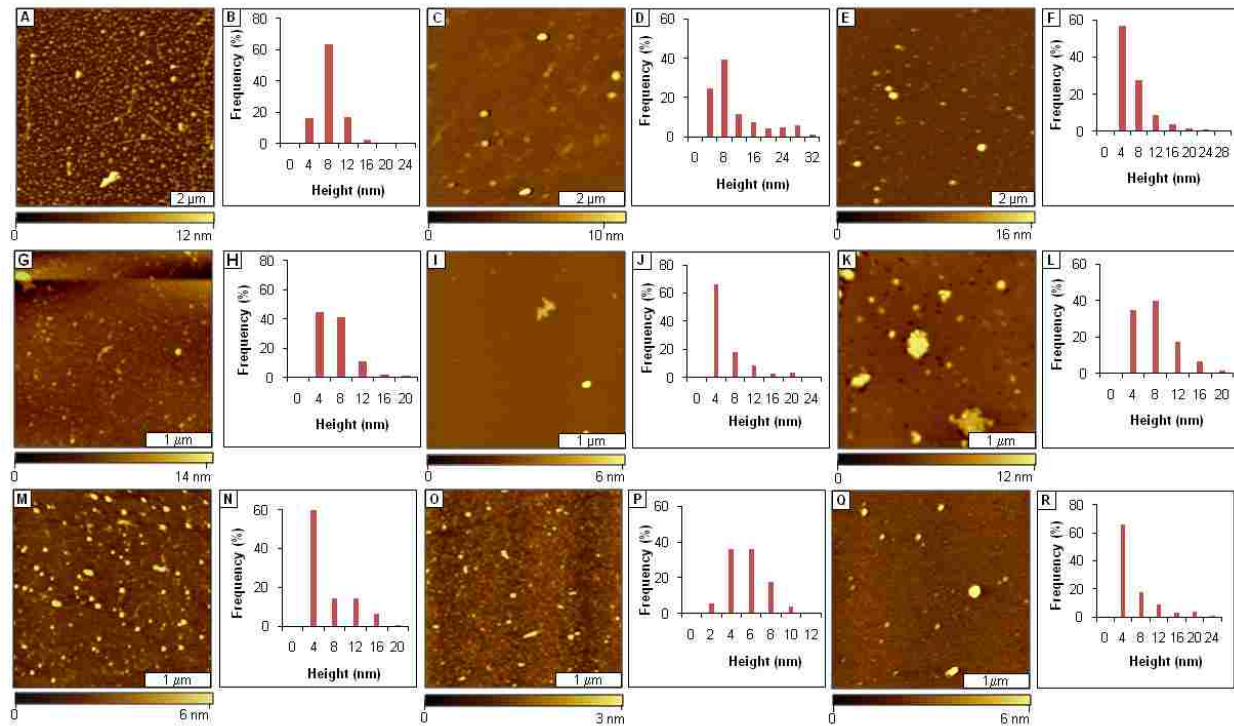


Figure 3.4 Spherical aggregates observed after 1 week aging the various AAMPs alone. Topographic AFM views of spherical structures formed by:- [A] AAMP-0 [B] Corresponding height analysis for A; [C] AAMP-1 [D] Height analysis for C; [E] AAMP-2; [F] Height analysis for E; [G] AAMP-3; [H] Height distribution histogram for G; [I] AAMP-4; [J] Height analysis for I; [K]AAMP-5; [L] Height histogram for K; [M] AAMP-6; [N] Height analysis for M; [O]AAMP-7; [P] Height distribution analysis for O;[Q]AAMP-8; [P] Height distribution analysis for Q;

AFM was used to characterize $\text{A}\beta_{1-40}$ or $\text{A}\beta_{1-40}/\text{AAMP}$ sample aliquots taken at the same time intervals as those used for ThT fluorescence assay. Images obtained from AFM topography of aliquots taken at different aging times for $\text{A}\beta_{1-40}$, and in presence of AAMP-0, and AAMP-1 are shown in Figure 3.5. Fibrils were the predominant structures observed after 1 week of aging $\text{A}\beta_{1-40}$ alone (Figure 3.5A). These fibrils had a mean height of 4.2 ± 2.3 nm which is smaller than the reported mean height of about 7-10 nm for mature fibrils.^{47, 56} The mean height is obtained by taking multiple cursor measurements of the thickness of the fibrils throughout several representative images and is presented in Table 3.3.

Table 3.3. Comparison for nanostructures observed by AFM for A β ₁₋₄₀ alone and with the various mitigators.

entry	mitigator	type/size of nanostructures formed					
		3 days		7 days		90 days	
		aggregate type	mean height (nm)	aggregate type	mean height (nm)	aggregate type	mean height (nm)
1	A β ₁₋₄₀	proto/fibril	3.44 \pm 2.1	fibrils	4.2 \pm 2.3	fibrils	11.1 \pm 6.5
2	AAMP-0	protofibrils	8.6 \pm 5.7	fibrils	9.1 \pm 3.1	-	-
3	AAMP-1	spherical	10.7 \pm 5.9	spherical	9.6 \pm 7.5	linear	9.5 \pm 7.0
4	AAMP-2	spherical	5.8 \pm 3.6	spherical	8.0 \pm 4.4	spherical	8.5 \pm 3.7
5	AAMP-3	spherical	1.6 \pm 1.4	linear	1.7 \pm 1.4	linear	3.7 \pm 2.4
6	AAMP-4	spherical	10.2 \pm 4.1	spherical	18.1 \pm 8.5	spherical rods	43.22
7	AAMP-5	spherical	3.8 \pm 2.8	spherical	5.0 \pm 3.5	spherical	8.0 \pm 3.1
8	AAMP-6	protofibril/ linear	8.0 \pm 5.5	rod like fibrils	6.7 \pm 2.9	rod like fibrils	8.1 \pm 3.2
9	AAMP-7	spherical	8.6 \pm 4.3	spherical	12.7 \pm 6.8	spherical	16.0 \pm 8.8
10	AAMP-8	spherical	6.2 \pm 2.8	spherical	9.8 \pm 5.2	spherical	35.9 \pm 15.8

The distribution of heights is presented as a histogram for each AFM view. The individual plots shown for the surface topography of the various samples are representative views of the morphologies observed for multiple areas of the samples. The presence of smaller sized fibrils is an indication that protofibrils and some immature fibrils predominate at the early stage, which is supported by height distribution analysis showing fibrils with diameters 2-4 nm accounting for \geq 60% of total fibrils (Figure 3.5B). In contrast, bundles of fibrils (Figure 3.5C) were observed after 3 months of incubation as the predominant surface arrangements. The mean height of the fibrils in the clumps was 11.1 \pm 6.5 nm and more than 70% of these fibrils had heights ranging from 4 to 12 nm (Figure 3.5D) indicating mature fibrils (7-10 nm) had formed.

The assembly of A β ₁₋₄₀ into fibrils is consistent with the proposed hierarchical assembly model (HAM model), which predicts that protofilaments predominate at earlier incubation stages while protofibrils and fibrils are detected later. The HAM model also predicts that protofibrils

and fibrils will exhibit periodicity, variations in height, branching, and clumping at various stages of fibrillization. The unique arrangement of fibrils on the surface observed after 3 months is consistent with increased β -sheet character of the fibrils.^{57, 58}

The significance of $\alpha\alpha$ AAs in disrupting fibril formation was evaluated by aging equimolar mixtures of A β ₁₋₄₀ with AAMP-0 (no $\alpha\alpha$ AAs) and AAMP-1 (with $\alpha\alpha$ AAs). For instance, after 3 days of aging AAMP-0/A β ₁₋₄₀ mixture, protofibrils (Figure 3.5E) with mean height of 8.6±5.7 nm were the main structures observed. A dense network of fibrils (Figure 3.5G) with mean height of 9.1±3.1 nm was observed after 1 week of aging. The height analysis shows a time-dependent increase in fibril heights (Figure 3.5F and 3.5H). In contrast, mixtures of protofibrils and spherical aggregates (Figure 3I) with a mean height of 9.6±7.5 nm were observed with AAMP-1 after 1 week of incubation, and rod-like structures (Figure 3.5K) were formed after 3 months with a slight increase in mean height as displayed in Figures 3.5J and 3.5I.

The peptide AAMP-0 (no $\alpha\alpha$ AAs) was used as a control sample to evaluate the effects of $\alpha\alpha$ AAs. This peptide (AAMP-0) was shown previously to enhance the rate of aggregation of A β ₁₋₄₀ to form a dense network of fibrils.²⁸ The enhanced A β ₁₋₄₀ aggregation rates may also lead to thicker fibrils as compared to A β ₁₋₄₀ fibrils alone. The structural design for AAMP-0 and our AAMPs are similar except for $\alpha\alpha$ AAs incorporated in the latter (For example Dbg for Phe etc). The peptide mitigator AAMP-1 was previously communicated to block A β ₁₋₄₀ fibrillization even after 4.5 months of incubation at room temperature.³⁸ The different aggregate morphology observed from A β ₁₋₄₀ aggregation mitigated by AAMP-0 (fibrils) as compared to $\alpha\alpha$ AA-containing AAMP-1 (mixture of spherical aggregates and rod-like structures) reinforces the contrast in using $\alpha\alpha$ AA-containing AAMPs to disrupt fibril formation. The results for AAMP-1 with further characterization of the sizes and morphologies of nanostructures formed at different

stages of aggregation using high resolution AFM are presented in Figure 3.5I and 3.5K. Although, AAMP-1 was effective at altering $\text{A}\beta_{1-40}$ assembly, for optimal use *in vivo* and improved systemic bioavailability the molecular weight of AAMP-1 should be reduced as much as possible. The AAMP-1 analogs were screened for their ability to disrupt $\text{A}\beta_{1-40}$ assembly and were used as a control.

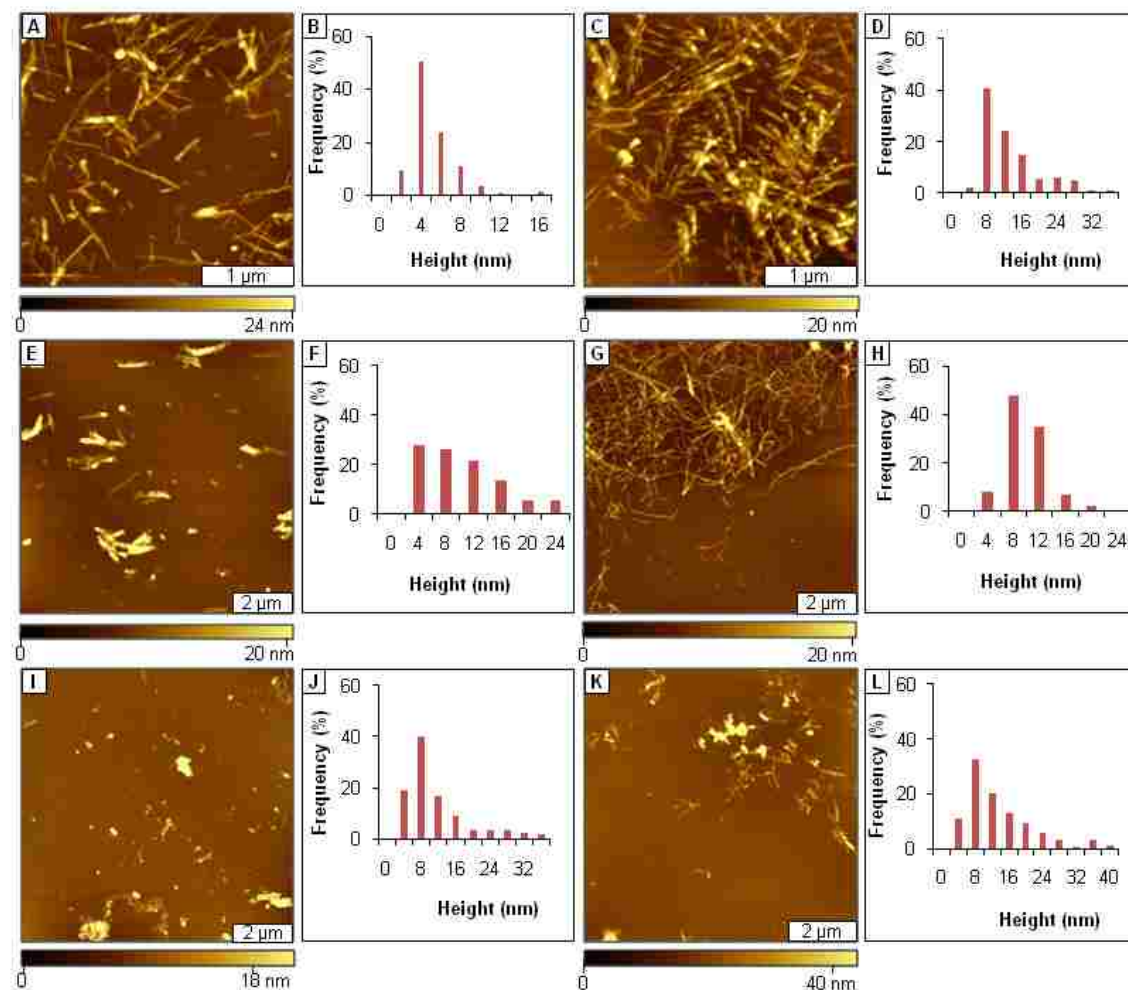


Figure 3.5. Aggregation of $\text{A}\beta_{1-40}$ with and without AAMPs. [A] Fibrils formed by $\text{A}\beta_{1-40}$ alone after 1 week of incubation; [B] Height analysis for A; [C] Fibril bundles formed by $\text{A}\beta_{1-40}$ alone after 3 months of incubation; [D] Height analysis for C; [E] Prototubers formed after 3 days $\text{A}\beta_{1-40}$ mitigation by AAMP-0; [F] Height distribution analysis for E; [G] Fibril network formed after 1 week $\text{A}\beta_{1-40}$ aggregation mitigation by AAMP-0; [H] Height distribution histogram for G; [I] Mixture of spherical and linear aggregates formed after 1 week $\text{A}\beta_{1-40}$ mitigation by AAMP-1; [J] Height analysis for I; [K] Spherical and prototubers observed after 3 months of $\text{A}\beta_{1-40}$ mitigation by AAMP-1; [L] Height distribution histogram for K

When AAMP-1 analogs with two $\alpha\alpha$ AAs were aged with equimolar $\text{A}\beta_{1-40}$, assemblies with different heights and morphologies were formed based on the side chain functionality of the $\alpha\alpha$ AAs used. Spherical aggregates (Figure 3.6A) with mean heights of 8.0 ± 4.4 nm and 60% of the particles with height range of 4-8 nm (Figure 3.6B) were observed after 1 week of aging $\text{A}\beta_{1-40}$ /AAMP-2 mixture. The spherical morphology of the aggregates did not change after 3 months incubation, but were observed to coalesce forming in some cases aggregate strings (Figure 3.6C). The only significant change observed was the slight increase in mean heights (8.5 ± 3.7 nm) as shown by height distribution analysis (Figure 3.6D). Smaller sized spherical aggregates (Figure 3.6E) with mean height 1.7 ± 1.4 nm were formed from coincubation of $\text{A}\beta_{1-40}$ in the presence of equimolar AAMP-3 as compared to AAMP-2. The same morphology was observed after 3 months incubation (Figure 3.6G), but with a larger mean height (3.7 ± 2.4 nm) as shown by AFM cursor analysis (Figure 3.6F and 3.6H). Mixtures of spherical aggregates and protofibrils/fibrils (visible in the background) with mean height of 18.1 ± 8.5 nm (Figure 3.6I) formed after 1 week of $\text{A}\beta_{1-40}$ mitigation by AAMP-4 as compared to mostly spherical particles observed after 3 days of incubation. After 3 months of incubation, the mean height of the spherical aggregates (Figure 3.6K) more than doubled (43.2 ± 25 nm) with maximum height spanning to 1 μm as shown in Figures 3.6J and 3.6L.

The disruption of fibril formation by AAMPs with two $\alpha\alpha$ AAs is an important finding in that these AAMPs portrayed the same or better disruptive properties as the original AAMP-1 peptide with three $\alpha\alpha$ AAs. The more interesting aspect of their disruption is the relation between size and morphology of the particles formed and the side chain functionality of incorporated $\alpha\alpha$ AAs. Larger particles with similar morphology were formed from $\text{A}\beta_{1-40}$ aggregation mitigation by AAMP-2 and AAMP-4 as compared to AAMP-3. The difference in

observed heights could be attributed to the side chain functionality of the $\alpha\alpha$ AAs incorporated in AAMP-2 (Dbg and Dpg), AAMP-3 (Dibg and Dpg), and AAMP-4 (Dbg and Dibg). Surprisingly, Dbg (aromatic)-containing AAMPs (AAMP-2 and AAMP-4) formed larger particles as compared to AAMP-3 without Dbg. Thus incorporation of the additional aromatic side-chain in Dbg containing AAMPs may play a role in determining the size and morphology of the resultant nanoparticles because aromatic residues are believed to supply energy, order, and directionality^{59, 60} to the $\text{A}\beta$ assembly process during fibril formation through aromatic-side chain stacking interactions.

Hydrophobic or steric effects from $\alpha\alpha$ AAs may also lead to the size and morphology of structures formed. For instance, larger spherical aggregates with a few protofibrils/fibrils were formed with AAMP-4 as compared to mainly spherical aggregates for AAMP-2. The different sizes and morphology of particles formed can thus be related to the combination of the $\alpha\alpha$ AAs used in each AAMP. They both have aromatic Dbg and a different second $\alpha\alpha$ AAs (Dpg and Dibg for AAMP-2 and AAMP-4 respectively). Thus, steric or hydrophobicity differences between Dpg (n-side chains) and Dibg (branched side chains) has influenced the size and morphology of the assemblies formed.

Positioning of $\alpha\alpha$ AAs relative to each other in the AAMP sequence could influence the size and morphology of assemblies formed. One of the ways to induce extended peptide conformations required for the interaction with $\text{A}\beta$ in short model peptides is to use $\alpha\alpha$ AAs with larger side-chain groups. For instance, smaller particles were formed by $\text{A}\beta_{1-40}$ mitigation by AAMP-3 as compared to either AAMP-2 or AAMP-4. The two $\alpha\alpha$ AAs are in an i, i+2 orientation in AAMP-2 and AAMP-4 as compared to an i, i+4 arrangement in AAMP-3. Other examples of i, i+2 design mitigators that were designed by replacement of amide backbone

include n-methyl groups, ester linkages, and isostructural E-olefin all of which were shown to mitigate fibril formation.^{31, 32, 34, 61} Thus placement of the disrupting elements on the same hydrogen bonding face is crucial for the mitigators to disrupt fibril formation than their arrangement. In addition, based on our findings with $\alpha\alpha$ AAs, the number of other disrupting elements reported such as N-methylated derivatives and ester linkages could be reduced without affecting their disruptive properties.

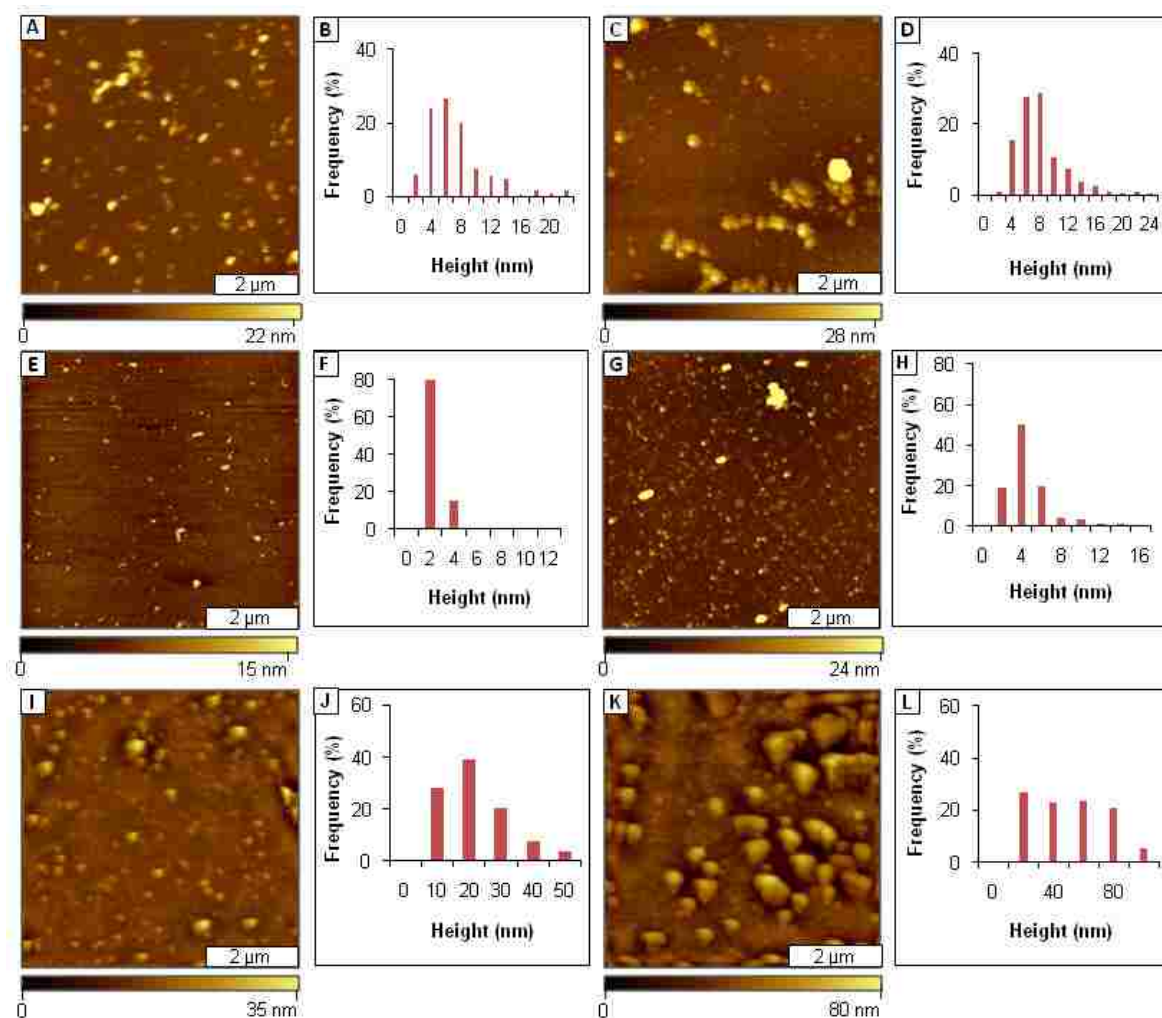


Figure 3.6. Disruption of $\text{A}\beta_{1-40}$ fibril formation by AAMPs with two $\alpha\alpha$ AAs; [A] Globular aggregates formed after 7 days aging $\text{A}\beta_{1-40}$ in presence of AAMP-2; [B] Corresponding height distribution analysis; [C] After 3 months aging; [D] Corresponding height distribution; [E] Spherical aggregates formed after 1 week aging $\text{A}\beta_{1-40}$ /AAMP-3 mixture; [F] Height analysis for E; [G] Spherical aggregates after 3 months aging; [H] Corresponding height analysis; [I] Mixture of spherical aggregates and protofibrils formed after 7 days aging $\text{A}\beta_{1-40}$ in presence of AAMP-4; [J] Corresponding height distribution analysis for I; [K] After 3 months aging; [L] Matching height distribution histogram.

The role of AAMPs with only one $\alpha\alpha$ AAs on mitigation of $\text{A}\beta_{1-40}$ aggregation was examined by aging $\text{A}\beta_{1-40}$ in the presence of equimolar amounts of AAMP-5 (Dibg), AAMP-6 (Dbg), and AAMP-7 (Dpg). Globular particles were observed to form with AAMP-5 (Figure 3.7A) which were stable (no fibrils) after 3 months of aging (Figure 3.7C). Height analysis shows that the percentage of the particles with heights ranging from 4-6 nm increased from ~30% for 1 week of incubation to over 50% after 3 months of aging (Figure 3.7B and 3.7D). Co-incubation of $\text{A}\beta_{1-40}$ /AAMP-6 mixture produced protofibrillar structures and rod-like fibrils (Figure 3.7E) after 1 week. The protofibrils (Figure 3.7G) observed after 3 months of incubation had increased in mean height as displayed by height analysis showing a 2-fold increase in the percentage of particles with heights of 4-6 nm as compared to after 1 week (Figures 3.7F and 3.7H). Aging of $\text{A}\beta_{1-40}$ with equimolar amounts of AAMP-7 resulted in mainly spherical particles after 3 days. However, a mixture of spherical aggregates and fibrils/protofibrils (Figure 3.7I) in the background were detected after 1-week of incubation with over 50% of the particles with heights ranging from 1-10 nm (Figure 3.7J). After 3 months of aging, the morphology of the particles (Figure 3.7K) did not change, but their sizes increased as shown by the increase in the percentage of particles with larger heights (Figure 3.7L). Spherical aggregates (Figure 3.7M) with mean heights of 9.8 nm were formed from $\text{A}\beta_{1-40}$ mitigation by AAMP-8 after aging for 1 week. Surprisingly, after 3 months, spherical aggregates (Figure 3.7O) observed earlier have grown in size to more than a micron in some cases as shown by height analysis (Figure 3.7N and 3.7P)

Results from $\text{A}\beta_{1-40}$ mitigation by AAMPs with one $\alpha\alpha$ AAs further confirms that side chain functionality of incorporated $\alpha\alpha$ AAs influences the size and morphology of the resulting nanoparticles. For example, the different morphology of the particles observed in AAMP-5 as compared to AAMP-6 is because of the steric difference between the $\alpha\alpha$ AAs incorporated.

Spherical aggregates formed with AAMP-5, which incorporate the more sterically, hindered Dibg (isobutyl side chains) as compared to rod-like fibrils in AAMP-6, which contains the less sterically hindered Dpg (n-propyl side chains). In addition, the size and morphology of fibrils formed by AAMP-6 were different from those of A β ₁₋₄₀ alone. Fibrils formed by AAMP-6 had larger mean heights (6.7 ± 2.9 nm) and smaller lengths (≤ 1 micron in length) as compared to mature A β ₁₋₄₀ fibrils, which were smaller in mean height (4.2 ± 2.3 nm) and several microns in length. The short fibril lengths suggest lateral interactions of protofilaments rather than the intertwining commonly identified during amyloid fibril formation, which can also be because of a slower growth rate of protofilaments by elongation and dissociation of monomers. The branching and polymorphic nature of the fibril lengths observed may have been caused by the interactions between protofibrils of unequal lengths.⁵⁸

Positioning of the $\alpha\alpha$ AAs relative to KLVFF core sequence also influences the morphology of the resulting nanoparticles. The core sequence KLVFF has been shown to be critical for the inhibitor peptide to interact with A β . Thus, mitigators with $\alpha\alpha$ AAs placed outside this core sequence should have less influence on the interaction with A β as compared to mitigators with $\alpha\alpha$ AAs incorporated into this region. An example is the different morphology of particles formed from A β ₁₋₄₀ mitigation by AAMP-8 (nonfibrillar assemblies) with Dpg incorporated in the KLVFF core (KLDpgFFAK₆) as compared to AAMP-6 (rod-like fibrils) with Dpg outside the KLVFF core (KLVFFDpgK₆). We speculate that the AAMPs with $\alpha\alpha$ AAs incorporated into the binding motif resulted in increased side-chain to side-chain hydrophobic interactions with the homologous core of A β . Thus, blocking one face from interchain hydrogen bonding disrupts the A β aggregation pathway.

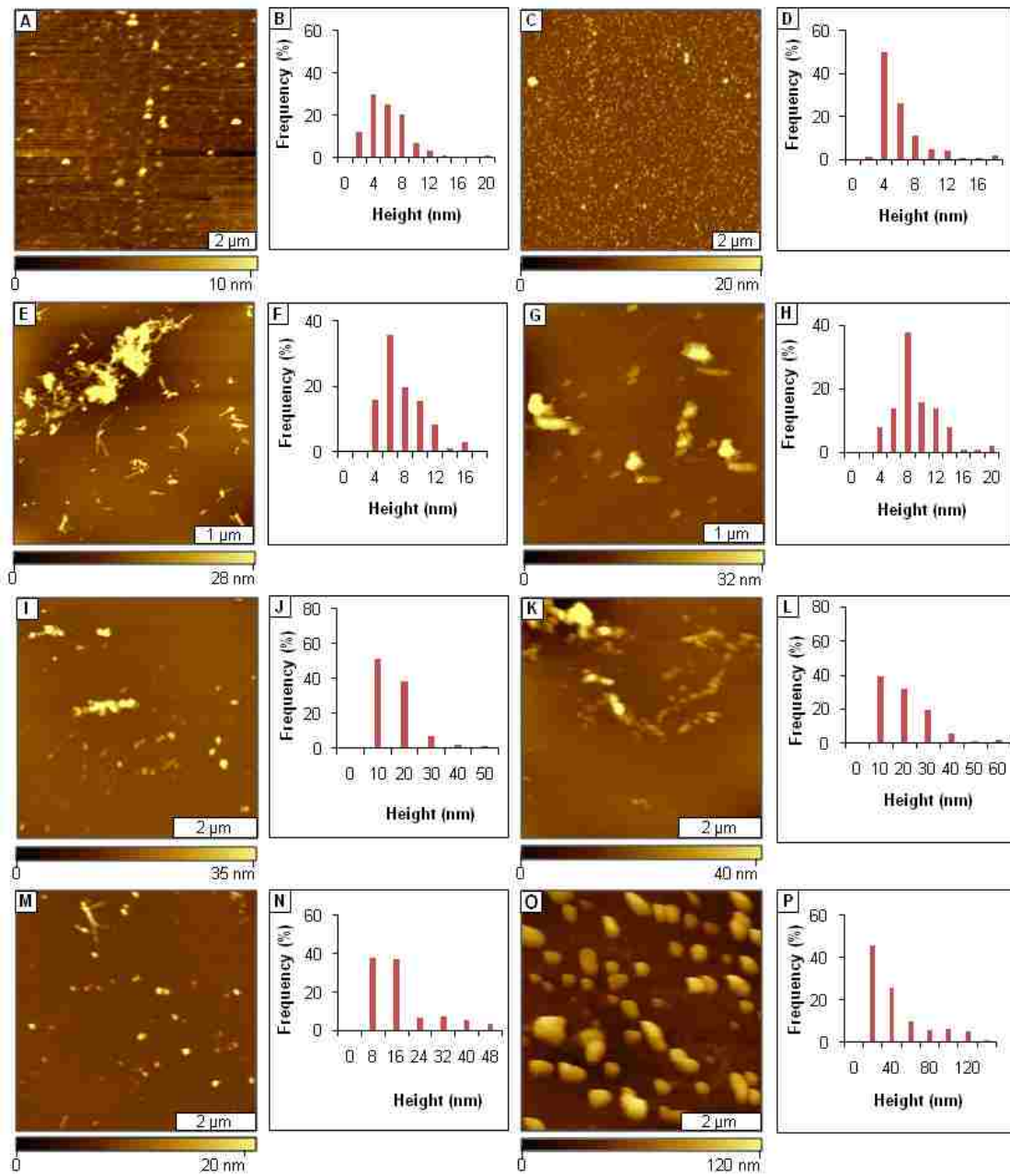


Figure 3.7 Topographic AFM images showing disruption of A β ₁₋₄₀ fibril formation by AAMPs with one $\alpha\alpha$ AAs [A]Views of nonfibrillar assemblies formed after 1 week A β aggregation mitigation by AAMP-5; [B] Corresponding height distribution; [C] After 3 months; [D] Height analysis for C; [E] Progressive AFM Views of rod-like fibrils detected after 1 week of aging A β ₁₋₄₀/AAMP-6 mixture; [F] Corresponding height distribution; [G] After 90 days; [H] Height distribution analysis for G; [I] Views of spherical and protofibrils/fibrils (background) formed by A β ₁₋₄₀/AAMP-7 mixture after 1 week aging; [J] Corresponding height analysis; [K]; After 90 days; [L] Height analysis for K; [M] Views of spherical particles formed by A β ₁₋₄₀ aggregation mitigation by AAMP-8; [N] Corresponding height distribution; [O] After 3 months; [P] Height analysis for O.

Interestingly, A β ₁₋₄₀ mitigation by AAMP-7 with aromatic Dbg yielded spherical aggregates after 3 days of aging. However, after 1 week of incubation a mixture of spherical particles and protofibrils/fibrils in the background with very different morphology relative to A β fibrils were formed. This was an unexpected result since it was predicted to disrupt formation of fibrillar structures similar to AAMP-5, which incorporates Dibg. A plausible explanation for the different morphology of particles formed by the two mitigators is the aromatic nature of Dbg versus Dibg. This could be due to the enhanced aromatic-stacking interactions asserted by the extra aromatic residue. In summary, after 3 days of incubation, AAMP-4 and AAMP-7 disrupted fibril formation. However, after 1 week of incubation, a mixture of spherical particles and protofibrils/fibrils were observed. This indicates that higher ratios of AAMP to A β ₁₋₄₀ are needed to prevent fibril formation.

3.3.2.4 Morphology of Structures Formed from A β ₁₋₄₀ Aggregation Mitigation by the Various AAMPs as Observed by TEM

Negatively stained samples of A β ₁₋₄₀ alone or mixed with equimolar AAMPs prepared at the same time as those of AFM and ThT were examined using TEM to confirm the various morphologies observed with AFM. The morphology of structures (Figure 3.8) formed by A β ₁₋₄₀ alone and with the various AAMPs after 1-week aging was consistent with AFM observations. For instance, A β ₁₋₄₀ sample showed a typical appearance of amyloid fibrils, shown as a dense network of fibrils extending several microns in length. In contrast, A β ₁₋₄₀/AAMP mixtures reveal disruption of A β ₁₋₄₀ fibrillization yielding particles with different morphologies.

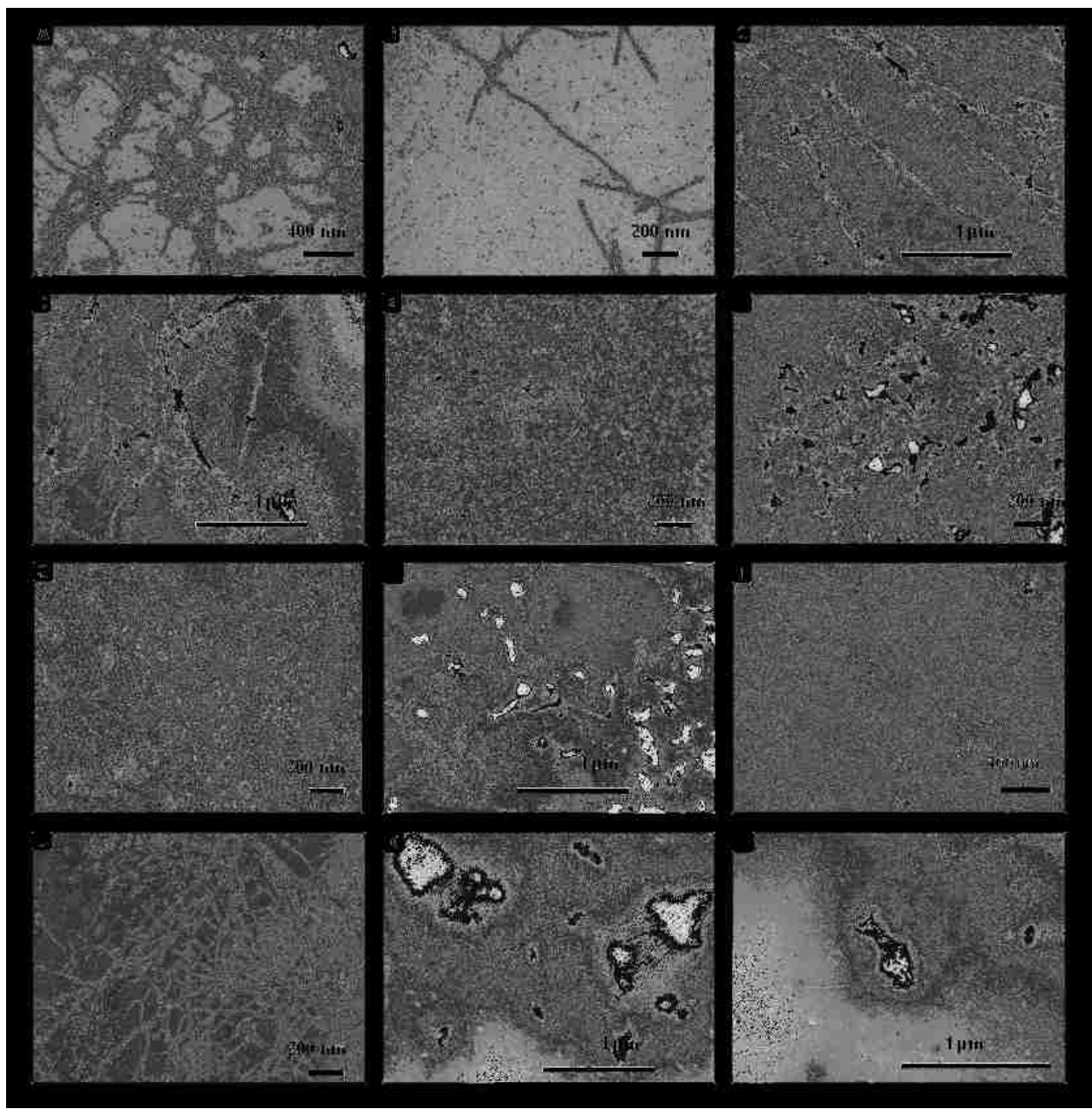


Figure 3.8 Morphologies of various particles observed after 1-week aging Aβ₁₋₄₀ in presence of the various AAMPs. [A] Fibrils formed by Aβ₁₋₄₀ alone; [B] Fibrils formed by Aβ₁₋₄₀ alone different view; [C] Fibrils formed by Aβ₁₋₄₀ alone different view; [D] Fibrils formed from Aβ₁₋₄₀ mitigation by AAMP-0; [E] Spherical particles formed from aging Aβ₁₋₄₀ in presence of AAMP-1; [F] Spherical particles were observed from aging Aβ₁₋₄₀/AAMP-2 mixture; [G] Spherical particles formed from Aβ₁₋₄₀ aggregation mitigation by AAMP-3; [H] Mixture of spherical aggregates and short fibrils were observed from incubating Aβ₁₋₄₀ in presence of AAMP-4; [I] Spherical particles formed from Aβ₁₋₄₀ aggregation mitigation by AAMP-5 [J] Fibrils observed from Aβ₁₋₄₀ aggregation mitigation by AAMP-6 [K] Mixture of spherical and short fibrils formed from Aβ₁₋₄₀ mitigation by AAMP-7; [L] Spherical particles were observed from aging Aβ₁₋₄₀/AAMP-8 mixture

3.3.3 A β ₁₋₄₀ Fibril Disassembly.

Several laboratories have reported that a dynamic equilibrium exists between A β ₁₋₄₀ monomers/dimers and fibrils.^{36, 62} Thus, a viable strategy to mimic possible dissolution of plaque deposits commonly present in the brains of patients with AD is to screen for compounds that can bind to preformed fibrils, shifting the equilibrium towards prefibrillar species. Soto^{36, 63} and Meredith^{31, 32} have shown that peptides, which incorporate proline (β -sheet breaker) and N-methylated amino acids, have the ability to disassemble mature A β ₁₋₄₀ fibrils.^{31, 32, 36} The design of N-methylated peptides and our $\alpha\alpha$ AA-containing AAMPs are similar in that both were designed to block one hydrogen-binding face thus preventing β -sheet stacking and extension. Therefore, we hypothesize that $\alpha\alpha$ AA-containing AAMPs should also disassemble preformed fibrils because of the more bulky side chains, as compared to the methyl group in N-methylated peptides.

3.3.3.1 Thioflavin T Fluorescence.

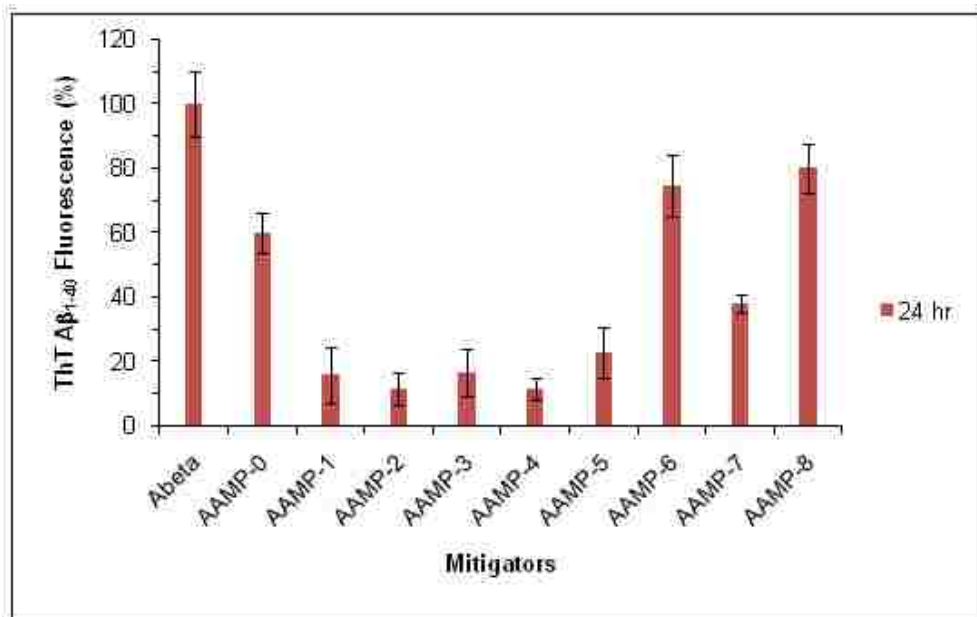


Figure 3.9. Disassembly of A β ₁₋₄₀ preformed fibrils. ThT fluorescence of A β ₁₋₄₀ fibril disassembly by the various AAMPs after 24 h incubation at 37 °C while shaking

To assess the ability of AAMPs to disassemble preformed fibrils, $\text{A}\beta_{1-40}$ was aged for 6 days at 37 °C while shaking. The mature fibrils that formed were mixed with the various AAMPs at 1:1 molar ratio (40 μM final concentration), and incubated while shaking for 24 h. The extent of disassembly was measured by ThT fluorescence. Results of ThT fluorescence for the disassembly of preformed fibrils by the various AAMPs after 24 h incubation are presented in Figure 3.9 as %ThT fluorescence relative to that of $\text{A}\beta_{1-40}$ fibrils.

The general reduction in ThT fluorescence for $\text{A}\beta_{1-40}$ fibril/AAMP mixtures relative to that of $\text{A}\beta_{1-40}$ alone indicates fibril disassembly occurred. For instance, AAMP-1, AAMP-2, AAMP-3, and AAMP-4 reduced $\text{A}\beta$ ThT fluorescence by nearly 80%. This is comparable to the disassembly of $\text{A}\beta_{1-40}$ fibrils reported for β -sheet breaker peptide (LPFFD),³⁶ RGTATEGKF peptide,⁶⁴ and N-methylated peptides,^{31, 32, 61} although this was at lower AAMP ratios. Coincidentally, these same mitigators disrupted $\text{A}\beta_{1-40}$ fibril formation by a similar degree.

The other AAMPs (AAMP-0 and Dpg-containing AAMP-6) reduced $\text{A}\beta_{1-40}$ ThT fluorescence by ~20%. The same mitigators only altered fibril morphology when aged with monomeric $\text{A}\beta_{1-40}$. It is possible that ThT Fluorescence could give false positive result for fibril disassembly, because reduction in ThT fluorescence can also result from inhibitor molecules displacing ThT molecules bound to the preformed fibrils.

3.3.3.2 Size and Morphology of Structures Formed from Disassembly of Preformed Fibrils by Various AAMPs as Determined Using AFM

Results for disassembly of preformed fibrils by AAMPs are summarized in Table 3.3. Topographic AFM image of $\text{A}\beta_{1-40}$ taken after six days aging showed a dense network of fibrils (Figure 3.10A) with a mean height of 6.2 nm. The height analysis (Figure 3.10B) reveals the

maturity of the fibrils formed, with more than 60% of the fibrils having heights between 4-8 nm, consistent with the height of mature fibrils (7-10 nm).

Table 3.3. Effect of various AAMPs on $\text{A}\beta_{1-40}$ disassembly.

entry	Mitigators	$\alpha\alpha\text{AAs}$	Aggregate type after 24 h			
			dominant structures	mean height (nm)	isolated structures	mean height (nm)
1	$\text{A}\beta_{1-40}$	-	Fibrils	6.2±2.6	-	-
2	AAMP-0	-	Fibrils	5.4±2.7	spherical	5.6±2.2
3	AAMP-1	Dibg, Dbg, Dpg	Spherical	5.5±2.9	fibrils	11.2±5.6
4	AAMP-2	Dbg, Dpg	Spherical	3.0±1.2	fibrils	12.4±4.6
5	AAMP-3	Dibg, Dpg	Spherical	7.9±5.0	fibrils	8.4±3.4
6	AAMP-4	Dbg, Dibg	Spherical	11.2±8.2	fibrils	5.2± 2.6
7	AAMP-5	Dibg	Spherical	5.0±4.2	fibrils	5.1±2.1
8	AAMP-6	Dpg	Fibrils	6.6±2.1	spherical	4.7±2.6
9	AAMP-7	Dbg	Spherical	11.3±5.9	fibrillar	5.2±2.5
10	AAMP-8	Dpg	Spherical	10.8±7.5	fibrillar	8.9±4.5

Topographic AFM images of $\text{A}\beta_{1-40}$ fibrils disassembled by AAMP-0 (no $\alpha\alpha\text{AAs}$) exhibit reduced surface coverage of fibrils and a few spherical particles (Figure 3.10C) consistent with the 20% reduction in ThT fluorescence observed relative to that of $\text{A}\beta_{1-40}$. Also, this is consistent with previous reports that AAMP-0 does not induce fibril disassembly. The height distribution shows a distribution similar to that of $\text{A}\beta_{1-40}$ fibrils (Figure 3.10D). In contrast, $\alpha\alpha\text{AA}$ -containing AAMPs induced disassembly of preformed fibrils to form nonfibrillar assemblies and isolated protofibrils/fibrils.

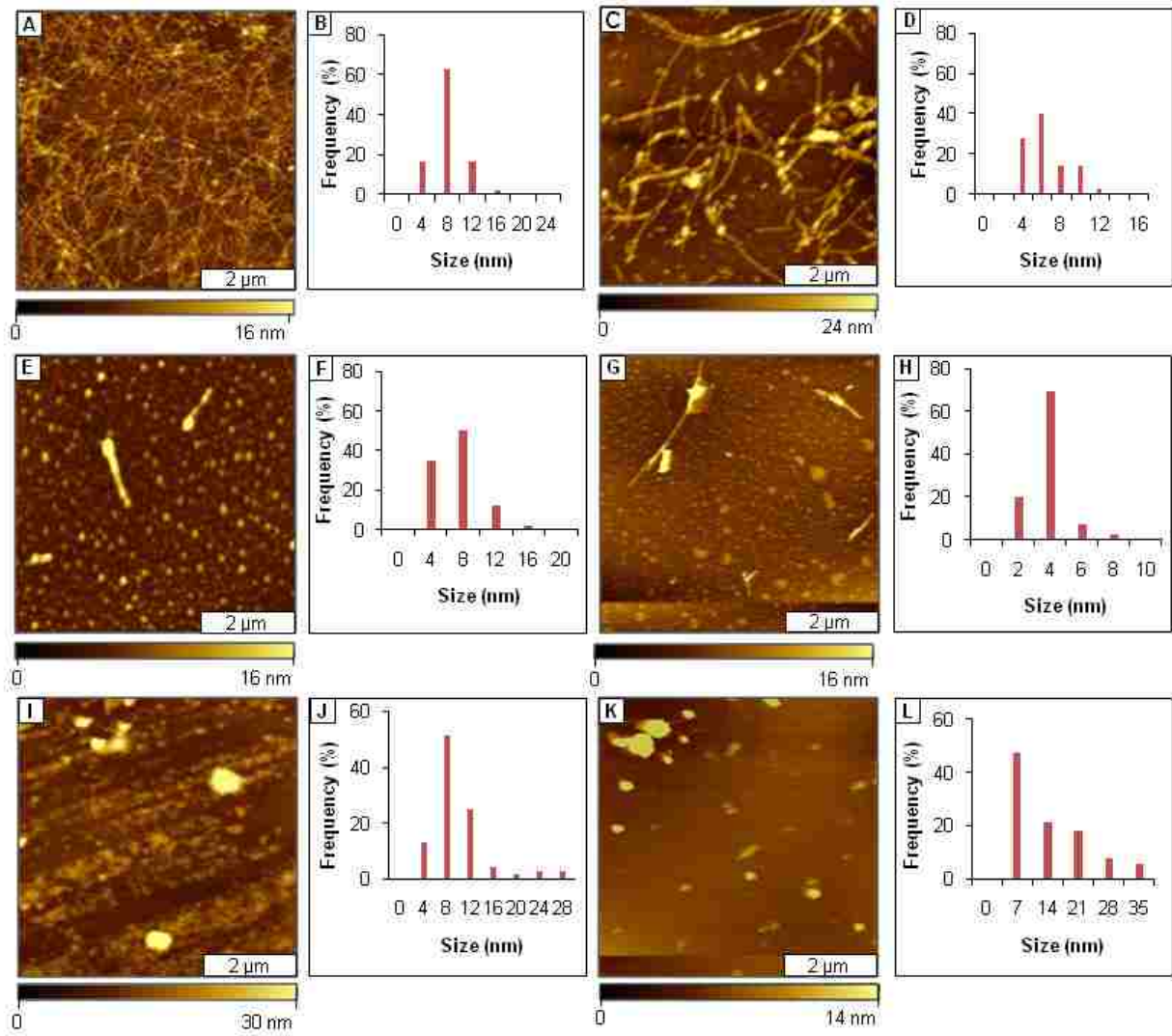


Figure 3.10. Disassembly of $\text{A}\beta_{1-40}$ preformed fibrils. [A] $\text{A}\beta_{1-40}$ fibrils; [B] Corresponding histogram; [C] Fibrils/protofibrils formed as a result of fibril disassembly by AAMP-0; [D] Height analysis for C; [E] Spherical aggregates induced by AAMP-1 fibril disassembly; [F] Height histogram analysis for E; [G] Spherical particles formed by AAMP-2 fibril disassembly; [H] Height analysis for G; [I] Spherical aggregates from disassembly by AAMP-3; [J] Corresponding height analysis; [K] Spherical assemblies formed from fibril disassembly by AAMP-4; [L] Height histogram for K

Nonfibrillar assemblies and a few isolated fibrillar structures were the main structures observed from $\text{A}\beta_{40}$ fibril disassembly by AAMP-1 (Figure 3.10E), with three $\alpha\alpha$ AAs. The same result (nonfibrillar assemblies) was also observed with AAMP-2 (Figure 3.10G), AAMP-3

(Figure 3.10I), and AAMP-4 (Figure 3.10K), incorporating two $\alpha\alpha$ AAs as compared to AAMP-1. In addition to observing nonfibrillar assemblies, isolated protofibrils (beaded morphology) and fibrils (smooth) were detected in these mixtures. The height distribution reveals that most of the particles formed were less than 10 nm in height (Figure 3.10D, 3.10F, 3.10H, 3.10J, and 3.10L). Coincidentally, these same AAMPs showed up to 80% reduction in ThT fluorescence. Thus, $\alpha\alpha$ AAs play a role in disassembly of preformed fibrils as seen from fibrils being the predominant species formed with AAMP-0 (no $\alpha\alpha$ AAs) as compared to nonfibrillar assemblies formed with $\alpha\alpha$ AA-containing AAMPs (for example AAMP-1, AAMP-2 etc). This is consistent with the ThT fluorescence observations. Significant also, was the increased heights of isolated fibrils formed by disassembly of preformed fibrils by $\alpha\alpha$ AA-containing AAMPs as compared to either $A\beta_{1-40}$ fibrils or AAMP-0 (Table 3.3). This may suggest that $\alpha\alpha$ AAMPs binds to fibrils or cause the fibrils to coalesce resulting in increased heights.

Disassembly by AAMPs with one $\alpha\alpha$ AA resulted in mixtures of spherical particles and protofibrils/fibrils. For instance, spherical particles and isolated fibrils/protofibrils were formed from $A\beta_{1-40}$ fibril disassembly by AAMP-5 (Figure 3.11A), AAMP-7 (Figure 3.11E) and AAMP-8 (Figure 3.11G). In contrast, disassembly of performed fibrils by AAMP-6 formed mainly fibrillar structures (Figure 3.11C) that exhibited a beaded morphology and a periodicity characteristic of protofibrils.

The spherical particles observed from disassembly by AAMP-7 and AAMP-8 is larger assemblies as compared to AAMP-5, as shown the height analysis (Figure 8B, 8F, and 8H). Surprisingly, similar trends were observed for the assembly of $A\beta_{1-40}$ in the presence of these AAMPs. Thus, aromaticity (AAMP-7) and steric effects (AAMP-8) play a part in the disassembly process. Isolated protofibrils/fibrils observed along with spherical particles for

AAMP-7 and AAMP-8, were shorter in length and in some with beaded morphology as compared to $\text{A}\beta_{1-40}$ fibrils. Also, the protofibrils/fibrils formed by AAMP-6 were shorter and with beaded morphology but with similar height distribution (Figure 3.11D) and mean height (Table 3.3) as compared to $\text{A}\beta_{1-40}$ fibrils. This suggests that these AAMPs induced partial disassembly or fibril breakage of preformed fibrils forming protofibrils (beaded morphology) and short fibrils with mean heights matching those of $\text{A}\beta_{1-40}$ fibrils (Table 3.3). The partial disassembly of $\text{A}\beta_{1-40}$ preformed fibrils and disruption of fibril formation by AAMP-6 shows that positioning of $\alpha\alpha$ AAs relative to KLVFF influences both disassembly and assembly processes.

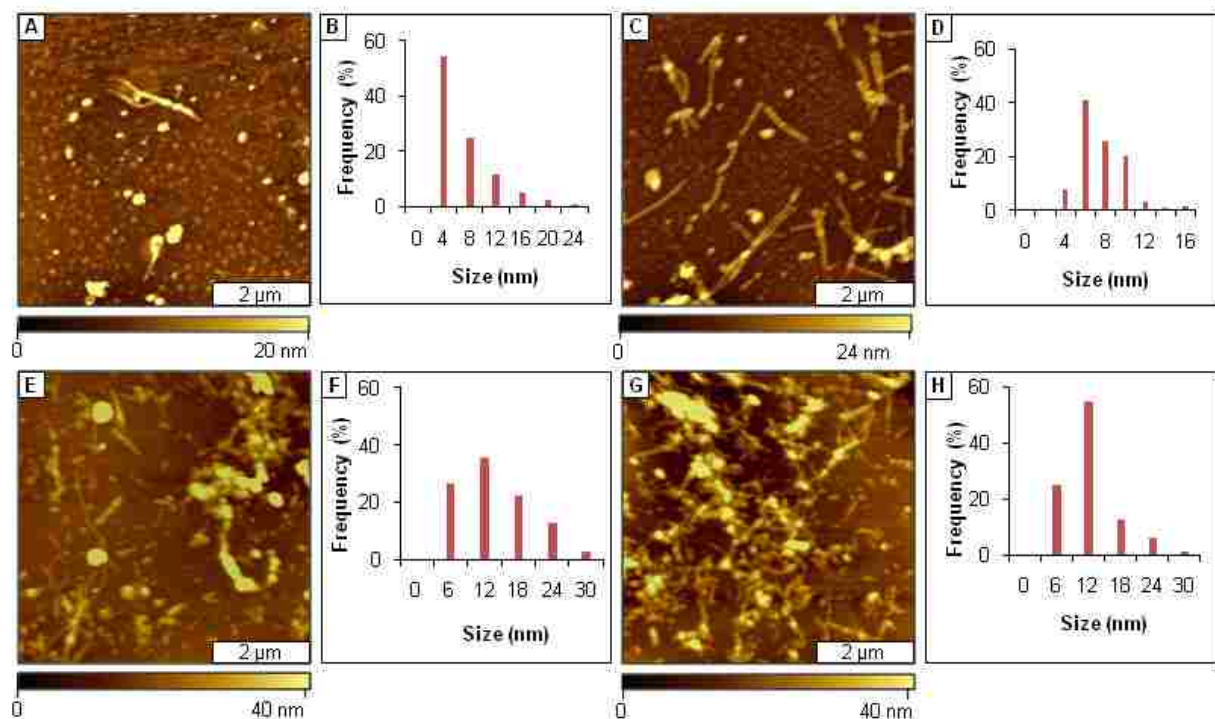


Figure 3.11. Disassembly of $\text{A}\beta_{1-40}$ preformed fibrils [A] Spherical aggregates induced by AAMP-5 fibril disassembly; [B] Height histogram analysis for A; [C] Fibrils/prototibrils formed as a result of fibril disassembly by AAMP-6; [D] Height analysis for C; [E] Spherical aggregates from disassembly by AAMP-7; [F] Corresponding height analysis; [G] Spherical assemblies formed from fibril disassembly by AAMP-8; [H] Height histogram for G.

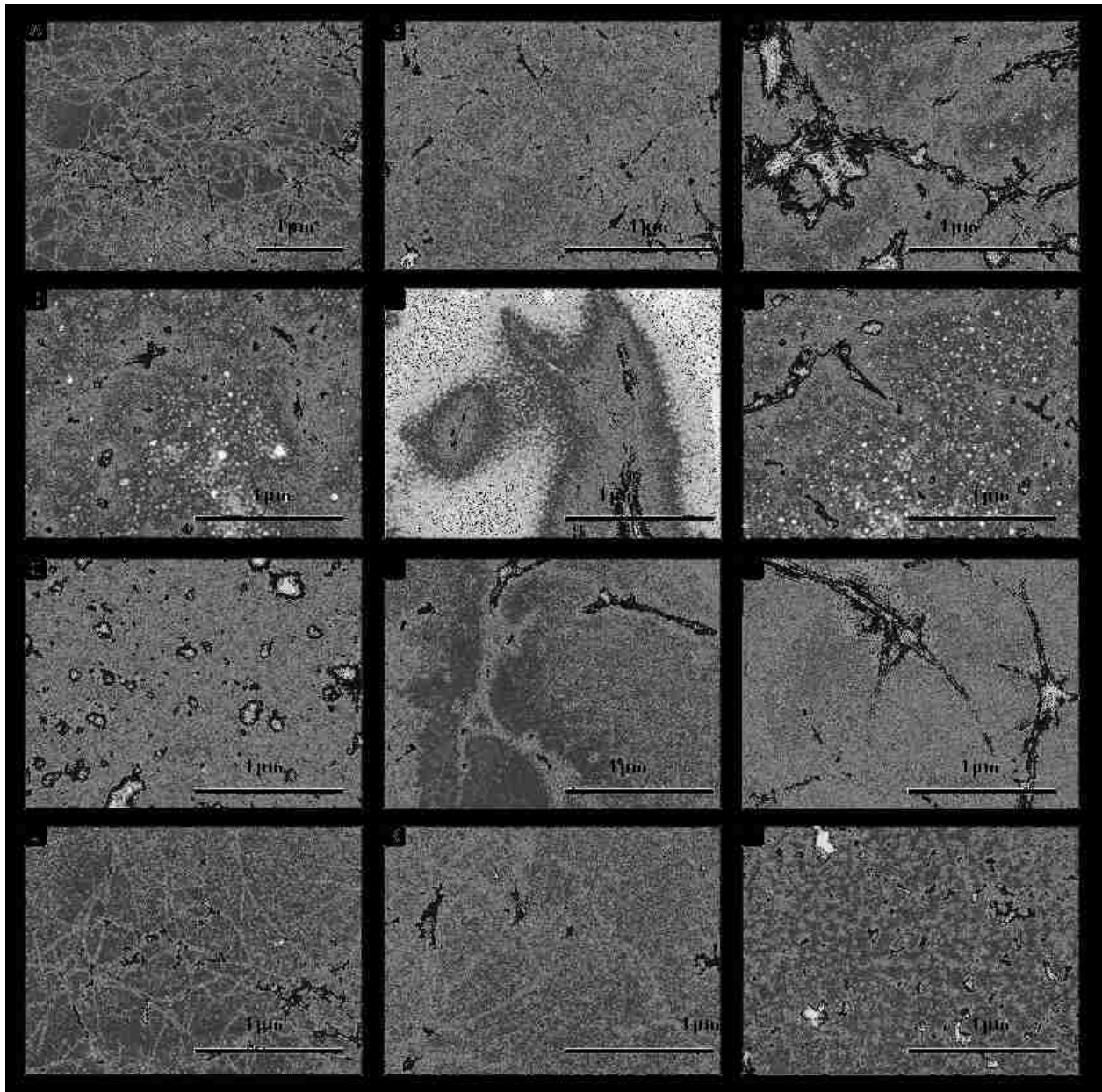


Figure 3.12 Disassembly of $\text{A}\beta_{1-40}$ preformed fibrils. [A] $\text{A}\beta_{1-40}$ preformed fibrils; [B]; $\text{A}\beta_{1-40}$ preformed fibrils zoom in view; [C] Fibrils disassembly by AAMP-0; [D] Mixtures of spherical aggregates and isolated fibrils formed from disassembly by AAMP-1; [E] Isolated short fibrils formed from disassembly by AAMP-2; [F] Mixtures of spherical aggregates and isolated fibrils formed from disassembly by AAMP-3; [G] View of only spherical aggregates formed from disassembly by AAMP-3; [H] Isolated fibrils formed from disassembly by AAMP-4; [I] Mixture of spherical aggregates and fibrils formed from disassembly by AAMP-5; [J] Fibrils formed from disassembly by AAMP-6; [K] Isolated fibrils formed from disassembly by AAMP-7; [L] Spherical particles formed by AAMP-8.

The observed disassembly of preformed fibrils into either oligomeric, or prefibrillar particles (precursors of fibril formation) indicates a shift in equilibrium. It has been shown that fibrils elongate by monomer addition to the fibril ends. Therefore, disassembly of fibrils suggests that AAMP possibly binds at the fibril end which shifts the thermodynamic equilibrium back towards oligomeric (AAMP-5, AAMP-7 and AAMP-8) and protofibrillar (AAMP-6) assemblies. Even in cases where fibrils/protofibrils were observed, the surface coverage was profoundly reduced as compared with the dense network of $\text{A}\beta_{1-40}$ fibrils, suggesting some amount of disassembly occurred.

3.3.3.3 Morphology of Structures Formed from Disassembly of Preformed Fibrils by Various AAMPs as Determined Using TEM.

Negatively stained samples of $\text{A}\beta_{1-40}$ pre-formed fibrils or those mixed with various AAMPs prepared at the same time as those of AFM and ThT were examined using TEM to confirm the various morphologies observed with AFM. The morphology of $\text{A}\beta_{1-40}$ pre-formed fibrils and structures resulting from disassembly by the various AAMPs observed after 24 hr aging (Figure 3.12) were consistent with AFM observations. For instance, $\text{A}\beta_{1-40}$ sample showed a typical appearance of amyloid fibrils, shown as a dense network of fibrils extending several microns in length. In contrast, $\text{A}\beta_{1-40}/\text{AAMP}$ mixtures reveal disassembly of $\text{A}\beta_{1-40}$ fibrils yielding particles with different morphologies.

Our study validates the use of $\alpha\alpha$ AAs as disrupting elements when incorporated into the KLVFF motif for designing amyloid aggregation mitigating peptides, as indicated by the absence of fibrillar assemblies in comparison to the control peptide (AAMP-0). We showed that the side chain interactions associated with the various $\alpha\alpha$ AAs are important in disrupting fibril formation. A major finding was that the mitigators incorporating one $\alpha\alpha$ AA were as effective in

disrupting A β ₁₋₄₀ fibril formation as the ones with two or three $\alpha\alpha$ AAs. Thus, these findings support our efforts to reduce the overall molecular weight of the peptide without affecting its efficacy for optimal *in vivo* use and improved systemic bioavailability.

Interestingly, we found that the mitigators, which disrupted fibril formation, also disassembled fibrils. This suggests the existence of an equilibrium between A β ₁₋₄₀ monomers/dimers and fibrils. Molecular dynamic simulations have been employed to study the mechanism of how these mitigators interact and disassemble fibrils.^{63, 65, 66} Recently, Yassmine et al showed through simulation the disassembly of A β ₁₆₋₂₂ protofibril by N-methylated inhibitors.⁶⁷ They reported that N-methylated inhibitors interact with the protofibril by both lateral and longitudinal association, thereby disrupting the β -sheet extension and its lateral association into layers. More importantly, they showed that the inhibitor peptides intercalate and possibly sequester the A β peptides, which we believe to be the mode of action for our designed $\alpha\alpha$ AA-AAMPs in disrupting A β ₁₋₄₀ fibrillogenesis. This is also true based on Tycko's structural model,⁶⁸ where we hypothesize that the interaction of $\alpha\alpha$ AA-AAMPs with A β ₁₋₄₀ at the region 17-20 disrupts the "bend" segment between the two β -strands, affecting β -sheet extension and packing during fibril formation.

The formation of oligomeric assemblies, as shown in computer simulations and experimental data, proceeds via two steps. The initial step is coalescence driven by the rapid formation of nonspecific hydrophobic interactions. This is followed by a conformational conversion to ordered β -sheet structures because of the slow formation of highly directional, interchain hydrogen bonds. Competition between hydrophobic interactions and hydrogen bonding is important for determining the morphology of aggregates that formed. Aging conditions can affect hydrogen bonding interactions to yield both fibrillar and non-fibrillar

assemblies with different morphologies but with the same β -sheet content. Based on our design strategy, we hypothesized that AAMPs bind $A\beta_{1-40}$ and block one face of aggregation, which affects the formation of hydrogen bonding interchains and takes $A\beta_{1-40}$ fibrillogenesis off the normal aggregation pathway. This favors hydrophobic interactions over hydrogen bonding and results in nonfibrillar assemblies.

One possible application of our findings is that $\alpha\alpha$ AAs can be used to control neuronal toxicity from $A\beta$ species. Neurotoxicity is believed to be a result of aberrant interactions between cellular components such as membranes, protasomes and/or molecular chaperons, and solvent-exposed hydrophobic surfaces of oligomeric assemblies. The size of aggregates affects these interactions, with the highest toxicity resulting from aggregates with a high surface area to volume ratio. This explains why fibrils and, to some extent, large oligomers are not very toxic compared to small oligomeric assemblies. We showed that position, distribution, and side chain functionality of $\alpha\alpha$ AAs incorporated in the binding core affects the size of the resulting assemblies. Thus, we can use $\alpha\alpha$ AAs to influence the desired size of aggregates formed, in hopes of controlling neurotoxicity.⁶⁹⁻⁷¹ Future cytotoxic experiments will be carried out to validate this hypothesis.

3.4 Conclusion

Experiments consistently demonstrate that mixtures with more than 50% $A\beta$ aggregation mostly likely contain fibrillar assemblies. This is an important observation because there are some reports that thioflavin-T binding yields ambiguous results. By comparing our $\alpha\alpha$ AAs-containing mitigators with the control peptide (no $\alpha\alpha$ AAs), we showed the effectiveness of $\alpha\alpha$ AAs as disrupting elements. Furthermore, we also showed that mitigators with one $\alpha\alpha$ AAs

were as effective as those with two or three, depending on their position. This is important because it helps us achieve our goal of reducing the molecular weight of the initial mitigator AAMP-1 but still maintain/enhance its mitigating properties.

We have demonstrated that AAMP-1, AAMP-2, AAMP-3, AAMP-4, AAMP-5, AAMP-7 and AAMP-8, which disrupted fibril formation, also disassembled fibrils forming nonfibrillar assemblies. We also showed that AAMP-0 and AAMP-5 not only mitigated $\text{A}\beta_{1-40}$ fibril formation yielding fibrils with a different morphology, but also disassembled preformed fibrils, forming fibrillar assemblies with similar morphologies to those of protofibrils. This is proof that there exists an equilibrium between $\text{A}\beta_{1-40}$ monomers/dimers and fibrils.

Mitigators incubated alone slowly aggregated to yield spherical aggregates which may explain the unexpected toxicity observed with AAMP-1. However, CD spectra showed that after 7 days of aging the random coil conformation seen for monomers was unchanged. This suggests that peptides can oligomerize without changes to β -sheet conformation, a property of nearly all polypeptides. If the AAMPs alone aggregated, they are expected to act as seeds and enhance abeta aggregation into fibrils. However, AFM and TEM results suggest a different mechanism. We have shown earlier that AAMP-1 disrupt $\text{A}\beta_{1-40}$ aggregation by acting as co-surfactants. This has been supported by molecular dynamic simulations using N-methylated amino acids to intercalate and sequester $\text{A}\beta_{1-40}$ peptide. There are reports that relate the size of nanoparticles formed with the maximum toxicity exhibited by particles with high surface area to volume ratios. Number, side chain functionality, and distribution of $\alpha\alpha\text{AA}$ nucleates the size and morphology of $\text{A}\beta/\text{AAMP}$ products. This is a major finding because $\alpha\alpha\text{AAs}$ may be employed as a means to control the size of resulting nanoparticles and possibly neurotoxicity.

3.5 References

1. Hardy, J.; Selkoe, D. J., Medicine - The amyloid hypothesis of Alzheimer's disease: Progress and problems on the road to therapeutics. *Science* **2002**, 297 (5580), 353-356.
2. Selkoe, D. J., Alzheimer's disease is a synaptic failure. *Science* **2002**, 298 (5594), 789-791.
3. Selkoe, D. J., The molecular pathology of Alzheimer's disease. *Neuron* **1991**, 6 (4), 487-98.
4. Sengupta, P.; Garai, K.; Sahoo, B.; Shi, Y.; Callaway, D. J. E.; Maiti, S., The amyloid beta peptide (A beta(1-40)) is thermodynamically soluble at physiological concentrations. *Biochemistry* **2003**, 42 (35), 10506-10513.
5. Bieschke, J.; Zhang, Q. H.; Powers, E. T.; Lerner, R. A.; Kelly, J. W., Oxidative metabolites accelerate Alzheimer's amyloidogenesis by a two-step mechanism, eliminating the requirement for nucleation. *Biochemistry* **2005**, 44 (13), 4977-4983.
6. Harper, J. D.; Lansbury, P. T., Models of amyloid seeding in Alzheimer's disease and scrapie: Mechanistic truths and physiological consequences of the time-dependent solubility of amyloid proteins. *Annu. Rev. Biochem* **1997**, 66, 385-407.
7. Zhang, Q. H.; Powers, E. T.; Nieva, J.; Huff, M. E.; Dendle, M. A.; Bieschke, J.; Glabe, C. G.; Eschenmoser, A.; Wentworth, P.; Lerner, R. A.; Kelly, J. W., Metabolite-initiated protein misfolding may trigger Alzheimer's disease. *Proc. Natl. Acad. Sci. U. S. A.* **2004**, 101 (14), 4752-4757.
8. Selkoe, D. J., Translating cell biology into therapeutic advances in Alzheimer's disease. *Nature* **1999**, 399 (6738), A23-A31.
9. Lansbury, P. T., Jr., Inhibition of amyloid formation: a strategy to delay the onset of Alzheimer's disease. *Curr. Opin. Chem. Biol.* **1997**, 1 (2), 260-267.
10. Haass, C.; Selkoe, D. J., Soluble protein oligomers in neurodegeneration: lessons from the Alzheimer's amyloid beta -peptide. *Nat. Rev. Mol. Cell Biol.* **2007**, 8 (2), 101-112.
11. Hartley, D. M.; Walsh, D. M.; Ye, C. P. P.; Diehl, T.; Vasquez, S.; Vassilev, P. M.; Teplow, D. B.; Selkoe, D. J., Protofibrillar intermediates of amyloid beta-protein induce acute electrophysiological changes and progressive neurotoxicity in cortical neurons. *J. Neurosci.* **1999**, 19 (20), 8876-8884.
12. Lee, S.; Carson, K.; Rice-Ficht, A.; Good, T., Hsp20, a novel alpha-crystallin, prevents A beta fibril formation and toxicity. *Protein Sci.* **2005**, 14 (3), 593-601.
13. Stefani, M.; Dobson, C. M., Protein aggregation and aggregate toxicity: new insights into protein folding, misfolding diseases and biological evolution. *J. Mol. Med.* **2003**, 81 (11), 678-699.

14. Walsh, D. M.; Selkoe, D. J., Oligomers in the brain: The emerging role of soluble protein aggregates in neurodegeneration. *Protein Peptide Lett.* **2004**, *11* (3), 213-228.
15. Walsh, D. M.; Townsend, M.; Podlisny, M. B.; Shankar, G. M.; Fadeeva, J. V.; El Agnaf, O.; Hartley, D. M.; Selkoe, D. J., Certain inhibitors of synthetic amyloid beta -peptide (Abeta) fibrillogenesis block oligomerization of natural Abeta and thereby rescue long-term potentiation. [Erratum to document cited in CA143:090706]. *J. Neurosci.* **2005**, *25* (18), No pp given.
16. Walsh, D. M.; Townsend, M.; Podlisny, M. B.; Shankar, G. M.; Fadeeva, J. V.; El Agnaf, O.; Hartley, D. M.; Selkoe, D. J., Certain inhibitors of synthetic amyloid beta-peptide (A beta) fibrillogenesis block oligomerization of natural A beta and thereby rescue long-term potentiation (vol 25, pg 2455, 2005). *J. Neurosci.* **2005**, *25* (18), CP8-CP8.
17. Kornilova, A. Y.; Wolfe, M. S., Secretase inhibitors for Alzheimer's disease. In *Annu. Rep. Med. Chem.*, 2003; Vol. 38, pp 41-50.
18. Bard, F.; Cannon, C.; Barbour, R.; Burke, R. L.; Games, D.; Grajeda, H.; Guido, T.; Hu, K.; Huang, J. P.; Johnson-Wood, K.; Khan, K.; Kholodenko, D.; Lee, M.; Lieberburg, I.; Motter, R.; Nguyen, M.; Soriano, F.; Vasquez, N.; Weiss, K.; Welch, B.; Seubert, P.; Schenk, D.; Yednock, T., Peripherally administered antibodies against amyloid beta-peptide enter the central nervous system and reduce pathology in a mouse model of Alzheimer disease. *Nat. Med.* **2000**, *6* (8), 916-919.
19. Bard, F.; Barbour, R.; Cannon, C.; Carretero, R.; Fox, M.; Games, D.; Guido, T.; Hoenow, K.; Hu, K.; Johnson-Wood, K.; Khan, K.; Kholodenko, D.; Lee, C.; Lee, M.; Motter, R.; Nguyen, M.; Reed, A.; Schenk, D.; Tang, P.; Vasquez, N.; Seubert, P.; Yednock, T., Epitope and isotype specificities of antibodies to beta-amyloid peptide for protection against Alzheimer's disease-like neuropathology. *Proc. Natl. Acad. Sci. U. S. A.* **2003**, *100* (4), 2023-2028.
20. Dodart, J. C.; Bales, K. R.; Gannon, K. S.; Greene, S. J.; DeMattos, R. B.; Mathis, C.; DeLong, C. A.; Wu, S.; Wu, X.; Holtzman, D. M.; Paul, S. M., Immunization reverses memory deficits without reducing brain A beta burden in Alzheimer's disease model. *Nat. Neurosci.* **2002**, *5* (5), 452-457.
21. Komatsu, M.; Waguri, S.; Chiba, T.; Murata, S.; Iwata, J.; Tanida, I.; Ueno, T.; Koike, M.; Uchiyama, Y.; Kominami, E.; Tanaka, K., Loss of autophagy in the central nervous system causes neurodegeneration in mice. *Nature* **2006**, *441* (7095), 880-884.
22. Cohen, E.; Bieschke, J.; Perciavalle, R. M.; Kelly, J. W.; Dillin, A., Opposing activities protect against age-onset proteotoxicity. *Science* **2006**, *313* (5793), 1604-1610.
23. Hara, T.; Nakamura, K.; Matsui, M.; Yamamoto, A.; Nakahara, Y.; Suzuki-Migishima, R.; Yokoyama, M.; Mishima, K.; Saito, I.; Okano, H.; Mizushima, N., Suppression of basal autophagy in neural cells causes neurodegenerative disease in mice. *Nature* **2006**, *441* (7095), 885-889.
24. Findeis, M. A., Approaches to discovery and characterization of inhibitors of amyloid beta -peptide polymerization. *Biochim. Biophys. Acta, Mol. Basis Dis.* **2000**, *1502* (1), 76-84.

25. Tjernberg, L. O.; Naslund, J.; Lindqvist, F.; Johansson, J.; Karlstrom, A. R.; Thyberg, J.; Terenius, L.; Nordstedt, C., Arrest of beta-amyloid fibril formation by a pentapeptide ligand. *J. Biol. Chem.* **1996**, *271* (15), 8545-8.
26. Liu, R. T.; McAllister, C.; Lyubchenko, Y.; Sierks, M. R., Residues 17-20 and 30-35 of beta-amyloid play critical roles in aggregation. *J. Neurosci. Res.* **2004**, *75* (2), 162-171.
27. Lowe, T. L.; Strzelec, A.; Kiessling, L. L.; Murphy, R. M., Structure-Function Relationships for Inhibitors of b-Amyloid Toxicity Containing the Recognition Sequence KLVFF. *Biochemistry* **2001**, *40* (26), 7882-7889.
28. Pallitto, M. M.; Ghanta, J.; Heinzelman, P.; Kiessling, L. L.; Murphy, R. M., Recognition sequence design for peptidyl modulators of beta-amyloid aggregation and toxicity. *Biochemistry* **1999**, *38* (12), 3570-3578.
29. Lowe, T. L.; Strzelec, A.; Kiessling, L. L.; Murphy, R. M., Structure-function relationships for inhibitors of beta-amyloid toxicity containing the recognition sequence KLVFF. *Biochemistry* **2001**, *40* (26), 7882-7889.
30. Ghanta, J.; Shen, C.-L.; Kiessling, L. L.; Murphy, R. M., A strategy for designing inhibitors of b-amyloid toxicity. *J. Biol. Chem.* **1996**, *271* (47), 29525-29528.
31. Gordon, D. J.; Tappe, R.; Meredith, S. C., Design and characterization of a membrane permeable N-methyl amino acid-containing peptide that inhibits A β .1-40 fibrillogenesis. *J. Pept. Res.* **2002**, *60* (1), 37-55.
32. Gordon, D. J.; Sciarretta, K. L.; Meredith, S. C., Inhibition of β -Amyloid(40) Fibrillogenesis and Disassembly of β -Amyloid(40) Fibrils by Short β -Amyloid Congeners Containing N-Methyl Amino Acids at Alternate Residues. *Biochemistry* **2001**, *40* (28), 8237-8245.
33. Gordon, D. J.; Tappe, R.; Meredith, S. C., Design and characterization of a membrane permeable N-methyl amino acid-containing peptide that inhibits A β 1-40 fibrillogenesis,. *J. Pept. Res.* **2002**, *60* (1), 37-55.
34. Bieschke, J.; Siegel, S. J.; Fu, Y. W.; Kelly, J. W., Alzheimer's A beta peptides containing an isostructural backbone mutation afford distinct aggregate morphologies but analogous cytotoxicity. Evidence for a common low-abundance toxic Structure(s). *Biochemistry* **2008**, *47* (1), 50-59.
35. Fu, Y. W.; Gao, J. M.; Bieschke, J.; Dendle, M. A.; Kelly, J. W., Amide-to-E-olefin versus amide-to-ester backbone H-bond perturbations: Evaluating the O-O repulsion for extracting H-bond energies. *J. Am. Chem. Soc.* **2006**, *128* (50), 15948-15949.
36. Soto, C.; Sigurdsson, E. M.; Morelli, L.; Kumar, R. A.; Castano, E. M.; Frangione, B., beta-sheet breaker peptides inhibit fibrillogenesis in a rat brain model of amyloidosis: Implications for Alzheimer's therapy. *Nat. Med.* **1998**, *4* (7), 822-826.

37. Etienne, M. A.; Aucoin, J. P.; Fu, Y.; McCarley, R. L.; Hammer, R. P., Stoichiometric Inhibition of Amyloid beta -Protein Aggregation with Peptides Containing Alternating alpha ,alpha -Disubstituted Amino Acids. *J. Am. Chem. Soc.* **2006**, 128 (11), 3522-3523.
38. Etienne, M. A.; Aucoin, J. P.; Fu, Y. W.; McCarley, R. L.; Hammer, R. P., Stoichiometric inhibition of amyloid beta-protein aggregation with peptides containing alternating alpha,alpha-disubstituted amino acids. *J. Am. Chem. Soc.* **2006**, 128 (11), 3522-3523.
39. Fu, Y. W.; Hammer, R. P., Efficient acylation of the N-terminus of highly hindered C-alpha,C-alpha-disubstituted amino acids via amino acid symmetrical anhydrides. *Org. Lett.* **2002**, 4 (2), 237-240.
40. Fu, Y. W.; Hammarstrom, L. G. J.; Miller, T. J.; Fronczek, F. R.; McLaughlin, M. L.; Hammer, R. P., Sterically hindered C-alpha,C-alpha-disubstituted alpha-amino acids: Synthesis from alpha-nitroacetate and incorporation into peptides. *J. Org. Chem.* **2001**, 66 (21), 7118-7124.
41. Fu, Y. W.; Etienne, M. A.; Hammer, R. P., Facile synthesis of alpha,alpha-diisobutylglycine and anchoring its derivatives onto PAL-PEG-PS resin. *J. Org. Chem.* **2003**, 68 (25), 9854-9857.
42. Etienne, M. A.; Edwin, N. J.; Aucoin, J. P.; Russo, P. S.; McCarley, R. L.; Hammer, R. P., beta -Amyloid protein aggregation. *Methods Mol. Biol. (Totowa, NJ, U. S.)* **2007**, 386 (Peptide Characterization and Application Protocols), 203-225.
43. Pavone, V.; Lombardi, A.; Saviano, M.; De Simone, G.; Nastri, F.; Maglio, O.; Omote, Y.; Yamanaka, Y.; Yamada, T., Conformational behavior of C-alpha,C-alpha-diphenyl glycine: Extended conformation in tripeptides containing consecutive D phi G residues. *Biopolymers* **2000**, 53 (2), 161-168.
44. Toniolo, C.; Crisma, M.; Formaggio, F.; Peggion, C., Control of peptide conformation by the Thorpe-Ingold effect (C-alpha-tetrasubstitution). *Biopolymers* **2001**, 60 (6), 396-419.
45. Nilsson, M. R., Techniques to study amyloid fibril formation in vitro. *Methods* **2004**, 34 (1), 151-160.
46. Wood, S. J.; Maleeff, B.; Hart, T.; Wetzel, R., Physical, Morphological and Functional Differences between pH 5.8 and 7.4 Aggregates of the Alzheimer's Amyloid Peptide A [beta]. *J. Mol. Biol.* **1996**, 256 (5), 870-877.
47. Harper, J. D.; Lieber, C. M.; Lansbury, P. T., Atomic force microscopic imaging of seeded fibril formation and fibril branching by the Alzheimer's disease amyloid-beta protein. *Chemistry & Biology* **1997**, 4 (12), 951-959.
48. Legleiter, J.; Czilli, D. L.; Gitter, B.; DeMattos, R. B.; Holtzman, D. M.; Kowalewski, T., Effect of different anti-A beta antibodies on A beta fibrillogenesis as assessed by atomic force microscopy. *J. Mol. Biol.* **2004**, 335 (4), 997-1006.

49. Goldsbury, C.; Kistler, J.; Aebi, U.; Arvinte, T.; Cooper, G. J. S., Watching amyloid fibrils grow by time-lapse atomic force microscopy. *J. Mol. Biol.* **1999**, 285 (1), 33-39.
50. Harper, J. D.; Wong, S. S.; Lieber, C. M.; Lansbury, P. T., Assembly of A beta amyloid protofibrils: An in vitro model for a possible early event in Alzheimer's disease. *Biochemistry* **1999**, 38 (28), 8972-8980.
51. Liu, R. T.; Yuan, B.; Emadi, S.; Zameer, A.; Schulz, P.; McAllister, C.; Lyubchenko, Y.; Goud, G.; Sierks, M. R., Single chain variable fragments against beta-amyloid (A beta) can inhibit A beta aggregation and prevent A beta-induced neurotoxicity. *Biochemistry* **2004**, 43 (22), 6959-6967.
52. Kad, N. M.; Myers, S. L.; Smith, D. P.; Smith, D. A.; Radford, S. E.; Thomson, N. H., Hierarchical assembly of beta(2)-microglobulin amyloid in vitro revealed by atomic force microscopy. *J. Mol. Biol.* **2003**, 330 (4), 785-797.
53. Anon, *Peptide Characterization and Application Protocols. Methods in Molecular Biology*, 386 edited by Gregg B. Fields. 2007; Vol. 129, p 14104.
54. Laczkó, I.; Vass, E.; Soos, K.; Fulop, L.; Zarandi, M.; Penke, B., Aggregation of A beta(1-42) in the presence of short peptides: conformational studies. *J. Pept. Sci.* **2008**, 14 (6), 731-741.
55. Li, Q.; Gordon, M.; Etienne Marcus, A.; Hammer Robert, P.; Morgan, D., Contrasting in vivo effects of two peptide-based amyloid-beta protein aggregation inhibitors in a transgenic mouse model of amyloid deposition. *Cell Transplant* **2008**, 17 (4), 397-408.
56. Ionescu-Zanetti, C.; Khurana, R.; Gillespie, J. R.; Petrick, J. S.; Trabachino, L. C.; Minert, L. J.; Carter, S. A.; Fink, A. L., Monitoring the assembly of Ig light-chain amyloid fibrils by atomic force microscopy. *Proc. Natl. Acad. Sci. U. S. A.* **1999**, 96 (23), 13175-13179.
57. Ward, R. V.; Jennings, K. H.; Jepras, R.; Neville, W.; Owen, D. E.; Hawkins, J.; Christie, G.; Davis, J. B.; George, A.; Karran, E. H.; Howlett, D. R., Fractionation and characterization of oligomeric, protofibrillar and fibrillar forms of beta-amyloid peptide. *Biochem. J.* **2000**, 348, 137-144.
58. Khurana, R.; Ionescu-Zanetti, C.; Pope, M.; Li, J.; Nielson, L.; Ramirez-Alvarado, M.; Regan, L.; Fink, A. L.; Carter, S. A., A general model for amyloid fibril assembly based on morphological studies using atomic force microscopy. *Biophys. J.* **2003**, 85 (2), 1135-1144.
59. Gazit, E., A possible role for pi-stacking in the self-assembly of amyloid fibrils. *FASEB J.* **2002**, 16 (1), 77-83.
60. Gazit, E., Mechanisms of amyloid fibril self-assembly and inhibition. *FEBS J.* **2005**, 272 (23), 5971-5978.

61. Gordon, D. J.; Meredith, S. C., Probing the role of backbone hydrogen bonding in beta-amyloid fibrils with inhibitor peptides containing ester bonds at alternate positions. *Biochemistry* **2003**, *42* (2), 475-485.
62. Carulla, N.; Caddy, G. L.; Hall, D. R.; Zurdo, J.; Gairi, M.; Feliz, M.; Giralt, E.; Robinson, C. V.; Dobson, C. M., Molecular recycling within amyloid fibrils. *Nature* **2005**, *436* (7050), 554-558.
63. Soto, P.; Griffin Mary, A.; Shea, J.-E., New insights into the mechanism of Alzheimer amyloid-beta fibrillogenesis inhibition by N-methylated peptides. *Biophys J* **2007**, *93* (9), 3015-25.
64. Sato, T.; Kienlen-Campard, P.; Ahmed, M.; Liu, W.; Li, H. L.; Elliott, J. I.; Aimoto, S.; Constantinescu, S. N.; Octave, J. N.; Smith, S. O., Inhibitors of amyloid toxicity based on beta-sheet packing of A beta 40 and A beta 42. *Biochemistry* **2006**, *45* (17), 5503-5516.
65. Tjernberg, L. O.; Lilliehook, C.; Callaway, D. J. E.; Naslund, J.; Hahne, S.; Thyberg, J.; Terenius, L.; Nordstedt, C., Controlling amyloid beta-peptide fibril formation with protease-stable ligands. *J. Biol. Chem.* **1997**, *272* (19), 12601-12605.
66. Chen, Z. J.; Krause, G.; Reif, B., Structure and orientation of peptide inhibitors bound to beta-amyloid fibrils. *J. Mol. Biol.* **2005**, *354* (4), 760-776.
67. Chebaro, Y.; Derreumaux, P., Targeting the early steps of Abeta 16-22 protofibril disassembly by N-methylated inhibitors: a numerical study. *Proteins: Struct., Funct., Bioinf.* **2009**, *75* (2), 442-452.
68. Tycko, R., Insights into the amyloid folding problem from solid-state NMR. *Biochemistry* **2003**, *42* (11), 3151-3159.
69. Raman, B.; Chatani, E.; Kihara, M.; Ban, T.; Sakai, M.; Hasegawa, K.; Naiki, H.; Rao, C. M.; Goto, Y., Critical balance of electrostatic and hydrophobic interactions is required for beta(2)-microglobulin amyloid fibril growth and stability. *Biochemistry* **2005**, *44* (4), 1288-1299.
70. Mu, Y.; Gao, Y. Q., Effects of hydrophobic and dipole-dipole interactions on the conformational transitions of a model polypeptide. *J. Chem. Phys.* **2007**, *127* (10).
71. Kim, W.; Hecht, M. H., Generic hydrophobic residues are sufficient to promote aggregation of the Alzheimer's A beta 42 peptide. *Proc. Natl. Acad. Sci. U. S. A.* **2006**, *103* (43), 15824-15829.

CHAPTER 4

EFFECTS OF TERMINAL MODIFICATIONS OF PEPTIDES DERIVED FROM A β CENTRAL HYDROPHOBIC CORE ON A β_{1-40} -PEPTIDE AGGREGATE SIZE AND MORPHOLOGY

4.1 Introduction

A standing hypothesis associated with Alzheimer's Disease (AD) is that aggregation of monomeric β -amyloid ($A\beta$) fibrils into neurotoxic misfolded forms is the key event associated with the disease pathogenesis.¹⁻³ Recently, extensive investigation of the aggregation pathway reveals that oligomeric assemblies and not mature fibrils are responsible for $A\beta$ neurotoxicity.⁴⁻⁸ Several approaches have been designed to target the $A\beta$ assembly process in an effort to reduce toxic species in the brain. Peptide-based approaches in particular, are increasingly becoming a vital constituent of new therapeutics because of their high specificity and low toxicity as compared to small organic molecules.⁹

Several groups have developed amyloid aggregation mitigating peptides (AAMPs) based on designed changes to the $A\beta_{16-20}$ central hydrophobic core, KLVFF fragment, which Tjenberg^{10, 11} showed to be critical for $A\beta$ self-assembly and self-recognition. To the KLVFF core, a "disrupter" group is added that solubilizes either inhibitor- $A\beta$ aggregates or blocks further addition of β -sheets through hydrogen bonding. Disrupters that have been added to peptides can be classified as N- or C-terminal modifications,¹² conformationally constrained amino acids,¹³ peptide backbone modifications,¹⁴ or the use of D-amino acids.¹⁵

An example for N- or C-terminal modifications was the addition of oligolysine chains to the C-terminus of the KLVFF motif to design peptide KLVFFKKKKKK that was shown to enhance the rate of $A\beta_{1-40}$ aggregation into fibrils and thereby prevent toxicity against PC12 cells.^{12, 16} Also, the rate of $A\beta$ assembly into fibrils was shown to depend on the number of lysine

groups present in the mitigator. Several modifications of the peptide backbone for the KLVFF binding motif have been reported. These include replacement of amide hydrogen with methyl groups,^{14, 17} and replacement of the amide bond with either an ester bond¹⁸ or isostructural E-olefin.¹⁹ These modifications were designed to block proliferation of hydrogen bonding between β -sheets that is necessary for A β fibrillization. Peptides derived from these modifications were found to disrupt A β ₁₋₄₀ fibril formation and to disassemble pre-formed fibrils. For instance, *N*-methylated peptide A β 16-22m¹⁴ and esterified A β 16-20e¹⁸ disrupted fibril formation and caused the disassembly of pre-formed fibrils. Also, it was demonstrated that mutations of the Phe19-Phe20 amide bond of A β ₁₋₄₀ with an E-olefin bond exclusively produced spherical aggregates and fibrillization was not detected despite incubation periods of up to 6 weeks.^{19, 20}

Conformationally constrained peptides have been shown to be effective at disrupting A β fibril formation through unfavorable steric interactions. For instance, a β -sheet breaker peptide, iA β 5 containing one proline residue was shown to disrupt fibril formation, disassemble pre-formed fibrils and protect against neurotoxicity.²¹ Our approach for this report involves replacing the hydrogen atom of the α -carbon of natural amino acid residues in the KLVFF motif with an alkyl substituent. Thus, the conformational freedom of the peptide is restricted and it is forced to adopt an extended conformation that is ideal for interaction with A β ₁₋₄₀. Peptides in an extended conformation form two faces where one face is available for interaction with A β , while the other is sterically blocked, limiting β -sheet extensions required for amyloid fibril propagation.

Apart from blocking hydrogen bonding between β -sheets, incorporation of $\alpha\alpha$ AAs within the KLVFF motif also increases the overall hydrophobicity of the mitigator peptide and in turn strengthens the hydrophobic interactions with A β ₁₋₄₀ target. Polar groups are normally

added to the highly hydrophobic $\alpha\alpha$ AAs-containing KLVFF core to increase the overall solubility of the peptide. Also, modification of the α -carbon helps to decrease susceptibility of the mitigator to proteolytic degradation, which will ensure effective delivery of the inhibitor to the target organ during *in vivo* studies. In general, our design for mitigators combines the advantages of both *C*-terminal and α -carbon modification.

We have previously developed a mitigator peptide (AMY-1) with *C*-terminal oligolysine chain (KDibgVDbgFDpgK₆) and a peptide (AMY-2) with an *N*-terminal oligolysine chain (K₇KDibgVDbgFDpg). Both mitigator peptides AMY-1 and AMY-2 disrupted fibril formation and formed spherical aggregates of different heights.²² For optimal use *in vivo* and improved systemic bioavailability, the charge and molecular weight of the mitigator should be greatly reduced. Incorporation of one or two $\alpha\alpha$ AAs in the KLVFF binding motif was previously shown to be as effective at disrupting A β ₁₋₄₀ fibrillization as compared to the original peptide (AAMP-1) with three $\alpha\alpha$ AAs. Herein, effects of forming A β fibrils in the presence of (define acronym) AAMPs incorporating different polar solubilizing groups (*C*- or *N*-terminal) are studied, in an effort to evaluate the effectiveness of reducing the overall charge of the mitigator. Also, the effects of $\alpha\alpha$ AA-containing AAMPs with fewer polar groups as compared to the original mitigator AAMP-1 with six Lys are presented.

Peptide analogs modified with α -amino isobutyric acid (also called α -methyl alanine) have been shown to be more effective at inducing disassembly of A β fibrils than either L-proline or D-amino acids in short model peptides.^{23, 24} The restrictions imposed by α -methyl alanine or C ^{α} -tetra substituted-amino acid on conformational freedom are more severe than those of proline. Thus, mitigators containing bulky substituent's ($\alpha\alpha$ AAs) could be more effective at inducing β -sheet disassembly than peptides that incorporate proline. Simulation experiments

have shown *N*-methylated peptide A β 16-22m interacts with A β ₁₆₋₂₂ blocking β -sheet extension, preventing lateral association into layers and more importantly blocking inhibitor intercalation for sequestering A β peptides. Our $\alpha\alpha$ AAs are bulkier than either *N*-methylated or α -methyl alanine model peptide derivatives. Thus, we hypothesize that $\alpha\alpha$ AA-AAMPs could be more effective at both disrupting fibril formation as well as inducing disassembly of pre-formed fibrils.

4.2 Materials and Methods

All the materials and methodologies used were described in Chapters 2 and 3.

4.3 Results and Discussion

4.3.1 Design of Peptides for Mitigating A β Aggregation

Initial work by Tjernberg identified the A β central hydrophobic core KLVFF as the key scaffold for designing disrupters of A β ₁₋₄₀ fibrillization.^{10, 11} Disrupting elements have been strategically placed at various positions within the A β hydrophobic core that either solubilizes AAMP-A β aggregate (Lys or Arg) or blocks one hydrogen bonding face inhibiting β -sheet extension or propagation as with N-Me amino acid or ester bonds. Thus, polar groups such as Arg, Lys, Glu, and PEG chains were added to increase the solubility of peptides. Certain mitigators incorporating these polar groups have been shown to be effective at disrupting fibril formation.¹⁶

Surface Plasmon resonance (SPR) was employed by Murphy and coworkers²⁵ to study the binding of variants related to KLVFF on immobilized A β ₁₀₋₃₅ fibrils.¹¹ Variants with positively charged residues (KLVFFK_n) added to the *C*-terminus had higher affinities for immobilized A β ₁₀₋₃₅ fibrils than the KLVFF control, while negatively charged residues (KLVFFE_n) also placed on the *C*-terminus had a significantly lower binding affinity. In contrast, *N*-terminal addition (K_nKLVFF) of positively charged residues resulted in lower affinity.

Binding affinity also is affected by additions of polar groups that do not precede the KLVFF region in the parent A β sequence. Therefore, amino acids (for example Gly) that are conformationally unrestricted can be used as a “spacer” between the KLVFF motif and solubilizing residues. Using Gly as a spacer between the mitigator KLVFF core and Arg residues (solubilizing agents) on both the *C*- and *N*- terminus, Brian et al designed the peptide RGKLVFFGR.²⁶ This peptide was shown to be an effective disrupter of A β ₁₋₄₀ fibril formation and prevent neurotoxicity towards human neuroblastoma SHSY5Y cells.

Table 4.1. Modified AAMPs used to probe the assembly and dissolution of A β fibrils.

Entry	AAMP	Sequence
1	AAMP-11	RGKLVFFGR
2	AAMP-12	KGKLVFFGK
3	AAMP-13	EGKLVFFGE
4	AAMP-14	(MiniPEG)GKLVFFG(MiniPEG)
5	AAMP-15	RRRGKLVFFGRRR
6	AAMP-16	KLVFFGR
7	AAMP-17	KLVFFG(MiniPEG)
8	AAMP-18	KLVFFGK
9	AAMP-19	RGKLVFF
10	AAMP-20	KLVFFDpgGK
11	AAMP-21	KGKDibgVFFGK
12	AAMP-22	KDibgVFFDpgGKKK
13	AAMP-23	KKKGKLVFFDpgGKKK
14	AAMP-24	KDibgVFFGKKK
15	AAMP-25	KLVFFF DpgGKKK
16	A β _{16-22m}	K(Me)LV(Me)FF(Me)AE

*Red color denotes the various polar groups. Blue color denotes $\alpha\alpha$ AAs.

As part of our continuing work to design more effective $\alpha\alpha$ AA-containing AAMPs, we employed similar strategies for placing spacers between the AAMP core KLVFF and the solubilizing groups. We have previously shown that AAMP-1 disrupted A β fibril formation.²² In vivo studies of AAMP-1 on APP transgenic mice displayed elevated toxicity at higher concentrations.²⁷ The toxicity observed could be related to the six cationic lysine's which also affect the delivery of drugs across the hydrophobic brain barrier during in vivo studies. Thus, positively and negatively charged polar amino acids as well as neutral polar groups such as MiniPEG was evaluated for effects on the resulting morphology of seed particles and protofibrils. Our goal was to reduce the overall charge of the original peptide (AAMP-1) without sacrificing the mitigator ability to disrupt fibril formation and induce disassembly of pre-formed fibrils.

Peptide mitigator AAMP-11 previously described by Brian and coworkers was used as a control peptide. First, variants of AAMP-11 were investigated where Arg was replaced with Lys (AAMP-12), Glu (AAMP-13), and MiniPEG (AAMP-14) to evaluate effects of polar groups on A β ₁₋₄₀ aggregation (Table 1. entries 1-4). Mitigator AAMP-15 allowed us to probe the effect of increasing the number of Arg in the chain to three on both the *C*-and *N*-terminus on A β fibrillogenesis (entry 5). Peptide mitigators (entries 6-8) were designed to evaluate the effect of placing polar groups only on the *C*-terminus. The effect of placing polar groups on the *N*-terminus was evaluated using AAMP-19 with Arg added only to the *N*-terminus (entry 9). We have previously shown that three $\alpha\alpha$ AAs incorporated in a mitigator sequence was efficient in disrupting the process of A β fibrillization. Thus, mitigators (entries 10-15) were designed to probe the effect of the reducing both the number of $\alpha\alpha$ AAs as well polar groups for A β fibrillization. We hypothesize that addition of a spacer between the $\alpha\alpha$ AA containing

KLVFF mitigator core and solubilizing residues, would improve the interaction between the AAMP and the A β full sequence length. The *N*-methylated peptide, A β 16-22m (entry 16) previously described to disrupt fibril formation and disassemble pre-formed fibrils was used as a control peptide because it is similarly designed to block one hydrogen face from β -sheet extension and packing.

4.3.2 Effects of AAMPs on A β ₁₋₄₀ThT Fluorescence

Thioflavin T (ThT) undergoes a characteristic spectral change upon binding to fibrillar species, with maximum emission shifting from 445 to 482 nm.²⁸⁻³⁰ The intensity of ThT fluorescence is directly proportional to amyloid fibril formation. However, it has also been shown that fluorescence can result from ThT dye binding to amorphous aggregates.^{19, 31} Despite this, ThT fluorescence is still widely used to monitor the process of A β fibrillization. Prior to investigating the effects of AAMPs on A β ₁₋₄₀ aggregation, the individual peptides were first tested alone to evaluate tendencies to self-aggregate. The individual AAMP solutions were aged in 80 μ M in PBS (pH 7.4) for 1 week at 37 ° with periodic agitation. Under these conditions, all of the AAMPs exhibited < 10 % reduced fluorescence (Figure 4.1) relative to that of A β ₁₋₄₀, which indicates minimal aggregation into amyloid species.

When A β ₁₋₄₀ was aged with the various AAMPs at 1:1 molar ratios (40 μ M final concentration) with periodic agitation, a reduction of A β ₁₋₄₀ ThT fluorescence was observed (Figure 4.2). This suggest a disruption of the assembly process for solutions of A β ₁₋₄₀ alone, to form either nonfibrillar or fibrillar assemblies with different sizes, lengths and morphologies relative to those of A β ₁₋₄₀ alone. The AAMPs with *N*- and *C*-termini modified using various polar groups showed a reduction in ThT fluorescence between 40-70% relative to that of A β ₁₋₄₀ after 1-week incubation. In particular, AAMP-11 with polar Arg was the only AAMP with less

than 50% reduced fluorescence. The similarity in the percentage of reduced ThT fluorescence indicates that comparable amounts of amyloid were formed. When using ThT alone one, could falsely argue that AAMP-11 is a better disrupter of A β fibril formation than the other AAMPs incorporating a polar group on both termini.

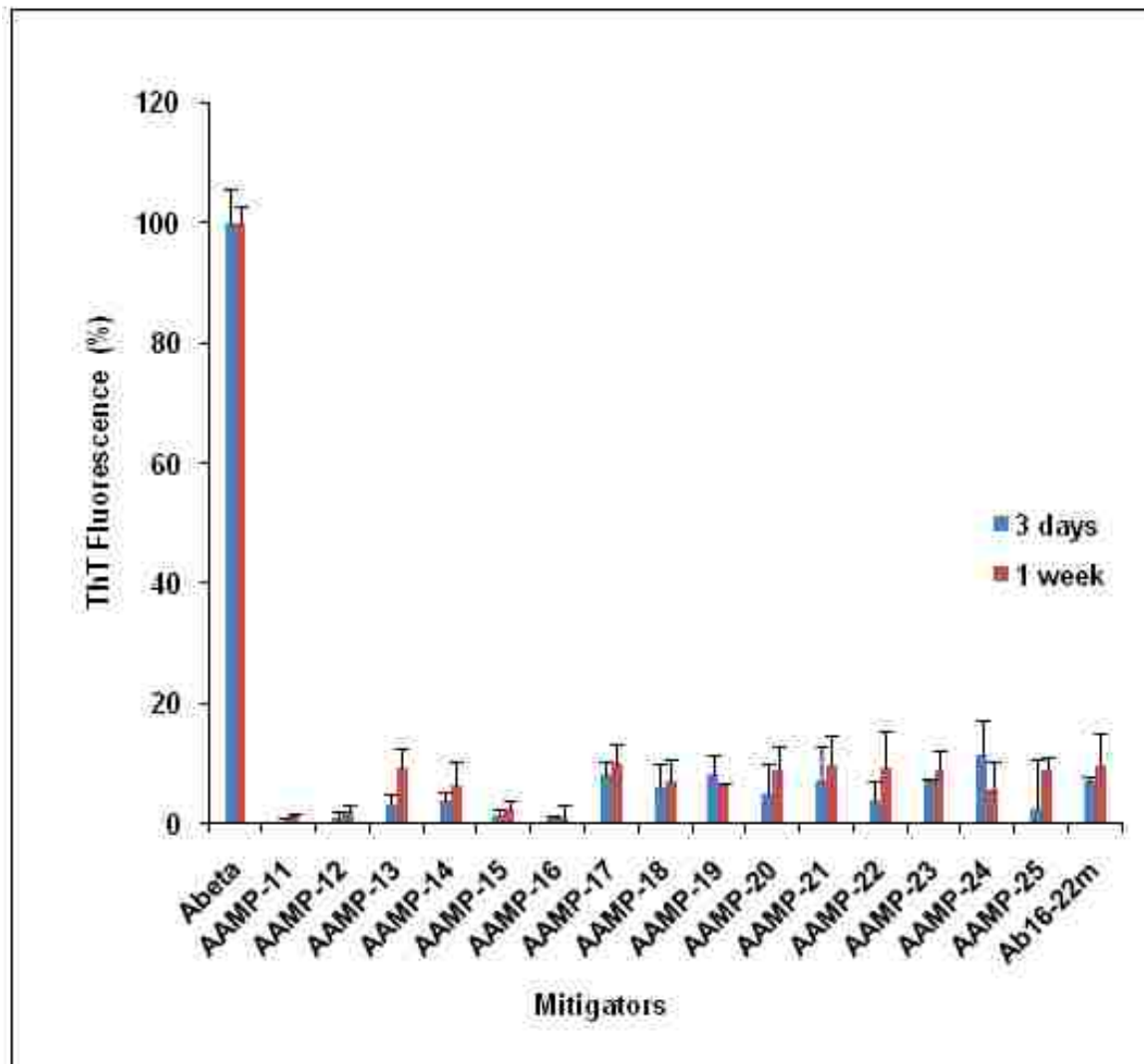


Figure 4.1. Time dependent ThT fluorescence assay of A β alone and AAMPs alone.

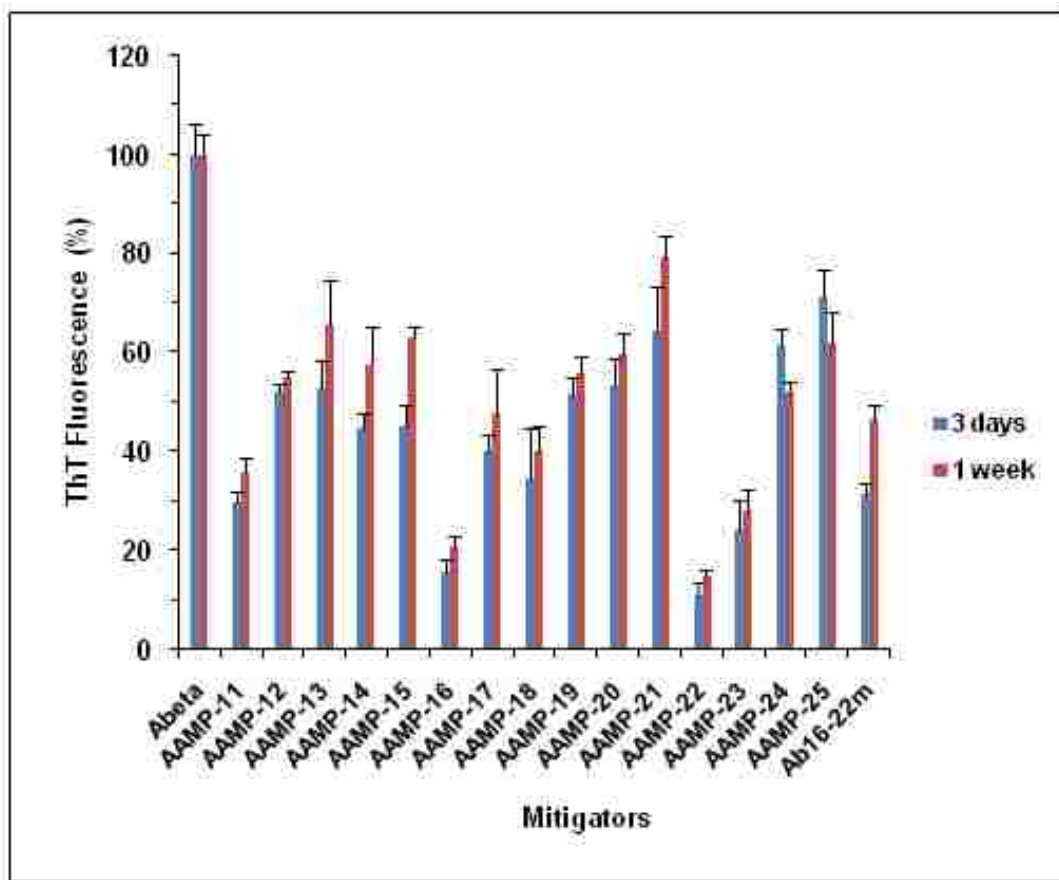


Figure 4.2. Time dependent ThT fluorescence assay of A β /AAMPs.

The addition of a polar Arg group to only the *C*-terminus in AAMP-11 was found to exhibit 80% reduced ThT fluorescence. Other AAMPs in the series incorporating MiniPEG (AAMP-17), Lys (AAMP-18) exhibited a 60% reduction of ThT fluorescence after 1 week of incubation. This indicates that the morphology or size of aggregates formed by AAMP-16 is different from those formed by either AAMP-17 or AAMP-18. Interestingly, mitigators with polar residues placed on the *C*-terminus had an increased reduction in ThT fluorescence as compared to the corresponding mitigators with polar groups added to both *C*- and *N*-termini. The AAMP-19 with Arg on the *N*-terminus showed a reduced fluorescence of 40% as compared to 80% when Arg (AAMP-16) was placed on the *C*-terminus.

As part of continuing work for optimizing charge and size of , AAMP-20, AAMP-21, AAMP-24 and AAMP-25 exhibited reduced fluorescence by less than 40% implying that they might have comparable amounts of amyloid or similar morphology. However, a potent mitigator AAMP-22 with two $\alpha\alpha$ AAs and three lysine's exhibited 80% reduced ThT fluorescence relative to that of $\text{A}\beta_{1-40}$. Based on ThT results only AAMP-11, AAMP-16, AAMP-22 and AAMP-23 exhibited a higher reduction in ThT fluorescence relative to $\text{A}\beta$ than *N*-methylated peptide, mA β_{16-22} previously reported to disrupt fibril formation and to disassemble pre-formed fibrils.¹⁴

As previously described by Austen and coworkers²⁶ AAMP-11 was found to inhibit oligomer formation and prevent $\text{A}\beta_{1-40}$ toxicity towards neuroblastoma SH-5Y5Y cells. They reported that an equimolar mixture of $\text{A}\beta_{1-40}$ /AAMP-11 aged for 12 days under quiescent conditions showed reduced fluorescence of over 80% relative to that of $\text{A}\beta_{1-40}$.²⁶ For the same peptide after 7 days aging, however we report a lower ThT fluorescence of 63% with a condition of periodic agitation, as compared to the previously reported result of over 80% reduction. Agitation is normally employed to enhance $\text{A}\beta$ aggregation so that it can be analyzed on a laboratory time scale, although fibrils formed are less stable and more toxic.^{32, 33}

4.3.3 Effect of Various AAMPs on $\text{A}\beta_{1-40}$ CD Spectra

The effect of $\alpha\alpha$ AA-AAMPs on $\text{A}\beta_{1-40}$ assembly into β -sheet structure, was examined using far-UV circular dichroism (CD). The CD spectra of monomeric AAMPs and $\text{A}\beta_{1-40}$ had a strong minimum near 200 nm and maxima near 220 nm, consistent with an unstructured conformation commonly referred to as random coil conformation. After 1-week of aging at 37 C while shaking, all the mitigators exhibited minima in their CD spectra around 200 nm, consistent with unchanged random coil conformation. However, the assembly of $\text{A}\beta_{1-40}$ alone after 1-week incubation exhibited a CD spectra with minima around 217 nm (Figure 4.3), consistent with

formation of β -sheet rich assemblies.^{22, 34} In contrast, when $A\beta_{1-40}$ was aged in the presence of equimolar AAMPs, an unusual CD signature with characteristics of random coil and beta sheet was observed, consistent with our previous results for an AAMP-1/ $A\beta_{1-40}$ mixture.²² This suggests that our AAMPs delay or disrupt $A\beta_{1-40}$ aggregation into β -sheet rich assemblies.

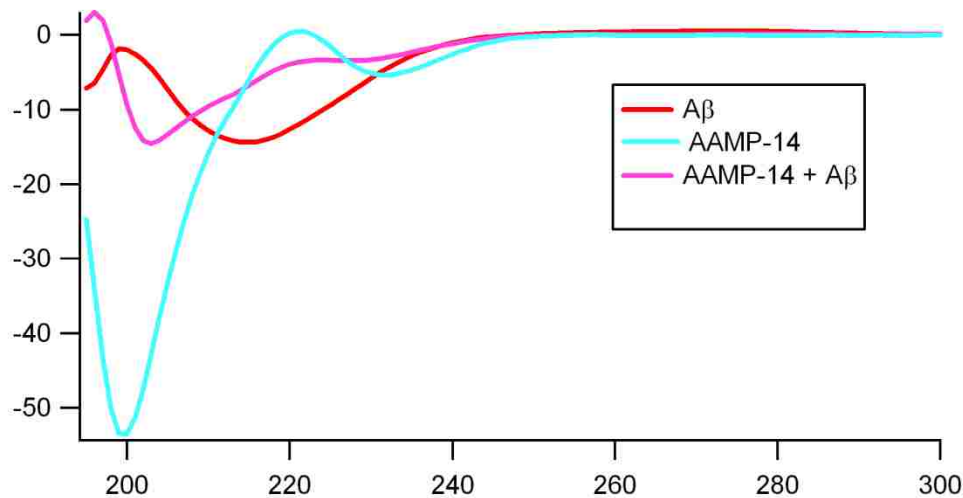


Figure 4.3. An example of a CD spectra for AAMP-14 alone, $A\beta_{1-40}$ alone and $A\beta_{1-40}$ /AAMP-14 equimolar mixture.

4.3.4 Assembly of $A\beta_{1-40}$ Alone and with the Various AAMPs Analyzed Using AFM

Samples of AAMPs alone, $A\beta_{1-40}$ alone, and mixtures of $A\beta_{1-40}$ /AAMPs mixture, which were prepared for the same time intervals as those of the ThT fluorescence assay were examined using TEM and AFM. First, samples from mitigator aged alone were examined to determine the morphology of the aggregates responsible for the observed ThT fluorescence. This is important because $A\beta_{1-40}$ has been shown to aggregate via a nucleation dependent polymerization process.^{35, 36} Thus, aggregates formed by AAMPs could act as seeds, rapidly increasing the rate of $A\beta$ assembly into fibrils. Also, AAMP monomer could be added instead to a growing protofibril in place of $A\beta$ monomer capping the $A\beta$ fibrillization or altering the normal aggregation pathway leading to formation of fibrils with different morphology. Peptide

mitigators were aged in the absence of A β ₁₋₄₀ PBS (50 mM at 37 C with periodic agitation) to investigate their self-aggregation. Topographic images of various samples of AAMPs aged for 1-week displayed sparse distribution of aggregates on the surface (Figure 4.4) with mean heights ranging from 2- 8 nm (Table 4.2).

Table 4.2: Size and morphologies of assemblies obtained from topographic AFM measurements of products observed from aging AAMPs alone at 37°C.

Entry	AAMPs	Type and size of resulting assemblies			
		3 days		1 week	
		Aggregate type	Size (nm)	Aggregate type	Size (nm)
1	AAMP-11	spherical	2.5±2.1	spherical	3.0±2.1
2	AAMP-12	spherical	2.1±1.2	Spherical	3.1±1.6
3	AAMP-13	spherical	2.7±2.1	Spherical	5.5±3.4
4	AAMP-14	spherical	2.8±1.7	Spherical	7.4±4.7
5	AAMP-15	spherical	3.3±1.9	spherical	5.3±2.3
6	AAMP-16	spherical	2.3±1.5	spherical	2.8±1.8
7	AAMP-17	spherical	3.1±1.7	spherical	3.9±2.3
8	AAMP-18	spherical	2.4±1.5	spherical	7.9±4.2
9	AAMP-19	spherical	2.8±1.8	spherical	3.1±2.1
10	AAMP-20	spherical	3.1±2.2	spherical	4.1±2.5
11	AAMP-21	spherical	3.2±2.0	spherical	3.6±3.5
12	AAMP-22	spherical	2.5±1.6	spherical	4.4±2.3
13	AAMP-23	spherical	2.3±1.6	spherical	3.4±2.1
14	AAMP-24	spherical	1.9±1.4	spherical	4.4±2.1
15	AAMP-25	spherical	2.9±2.5	spherical	3.1±1.9
16	A β ₁₆₋₂₂	spherical	3.9±1.6	spherical	6.1±3.8

The mean heights of aggregates observed after 1 week of aging shows an increase in height consistent with aggregation. When the mean heights of aggregates formed by the various AAMPs were compared, no direct correlation was detected between the mean heights of aggregates formed and terminal modifications of the peptides. A significant observation was larger aggregates formed by AAMPs with longer polar groups such as AAMP-14 and AAMP-18 as compared to AAMP-11 or AAMP-12.

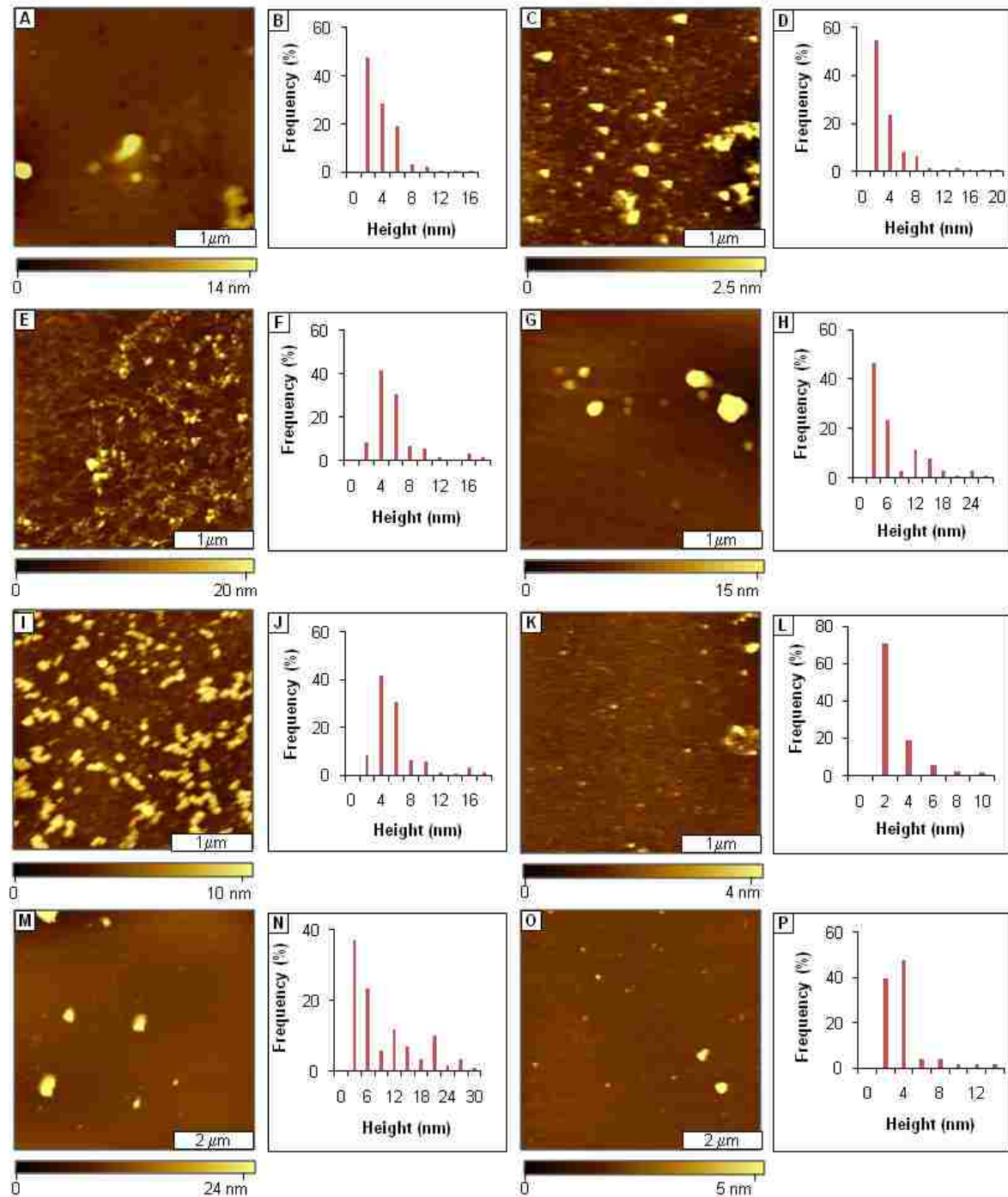


Figure 4.4 Assembly of AAMPs alone at 37°C and periodic agitation. Topographic AFM views of spherical structures formed by:- [A] AAMP-11 [B] Corresponding height analysis for A; [C] AAMP-12 [D] Height analysis for C; [E] AAMP-13; [F] Height analysis for E; [G] AAMP-14; [H] Height distribution histogram for G; [I] AAMP-15; [J] Height analysis for I; [K]AAMP-16; [L] Height histogram for K; [M] AAMP-17; [N] Height analysis for M; [O] AAMP-18; [P] Height distribution analysis for O;

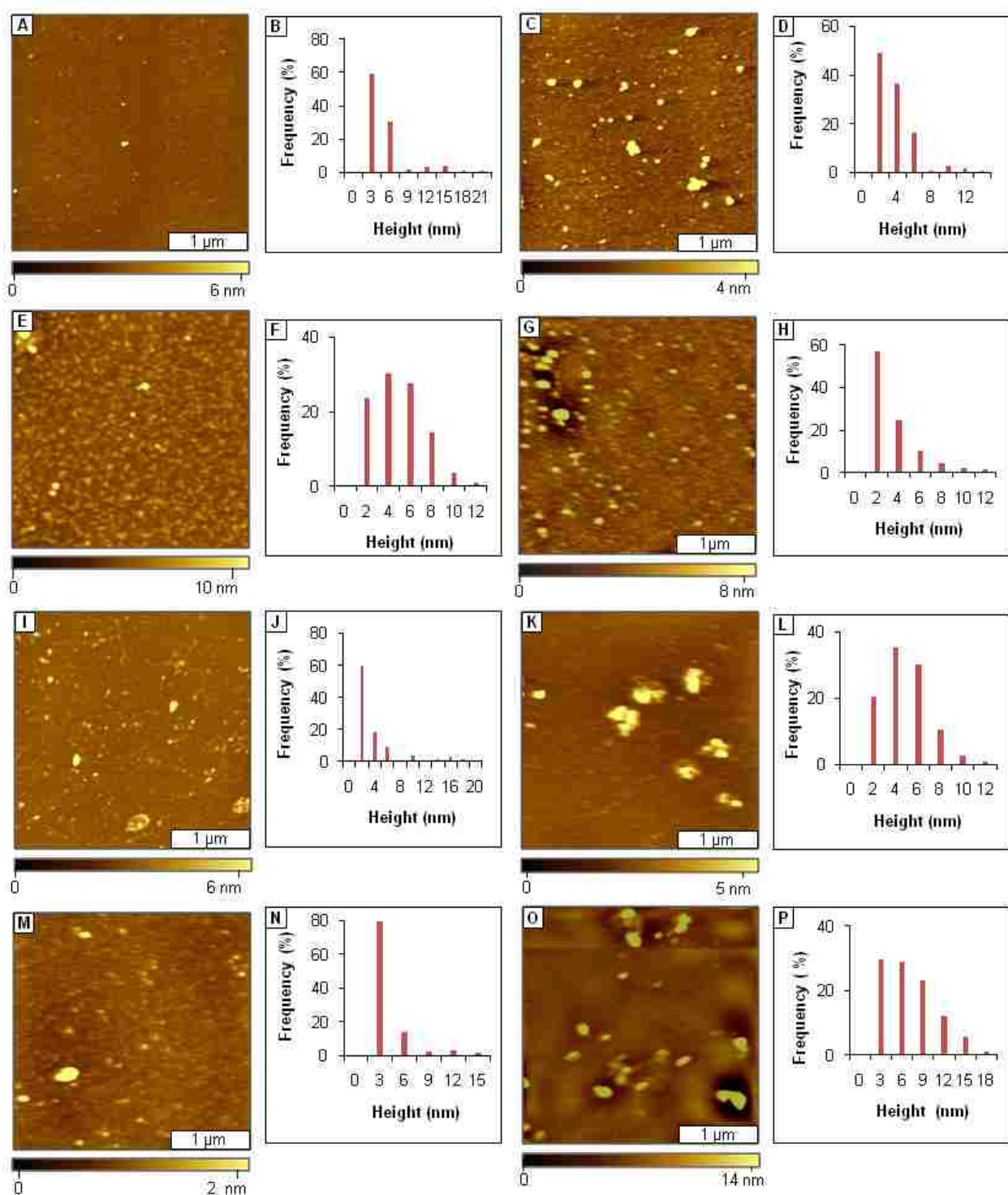


Figure 4.5 Assembly of AAMPs alone at 37°C and periodic agitation. Topographic AFM views of spherical structures formed by:- [A] AAMP-19 [B] Corresponding height analysis for A; [C] AAMP-20 [D] Height analysis for C; [E] AAMP-21; [F] Height analysis for E; [G] AAMP-22; [H] Height distribution histogram for G; [I] AAMP-23; [J] Height analysis for I; [K] AAMP-24; [L] Height histogram for K; [M] AAMP-25; [N] Height analysis for M; [O] A β ₁₆₋₂₂; [P] Height distribution analysis for O;

Spherical aggregates with mean height range between 3-5 nm were observed for all the mitigators incorporating $\alpha\alpha$ AAs into its sequence after 1 week of incubation. Surprisingly, smaller aggregates were observed from topographic images of AAMPs incorporating $\alpha\alpha$ AAs compared to the more hydrophobic *N*-methylated control peptide. This suggests that polar groups present in $\alpha\alpha$ AA-AAMPs play a role in aggregation. When the AAMPs solutions were aged under quiescent conditions, aggregates were hardly seen indicating that these mitigators are stable at room temperature.

4.3.4.1 Effect of *N*- and *C*-Terminal Modifications of AAMPs on $A\beta_{1-40}$ Fibrillization

The $A\beta_{1-40}$ sample aged alone showed a dense network of amyloid fibrils averaging 5.4 nm in height and extending several microns in length after 3 days aging (Figure 4.6A). A predominantly dense network of fibrils averaging 6.9 nm in height and spanning several microns in length was observed after 1 week of aging (Figure 4.6C). The fibrils that formed are consistent with the $A\beta_{1-40}$ aggregation process and fits the proposed hierarchical assembly model (HAM model).^{36, 37} The spherical particles observed within a sea of fibrils after 3 days aging are consistent with results expected with periodic or continuous sample agitation.³⁸ The height analysis (Figures 4.6B and 4.6D) shows that mature fibrils with diameter ≥ 7 nm were predominant after 1 week of aging, which coincides with the results observed with maximum ThT fluorescence.

When $A\beta_{1-40}$ was aged with the equimolar ratio of AAMPs incorporating differently charged polar groups to both *C*- and *N*-termini, the normal $A\beta_{1-40}$ aggregation process was disrupted to form either fibrils with different morphology (appearance, length) or spherical particles. A network of protofibrils and fibrils (Figure 4.6E) were the major species observed after 3 days of aging $A\beta_{1-40}$ with Arg-containing AAMP-11.

Table 4.3. Size and morphology of A β ₁₋₄₀/AAMP variants

Entry	AAMPs	Type and size of resulting assemblies			
		3 days		1 week	
		aggregate type	mean height (nm)	aggregate type	mean height (nm)
1	A β ₁₋₄₀	Fibrils	4.5±1.9	Fibrils	6.9±3.7
2	AAMP-11	Protoceribrils/fibrils	4.3±2.0	Protoceribrils/fibrils	6.6±3.1
3	AAMP-12	Protoceribrils/ amorphous	5.3±3.1	Rod shaped fibrils	7.4±3.2
4	AAMP-13	Amorphous	5.5±3.0	Amorphous	7.2±±
5	AAMP-14	Amorphous	27.8±13.4	Amorphous	40.1±21.2
6	AAMP-15	Protoceribril/linear	4.3±1.9	Protoceribril/rod like fibrils	5.6±2.2
7	AAMP-16	Spherical	20.9±10.1	Amorphous	36.0±15.3
8	AAMP-17	Amorphous	8.2±3.7	Amorphous	10.0±4.1
9	AAMP-18	Protoceribrils/amorphous	5.5±2.5	Fibrils	7.5±3.2
10	AAMP-19	Amorphous/protoceribrils	5.9±3.3	Linear/fibrils	9.4±3.8
11	AAMP-20	Protoceribrils	7.3±3.1	Amorphous/linear	23.9±12
12	AAMP-21	Protoceribrils	4.8±3.0	Fibrils	7.6±4.7
13	AAMP-22	Spherical	5.4±2.3	Amorphous	6.1±2.8
14	AAMP-23	Amorphous/linear	4.4±2.2	Linear/amorphous	10±5.1
15	AAMP-24	Spherical	8.7±3.6	Amorphous, linear	6.1±2.4
16	AAMP-25	Amorphous, protoceribrils	5.5±3.4	Fibrils	11.5±7.4
17	A β ₁₆₋₂₂	Amorphous	10.4±4.5	Amorphous	16.1±9.5

The morphology of the AAMP-11 structures (Figure 4.6G) observed after 1 week of aging for the most part did not change, except for an increase was observed for the mean heights as shown by the histogram analysis (Figures 4.6F and 4.6H). Similarly, fibrils/protoceribrils (Figure 4.6I) were observed after 3 days of aging A β ₁₋₄₀ with equimolar AAMP-12 containing another positively charged group (Lys). After 1 week incubation of AAMP-12 (Figure 4.6K, there was increase in both the mean height (Figures 4.6J and 4.6L) and surface coverage of fibrils. Also, when A β ₁₋₄₀ was aged with AAMP-13 containing a negatively charged Glu residue, protoceribrils and fibrils (Figure 4.6M) were observed after 3 days. Dense networks of beaded fibrils or protoceribrils (Figure 4.6O) were detected after 1-week incubation with AAMP-13 with height distribution (Figures 4.6N and 4.6P) showing increase in particles size. Interestingly,

spherical particles (Figure 4.6Q) were the major structures observed after 3 days aging A β ₁₋₄₀ with AAMP-14 incorporating a neutral MiniPEG group. No fibrillar species (Figure 4.6S) were observed after 1-week incubation, only spherical particle clumps were observed resulting in a height as shown by the height histograms (Figures 4.6R and 4.6T).

Fibrils were observed to form from aging mixtures of A β ₁₋₄₀ with AAMP-11 (Figure 4.6E), which is in disagreement with published results where fibrils were not detected.²⁶ The difference in morphology of the particles that formed could be attributed to differences in the aging conditions that were employed. Sample agitation is widely used to expedite amyloid fibril formation. This implies that under quiescent conditions, AAMP-11 disrupts fibril formation; however, fibril morphology is altered when aggregation rates are increased by agitation. A mixture of short fibrils with lengths spanning few microns and linear structures with protofibrillar morphology were observed with AAMP-12 incorporating positively charged Lys. Both AAMP-11 and AAMP-12 alter A β ₁₋₄₀ fibrillization pathway forming fibrils that are short in length, more branched, and with lower mean height as compared to those of A β ₁₋₄₀ fibrils. Surprisingly, this is consistent with SPR studies that showed mitigators with Lys and Arg polar residues had identical binding affinities for immobilized A β ₁₀₋₃₅.

However, a dense network of fibrils (Figure 4.6O) with a beaded morphology was observed when A β ₁₋₄₀ was aged with AAMP-13 containing negatively charged Glu, after 1-week incubation. The dense network of beaded fibrils observed in AAMP-13 as compared to AAMP-12 and AAMP-11 is also consistent with lower binding affinity for A β from mitigators with negatively charged polar groups as observed from SPR studies.²⁵

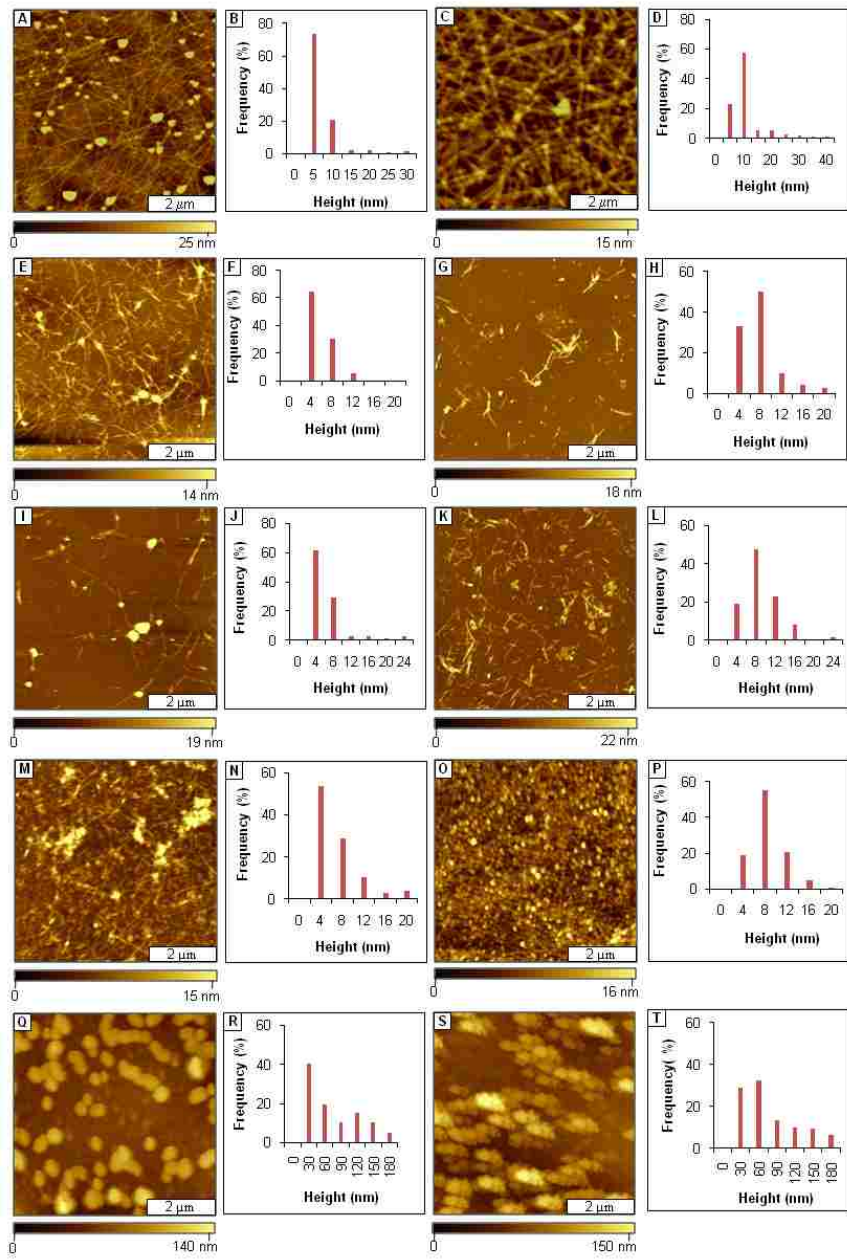


Figure 4.6. Mitigation of $\text{A}\beta_{1-40}$ aggregation by AAMPs with polar groups added to both the *C*- and *N*-terminus, as viewed by AFM topographs. [A] Fibrils formed after 3 days incubation by $\text{A}\beta_{1-40}$ alone; [B] Height analysis for A; [C] Fibrils present after 1 week; [D] Height analysis for C; [E] Fibrils formed after mitigation for 3 days by AAMP-11; [F] Height analysis for E; [G] Fibrils formed after 1 week; [H] Height distribution histogram for G; [I] Mixture of spherical and protofibril structures after 3 days mitigation by AAMP-12; [J] Height analysis for I; [K] Spherical and short sized fibrils observed after 1 week; [L] Height histogram for K; [M] Protofibrils present after 3 days with AAMP-13; [N] Height analysis for M; [O] Fibrils formed after 1 week; [P] Height distribution analysis for O; [Q] Spherical structures present after mitigation for 3 days by AAMP-14; [R] Height distribution for Q; [S] Spherical structures observed after 1 week; [T] Height analysis for S.

The lower binding affinities observed from mitigators with negatively charged polar groups was postulated to be from possible Coulombic interactions between the positively charged polar groups in the mitigator and negatively charged residues in A β (E22 and D23).¹¹ In contrast, spherical particles with diameters up to nearly 0.2 microns were observed from aging A β_{1-40} in the presence of AAMP-14 (Figure 4.6Q) with MiniPEG (neutral) group. The MiniPeg group is a glycol chain and increases the overall hydrophobicity of the peptide. Thus, in this case increased hydrophobicity is more of a factor as compared to Coulombic interaction (AAMP-12, AAMP-11) because A β assembly is initially controlled by hydrophobic interactions.

4.3.4.2 Effect of C-Terminal Modifications of AAMPs on A β_{1-40} Fibrillization

When three Arg residues were added on each terminus as in AAMP-15, fibrils (Figure 4.7A) with lengths up to 1-2 microns were observed in AFM topographs. The fibrils (Figure 4.7C) observed after 1-week incubation had increased height as shown by cursor analysis (Figures 4.7B and 4.7D). Surprisingly, AAMPs with polar groups added to only the C-terminus produced particles with a different morphology as compared to those with polar groups added to both termini. For instance, spherical particles (Figure 4.7E) were the major species observed from aging A β_{1-40} with AAMP-16 incorporating Arg on the C-terminus. The height of these particles (Figure 4.7G) increased up to 100 nm after 1-week incubation, shown by height distributions (Figures 4.7F and 4.7H). Mixtures of protofibrils and spherical particles (Figure 4.7I) were observed after 3 days aging A β_{1-40} in the presence of AAMP-17 containing the neutral MiniPEG group. After 1 week of aging, spherical and linear particles (Figure 4.7K) with increased heights (Figures 4.7J and 4.7L) were observed from samples imaged after 1 week.

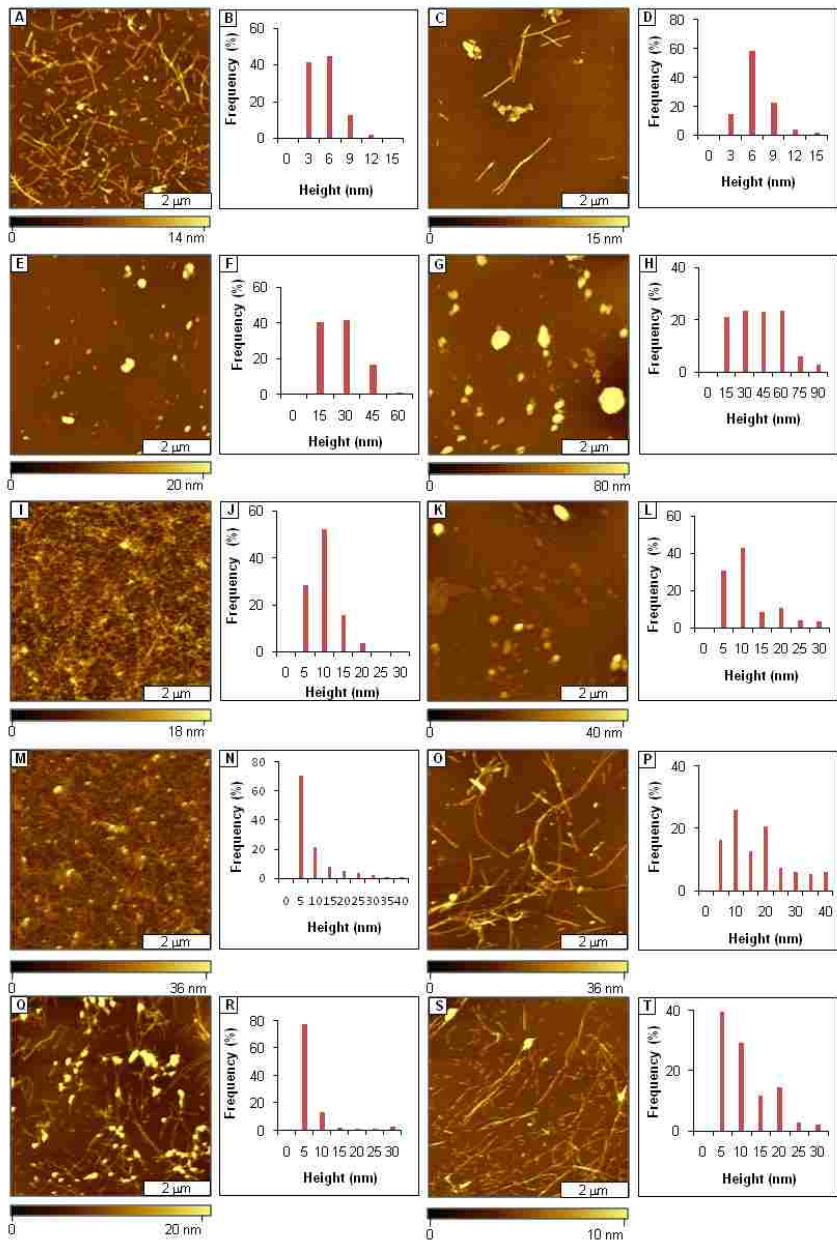


Figure 4.7 Disruption of $\text{A}\beta_{1-40}$ fibril formation by AAMPs with polar groups added to the *C*- or *N*-terminus, characterized by tapping mode AFM. [A] Views of short fibrils after 3 days aging $\text{A}\beta_{1-40}$ in the presence of AAMP-15; [B] Corresponding height distribution for A; [C] After 1 week; [D] Height analysis for C; [E] Spherical structures detected after 1 week of aging an $\text{A}\beta_{1-40}$ /AAMP-16 mixture; [F] Corresponding height distribution; [G] After 1 week; [H] Height distribution analysis for G; [I] Views of spherical and protofibrils formed by $\text{A}\beta_{1-40}$ /AAMP-17 mixture after 3 days aging; [J] Corresponding height analysis; [K]; After 1 week; [L] Height analysis for K; [M] Views of spherical particles and protofibrils formed by $\text{A}\beta_{1-40}$ aggregation mitigation by AAMP-18 after 3 days aging; [N] Corresponding height distribution; [O] Fibrils detected after 1 week; [P] Height analysis for O. [Q] Spherical aggregates and protofibrils observed after 3 days $\text{A}\beta_{1-40}$ mitigation by AAMP-19; [R] Height distribution histogram for Q; [S] Fibrils were present after 1 week aging; [T] Height analysis for S.

Also, when A β ₁₋₄₀ was aged with AAMP-18 containing another positively charged group (Lys), spherical particles, and protofibrils (Figure 4.7M) were detected for samples imaged after 3 days. Predominantly, fibrils (Figure O) were observed after 1-week incubation of AAMP-18 exhibiting an increased height distribution as compared to spherical/protofibrils observed after 3 days of aging (Figure 4.7N and 4.7P). When A β ₁₋₄₀ was aged in the presence of AAMP-19 with polar groups added to the *N*-terminus, a mixture of spherical and fibrillar structures (Figure 4.7Q) were observed for AFM images acquired of samples after 3 days aging. Predominantly, short fibrils spanning few microns (Figure 4.7S) and even distribution (Figures 4.7R and 4.7T) from those of A β were observed from samples taken after 1 week aging.

Contrary to results observed for AAMP-14, increasing the overall hydrophilicity of the peptide by addition of more positively charged Arg for AAMP-15 did not necessarily lead to increased disruptive properties. This suggests the importance of the overall hydrophobicity of the peptide, which has been shown to be involved in the initial process of A β assembly. Modification of the *C*-terminal of AAMPs with positively charged groups as in AAMP-16 and AAMP-17 led to disruption of fibrils yielding either non-fibrillar structures or fibrils with different morphologies (fibril length, fibril diameter, and fibril entanglement) as compared to structure of A β alone. Analogs of KLVF with *C*-terminal modification with Arg or Lys have been shown to have significantly larger binding affinities for A β .²⁵ Thus, the slight changes observed for the morphology of the particles could be attributed to the differences in the side chain functionality of the polar groups, where Arg has a more stable positive charge from delocalization as compared to Lys.

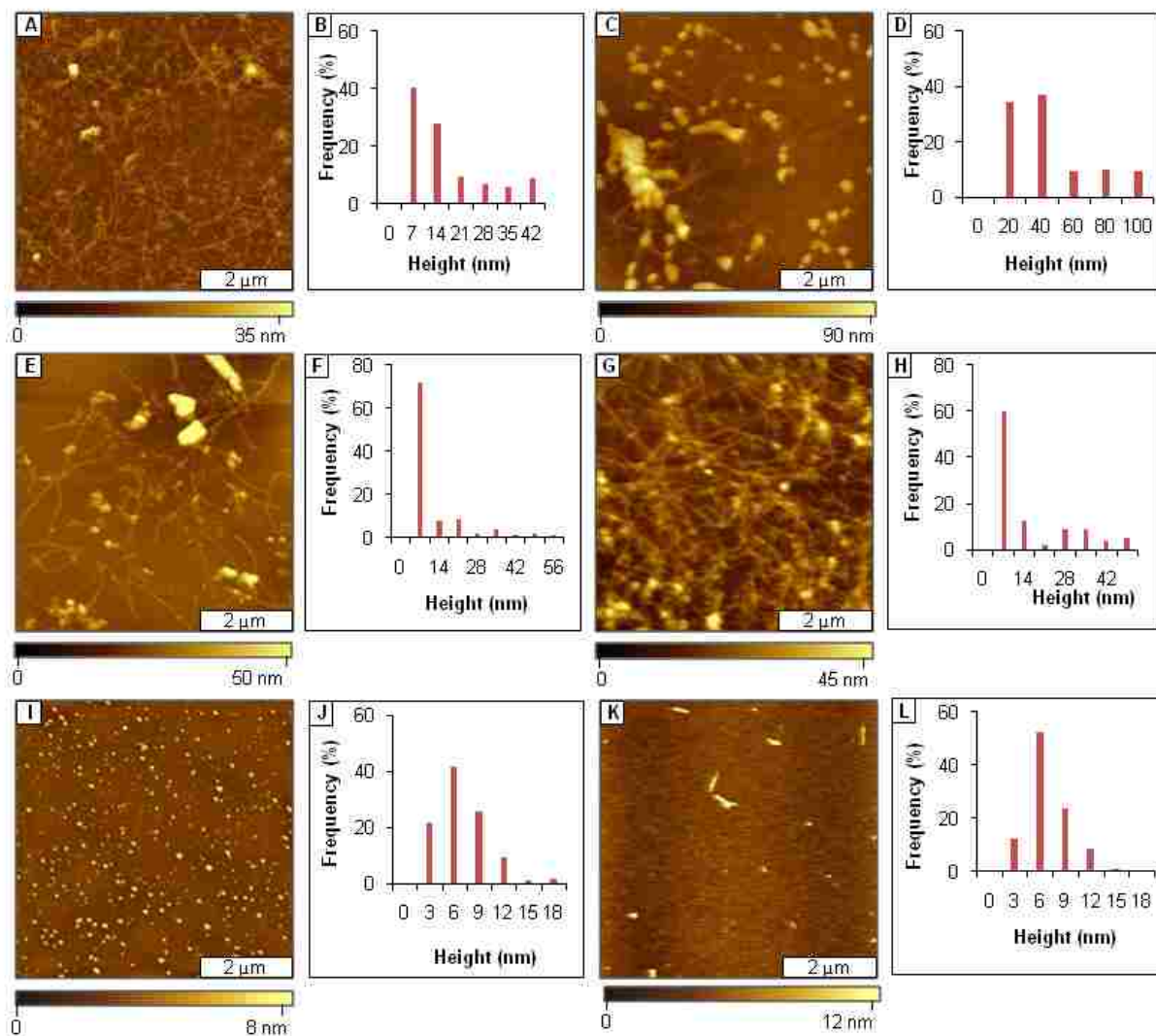


Figure 4.8. Disruption of $\text{A}\beta_{1-40}$ fibril formation by $\alpha\alpha\text{AAs}$ -containing AAMPs; [A] Protomibrils and spherical structures observed after 3 days aging $\text{A}\beta_{1-40}$ in the presence of AAMP-20; [B] Height distribution for A; [C] Spherical structures and fibrils (background) observed after 1 week; [D] Corresponding height analysis for C; [E] Views of fibrils with some spherical structures detected after 1 week of aging $\text{A}\beta_{1-40}/\text{AAMP-21}$ mixture; [F] Corresponding height distribution [G] After 1 week; [H] Height distribution analysis for G; [I] Spherical structures observed for $\text{A}\beta_{1-40}/\text{AAMP-22}$ mixture after 3 days aging; [J] Corresponding height analysis; [K]; spherical and linear aggregates after 1 week; [L] Height analysis for K.

When the positively charged residue is replaced with a neutral group (MiniPEG), similar disruption was observed, and could be attributed to enhancing hydrophobic-hydrophobic interactions between $\text{A}\beta$ and AAMP-17. Mitigators with their *N*- or *C*-terminus modified with

the same positively charged polar amino acid residue altered A β fibrillization forming particles with different morphology. For instance, fibrils were predominantly formed in AAMP-19 as compared to spherical particles in AAMP-16 with *N*- and *C*-terminal modified with Arg respectively. This is also consistent with binding studies that showed AAMPs with Lys y added to the N-terminus had 3-fold lower binding affinities as compared to AAMPs with Lys added to *C*-terminus.

4.3.4.3 Effect of *N*- or *C*-Terminal Modifications of AAMPs on A β ₁₋₄₀ Fibrillization

Analogs that incorporate $\alpha\alpha$ AAs were also tested to investigate the effects of $\alpha\alpha$ AAs on morphology of A β -AAMP aggregate. Spherical aggregates and isolated protofibrils (Figure 4.8A) were observed with Dpg-containing AAMP-20 after 3 days of aging. Spherical aggregates (Figure 4.8C) had grown to ~100 nm in diameter after 1 week of incubation as discerned from height distribution analysis (Figures 4.8B and 4.8D). Mixtures of spherical aggregates and fibrils/protofibrils (Figures 4.8E and 4.8G) were observed from aging Dibg-containing AAMP-21 after 3 and 7 days incubation. The height distribution of the particles increased over the same time (Figures 4.8F and 4.8H).

When A β ₁₋₄₀ was aged in the presence of AAMP-22 incorporating two $\alpha\alpha$ AAs, spherical particles (Figure 4.8I) were observed after 3 days while spherical and linear particles (Figure 4.8K) observed after 1 week aging. The diameters and distribution the particles increased at longer aging times as shown by height analysis (Figures 4.8J and 4.8L). AAMP-20 and AAMP-21 are similar in design with AAMP-18 and AAMP-12 except for $\alpha\alpha$ AA incorporated in their core. Mixtures of spherical aggregates and fibrils were observed with both AAMP-20 and AAMP-21 with diameters of spherical spanning up to a 0.1 micron as compared to primarily fibrils, although with different morphology as those of A β ₁₋₄₀.

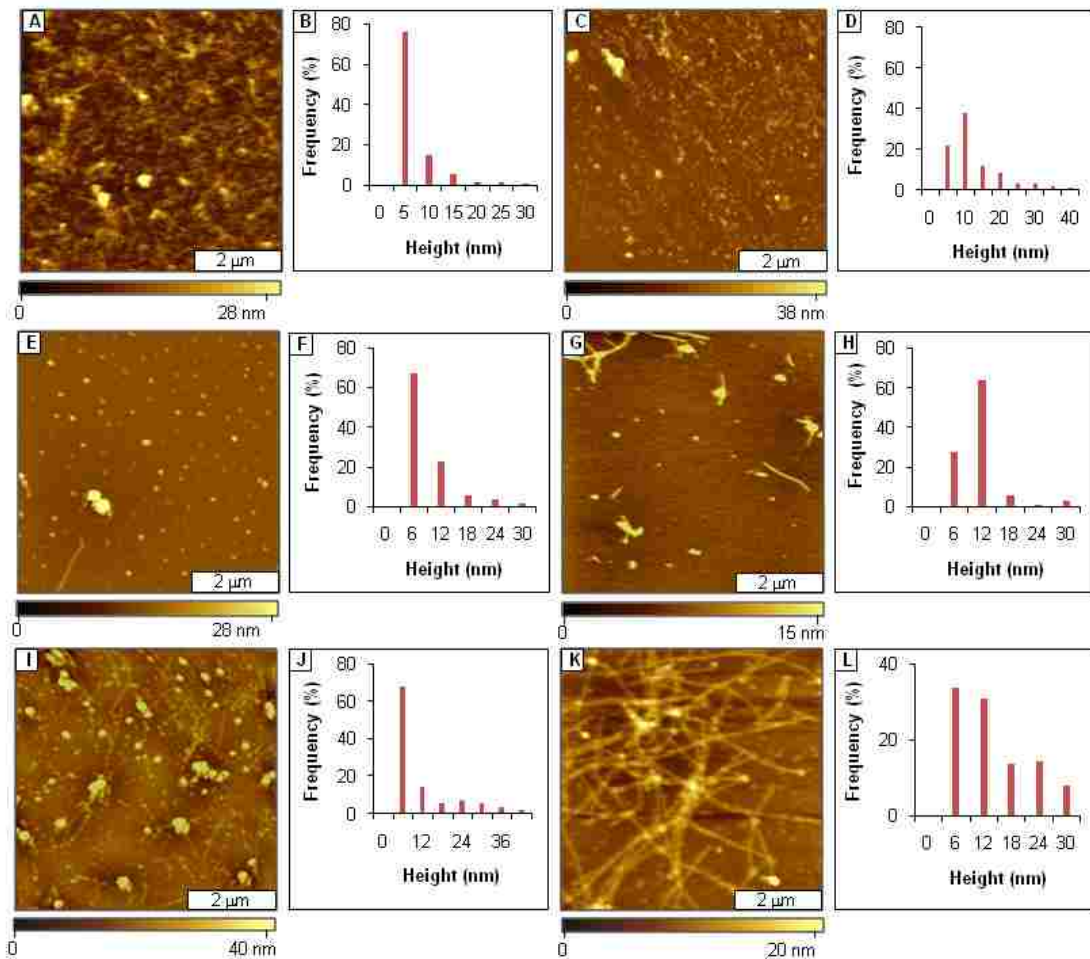


Figure 4.9. Effects of $\alpha\alpha$ AAs-containing AAMPs on $\text{A}\beta_{1-40}$ fibril formation; [A] Protomofibrils and spherical structures were observed after 3 days aging $\text{A}\beta_{1-40}$ in the presence of AAMP-23; [B] Height distribution for A; [C] Spherical structures and linear structures observed after 1 week; [D] Corresponding height analysis; [E] Spherical structures observed after 1 week of aging $\text{A}\beta_{1-40}$ /AAMP-24 mixture; [F] Height distribution analysis for E; [G] Rod-like fibrils and spherical aggregates observed after 1 week; [H] Corresponding histogram analysis; [I] Spherical and protomofibrillar structures observed after aging $\text{A}\beta_{1-40}$ /AAMP-25 for 3 days; [J] Corresponding height analysis; [K]; After 1 week [L] Height analysis for K.

These are good examples that show the effects of incorporating $\alpha\alpha$ AAs in a mitigator sequence. When the number of Lys were increased to three and another $\alpha\alpha$ AAs introduced as in AAMP-22, compared to AAMP-20 with only one Lys and $\alpha\alpha$ AA, no fibrillar structures were observed. This is consisted with increased solubility of $\text{A}\beta$ -AAMP aggregate and steric factors ,

crucial in our mitigator design. This is also consistent with 80% reduced fluorescence observed relative to that of A β ₁₋₄₀.

Spherical and linear structures (Figures 4.9A and 4.9C) were observed in AFM topographs of samples after three days and 1 week of incubating A β ₁₋₄₀ in the presence of AAMP-23 incorporating Dpg and three lysine residues added to both termini. Spherical structures (Figure 4.9E) were observed after 3 days of aging a mixture of A β ₁₋₄₀ and AAMP-24. After 1 week of incubation, spherical aggregates and protofibrils or linear structures (Figure 4.9G) were the predominant structures. On the other hand, after 3 days incubation of an A β ₁₋₄₀/AAMP-25 mixture, spherical aggregates and protofibrils (Figure 4.9I) were observed. After 1 week of aging, fibrils (Figure 4.9K) were more abundant. For all the AAMPs, particles that formed were observed to increase in height after longer aging ,as shown by height distributions (Figures 4.9B, 4.9D, 4.9F, 4.9H, 4.9J, and 4.9L).

Addition of three lysine residues to both termini as in AAMP-23, disrupted fibril assembly to generate linear structures. Addition of three lysines to both ends probably increased the solubility of A β -AAMP aggregates, resulting in disruption of fibrillogenesis. The different morphologies of the particles observed with AAMP-24 as compared to AAMP-25 can be attributed to the steric difference between the $\alpha\alpha$ AAs. Mixtures of spherical particles and protofibrils were formed with AAMP-24, which containing the Dibg (isobutyl side chains) as compared to fibrils in AAMP-25, which contains Dpg (n-propyl side chains). This highlights the important role of polar groups and steric hindrance to the mechanisms for disruption of A β fibrillization.

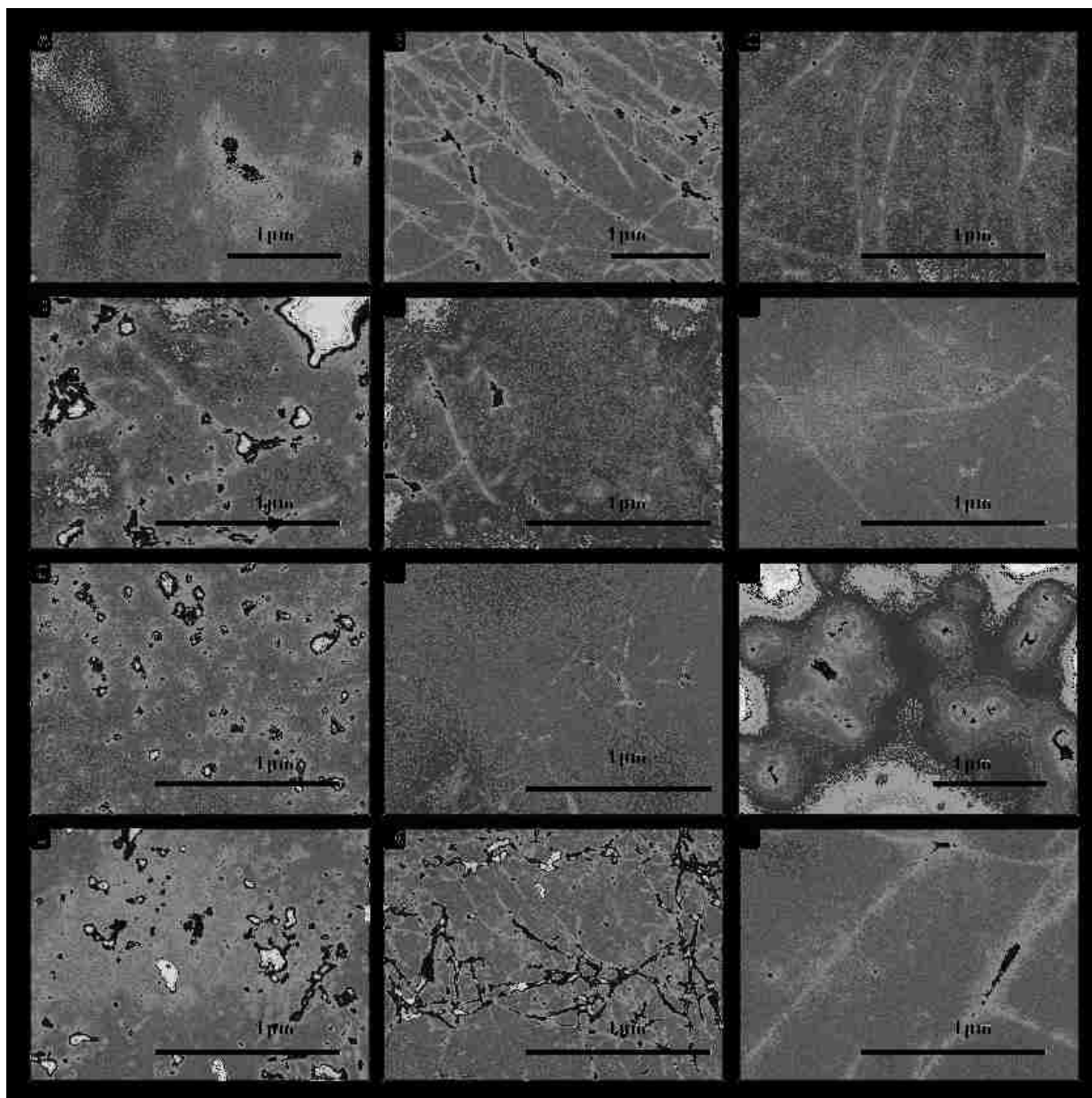


Figure 4.10 EM micrograph of particles observed after 1-week aging Aβ₁₋₄₀ in presence of the various AAMPs. [A] Fibrils formed by Aβ₁₋₄₀ alone; [B] Fibrils formed by Aβ₁₋₄₀ alone different view; [C]; Zoom in view of Aβ₁₋₄₀ fibrils observed in B [D] Fibrils formed from Aβ₁₋₄₀ mitigation by AAMP-11; [E] isolated fibrils formed from aging Aβ₁₋₄₀ in presence of AAMP-12; [F] isolated fibrils were observed from aging Aβ₁₋₄₀/AAMP-13 mixture; [G] mainly spherical particles and isolated protofibrils observed from aging Aβ₁₋₄₀ in presence of AAMP-14; [H] isolated fibrillar structures observed from incubating Aβ₁₋₄₀ in presence of AAMP-15; [I] Spherical particles formed from Aβ₁₋₄₀ aggregation mitigation by AAMP-16 [J] No fibrillar particles observed from Aβ₁₋₄₀ aggregation mitigation by AAMP-17 [K] Fibrillar structures formed from Aβ₁₋₄₀ mitigation by AAMP-18; [L] Fibrils observed from aging Aβ₁₋₄₀/AAMP-19 mixture.

4.3.5 Morphology of Structures Formed from A β ₁₋₄₀ Aggregation Mitigation by the Various AAMPs as Observed by TEM

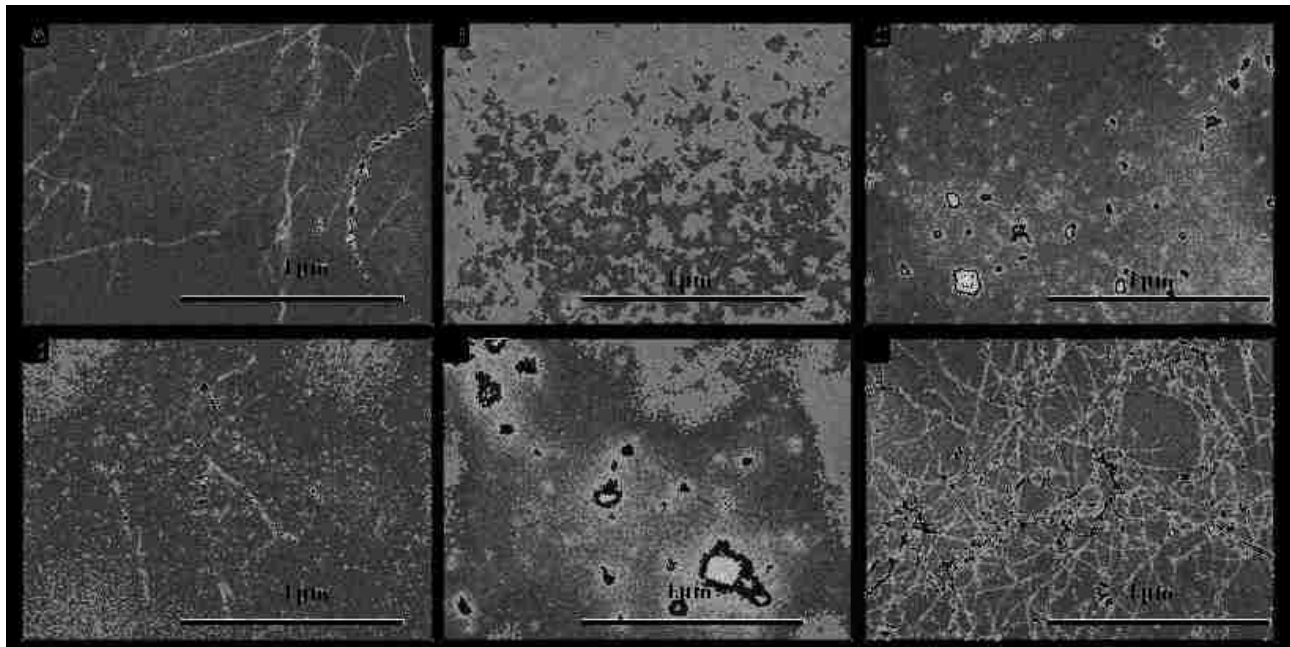


Figure 4.11 EM micrograph of particles observed after 1-week aging A β ₁₋₄₀ in presence of the various AAMPs. [A] Isolated fibrils observed from aging A β ₁₋₄₀/AAMP-20 mixture; [B] non-fibrillar structures formed from aging A β ₁₋₄₀ in presence of AAMP-21; [C] non-fibrillar structures formed from aging A β ₁₋₄₀ in presence of AAMP-22 [D] Isolated prefibrillar particles formed from A β ₁₋₄₀ mitigation by AAMP-23; [E] Mixture of spherical aggregates and isolated fibrils were formed from aging A β ₁₋₄₀ in presence of AAMP-24; [F] network of fibrils observed from aging A β ₁₋₄₀/AAMP-25 mixture.

Negatively stained samples of A β ₁₋₄₀ alone or mixed with equimolar AAMPs prepared at the same time as those of AFM and ThT were examined using TEM to confirm the various morphologies observed with AFM. The morphology of structures (Figure 3.8) formed by A β ₁₋₄₀ alone and with the various AAMPs after 1-week aging was consistent with AFM observations. For instance, A β ₁₋₄₀ sample showed a typical appearance of amyloid fibrils, shown as a dense network of fibrils extending several microns in length. In contrast, A β ₁₋₄₀/AAMP mixtures reveal disruption of A β ₁₋₄₀ fibrillization yielding particles with different morphologies.

4.3.6 A β ₁₋₄₀ Fibril Disassembly

It has been shown that the presence of fibrils in the brain nucleates further deposition of plaques in AD.³⁹ It was previously stated that a dynamic equilibrium exists between monomers/dimers and fibrils.^{21, 40, 41} This makes agents that induce fibril disassembly an attractive source for development of new therapeutics that will reduce or eliminate plaques in the brain. Previously, β -sheet breaker²¹ and *N*-methylated peptides^{14, 40} have been shown to disassemble pre-formed fibrils. Herein, we designed protocols to evaluate the effect of AAMPs on A β fibril disassembly. Mature fibrils, were formed by incubating A β ₁₋₄₀ for 1 week at 37 C in PBS (pH 7.4) while agitating. Equimolar mixtures of fibrils of AAMP/A β ₁₋₄₀ and A β ₁₋₄₀ alone were aged for 24 h. The extent to which AAMPs induced fibril disassembly was monitored using ThT fluorescence, as well as images acquired with AFM and TEM. Results of ThT fluorescence are shown in Figure 4.12 as percentage relative to that of A β ₁₋₄₀.

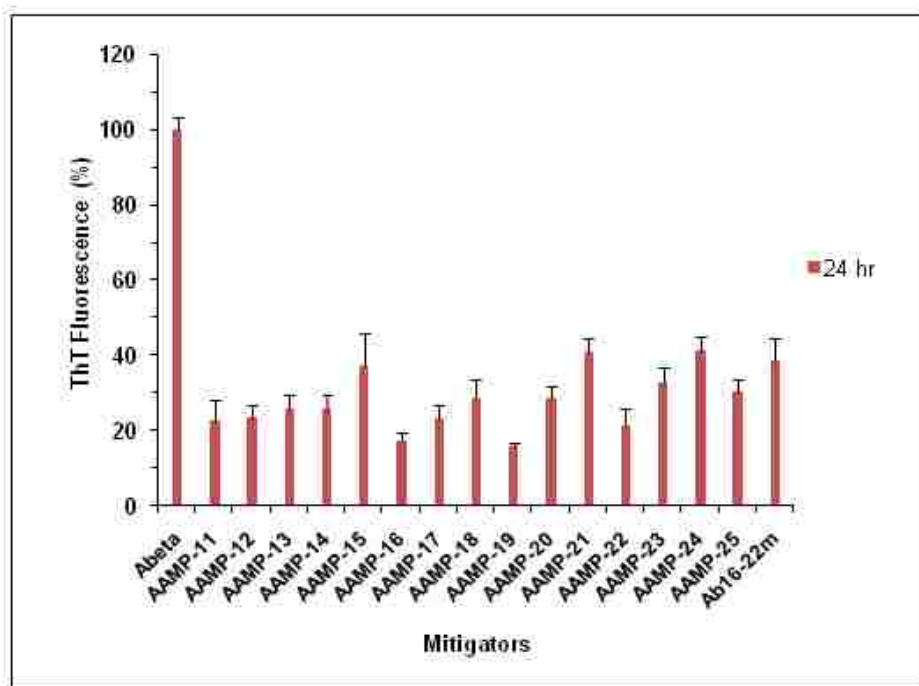


Figure 4.12. Fibril disassembly by various AAMPs as monitored by ThT fluorescence, presented as percent relative to that of A β ₁₋₄₀.

The various AAMPs exhibit reduced fluorescence of more than 50 % relative to that of $\text{A}\beta_{1-40}$. The *N*-methylated control peptide $\text{A}\beta_{16-22m}$, which has been shown to disassemble fibrils, displayed 40 % reduced fluorescence. Based on ThT fluorescence only, the various AAMPs tested exhibited reduced fluorescence comparable to the *N*-methylated control peptide. After 24 h, there is no significant difference in ThT fluorescence observed for AAMPs incorporating polar groups on the *N*-and *C*-terminus (AAMP-11-15), *C*-terminus (AAMP-16-18), *N*-terminus (AAMP-19) or $\alpha\alpha\text{AA}$ -containing AAMPs (AAMP-20-25). It should also be noted that the reduced fluorescence exhibited by the various AAMPs does not necessarily indicate the absence of fibrils. This is because inhibitor or disrupter molecules can bind fibrils displacing bound ThT molecule resulting in reduced fluorescence.

4.3.6.1 Size and Morphology of Structures Formed from $\text{A}\beta_{1-40}$ Disassembly by AAMPs

Table 4.4. Effect of various AAMPs on $\text{A}\beta$ disassembly

entry	AAMPs	size and morphology of resulting assemblies	
		24 hr	predominant/isolated structures
1	$\text{A}\beta_{1-40}$	fibrils	7.9 ± 3.2
2	AAMP-11	spherical /protofibrils	6.5 ± 4.3
3	AAMP-12	spherical/fibrils	6.3 ± 3.2
4	AAMP-13	spherical	15.8 ± 10.6
5	AAMP-14	protofibrils/amorphous	19.8 ± 11.1
6	AAMP-15	spherical	7.0 ± 4.0
7	AAMP-16	fibrils/spherical	7.5 ± 4.6
8	AAMP-17	spherical/protofibrils	7.2 ± 3.6
9	AAMP-18	protofibrils/fibrils	11.7 ± 6.7
10	AAMP-19	fibrils	5.3 ± 3.6
11	AAMP-20	protofibrils/fibrils	9.6 ± 4.6
12	AAMP-21	spherical/protofibrils	7.2 ± 3.5
13	AAMP-22	spherical/linear	11.2 ± 6.5
14	AAMP-23	spherical	13.4 ± 8.4
15	AAMP-24	spherical/protofibrils	8.4 ± 3.1
16	AAMP-25	fibrils	8.0 ± 3.8
17	$\text{A}\beta_{16-22m}$	spherical	35.6 ± 20.4

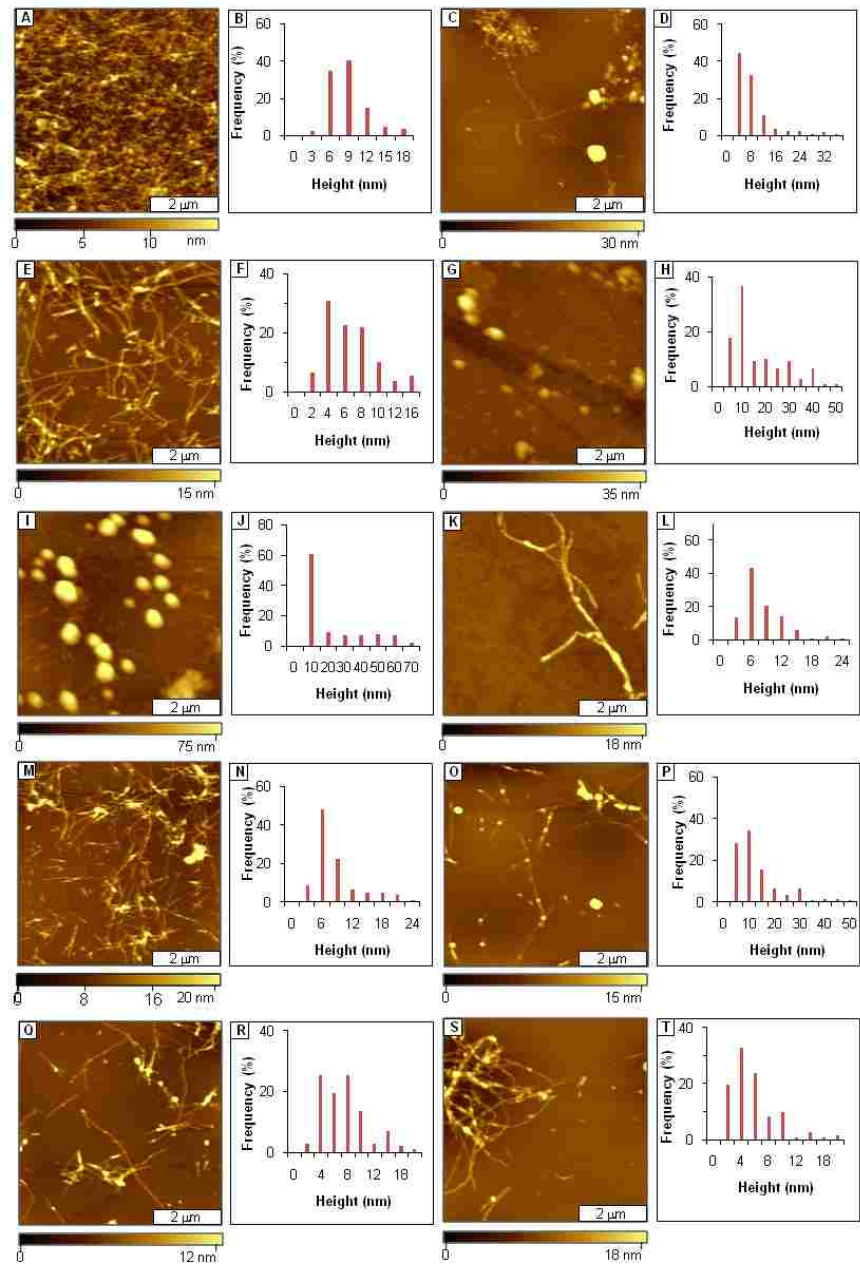


Figure 4.13. Disassembly of pre-formed fibrils of A β ₁₋₄₀. [A] Control sample of A β ₁₋₄₀ fibrils. [B] Corresponding height histogram. [C] Fibrils and spherical structures after disassembly by AAMP-11; [D] Histogram analysis for C; [E] Partial disassembly by AAMP-12; [F] Height histogram analysis for E; [G] Spherical particles formed by AAMP-13 fibril disassembly; [H] Height analysis for G; [I] Spherical aggregates and fibrils (background) formed from disassembly by AAMP-14; [J] Corresponding height analysis; [K] Isolated fibrils present from disassembly by AAMP-15; [L] Height histogram for K; [M] Mixture of short and long fibrils observed from disassembly by AAMP-16; [N] Corresponding height analysis; [O] Fibrils showing beaded sections for A β ₁₋₄₀ fibril disassembly by AAMP-17; [P] Corresponding height histogram; [Q] Fibrils showing nucleation units for mature fibrils after disassembly by AAMP-18; [R] Corresponding height analysis; [S] Partial pre-formed fibril disassembly observed with AAMP-19; [T] Height histogram for O.

Parallel AFM experiments were conducted for samples prepared at the same time as those for ThT fluorescence. A dense network of fibrils with mean height of 7.9 nm was observed from topographic AFM image of A β ₁₋₄₀ sample after 1 week of aging (Figure 4.13A). Similar observations were found with TEM micrographs, which displayed fibrils spanning several microns in length. Pre-formed fibrils were mixed with the various AAMPs at 1:1 molar ratio to evaluate their potential for disassembly. The mean heights and morphologies of the various structures formed from topographic AFM data are presented in Table 4. 4. Fibrils and protofibrils were the major structures observed with disassembly of pre-formed fibrils by AAMP-11 (Figure 4.13C), AAMP-12 (Figure 4.13E), and AAMP-15 (Figure 4.13K) which all have polar groups added to both the *C*- and *N*-terminus.

Spherical aggregates were the main structures observed after disassembly of pre-formed fibrils by AAMP-13 (Figure 4.13G) and AAMP-14 (Figure 4.13I), which incorporate Glu and PEG chains respectively into the ,*C*- and *N*-terminus. Predominantly, intact fibrils and isolated spherical particles were the major products observed for disassembly of pre-formed fibrils by AAMP-16 (Figure 4.13M), AAMP-17 (Figure 4.13O), and AAMP-18 (Figure 4.13Q) with different polar groups added only to the *C*-terminus. Partially disassembled fibrils were observed for AAMP-19 (Figure 4.13S) with polar groups added to *N*-terminus. Figures 4.13B, 4.13D, 4.13F, 4.13H, 4.13J, 4.13L, 4.13N, 4.13P, 4.13R and 4.13T are the corresponding height distributions from analysis of multiple cursor profiles.

The surface coverage and morphology (distribution, appearance, length, etc.) of fibrillar structures formed from disassembly by these mitigators indicates partial disassembly took place. For instance, fibrillar structures viewed with disassembly by AAMP-15, AAMP-17, and AAMP-18, showed nucleation units along the fibril length.

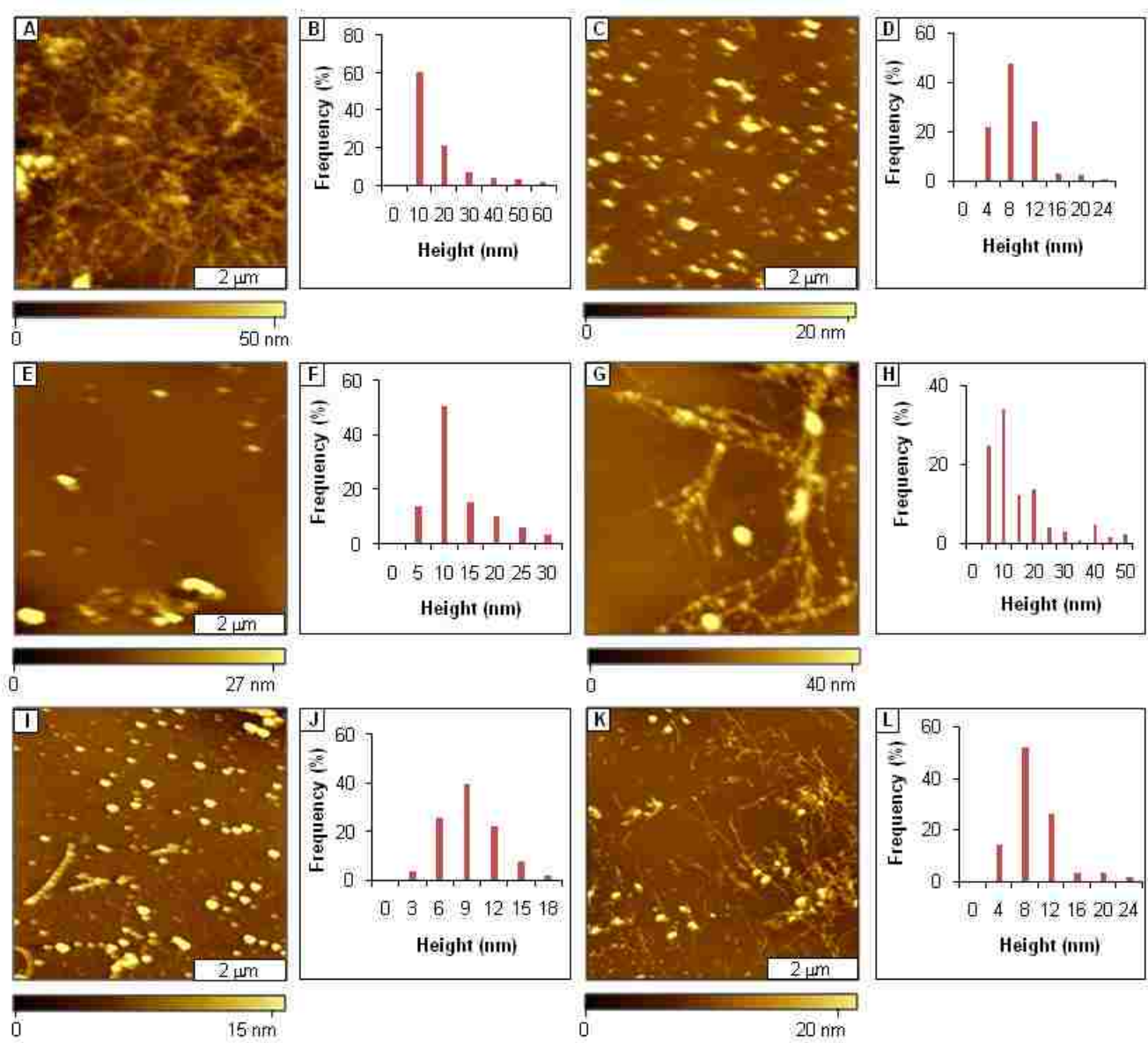


Figure 4.14. Disassembly of $\text{A}\beta_{1-40}$ pre-formed fibrils imaged using tapping mode AFM. [A] Fibril disassembly by AAMP-20; [B] Corresponding height histogram. [C] Spherical structures were observed with disassembly by AAMP-21; [D] Height analysis for C; [E] Spherical structures with disassembly by AAMP-22; [F] Corresponding height histogram; [G] Fibrils with beaded morphology observed from disassembly by AAMP-23 [H] Height analysis for G; [I] Spherical aggregates and isolated protofibrils formed from disassembly by AAMP-24; [J] Height analysis for I; [K] Fibrils and some spherical species observed from fibril disassembly by AAMP-25; [L] Corresponding height analysis.

This is an indication of immature fibrils or protofibrillar structures, which are precursors of mature fibril formation. In addition, there is evidence of fibril breakage as shown by the presence of fibrils with lengths less than a micron (AAMP-16) as compared to those of pre-formed A β ₁₋₄₀ fibrils. Spherical particles with diameters up to 0.1 micron were formed in the presence of AAMP-14. This underscores the importance of overall hydrophobicity and the length of polar group in the mechanism of disassembly for pre-formed fibrils.

4.3.6.2 Size and Morphology of Structures Formed from Fibril Disassembly by $\alpha\alpha$ AA-AAMPs

When $\alpha\alpha$ AA-containing AAMPs were mixed with pre-formed fibrils, the steric nature of $\alpha\alpha$ AAs played a role in the disassembly process. For instance, fibrils/protofibrils (Figure 4.14A) were the major species with disassembly by Dpg-containing AAMP-20 as compared to mainly spherical particles (Figure 4.14C) observed with Dibg containing AAMP-21. Similarly, spherical particles (Figure 4.14I) and fibrils (Figure 4.14K) were observed for Dibg-containing AAMP-24 and Dpg-containing AAMP-25. When another $\alpha\alpha$ AAs was introduced to AAMP-24 (Dpg) or AAMP-25 (Dibg) for AAMP-22, spherical particles (Figure 4.14E) with mean height of 11.2 nm were the major structures of disassembly. Addition of three Lys to both termini in Dpg-containing AAMP-23 (Figure 4.14G) evidenced no fibrils in AFM images, suggesting that adding polar groups contributes to the disassembly of pre-formed fibrils. Figures 4.14B, 4.14D, 4.14F, 4.14H, 4.14J and 4.14L, provide corresponding analysis of the height distribution of particles from AFM cursor measurements.

The distribution of $\alpha\alpha$ AAs in the KLVFF motif is a factor in the disassembly of pre-formed fibrils. For instance, fibrillar structures were the major species formed by AAMPs incorporating $\alpha\alpha$ AAs outside the KLVFF region as compared to spherical structures observed in AAMP-20 or AAMP-25 with $\alpha\alpha$ AAs placed in the KLVFF core. Increasing the hydrophobicity

or steric hindrance by introducing another $\alpha\alpha$ AA as in AAMP-22, induces disassembly of pre-formed fibrils to form mainly spherical particles. Although not conclusive, greater surface coverage of disassembled fibrils was observed with AAMP-20 than in the case of AAMP-25 with one and three C-terminal lysines, respectively. Also, AAMP-23 with three lysines were added to both termini and $\alpha\alpha$ AAs incorporated outside the KLVFF domain, was not expected to disassemble fibrils; however intact fibrils were not detected, suggesting that added polar groups also contributes to the disassembly of pre-formed fibrils. This shows that disassembly of pre-formed fibrils is synergistic combination of the influences of $\alpha\alpha$ AAs as well the number of polar groups added.

4.3.6.3 Morphology of Structures Formed from $A\beta_{1-40}$ Disassembly by the Various AAMPs as Observed by TEM

Negatively stained samples of $A\beta_{1-40}$ pre-formed fibrils or those mixed with various AAMPs prepared at the same time as those of AFM and ThT were examined using TEM to confirm the various morphologies observed with AFM. The morphology of $A\beta_{1-40}$ pre-formed fibrils and structures resulting from disassembly by the various AAMPs observed after 24 hr aging (Figure 3.12) were consistent with AFM observations. For instance, $A\beta_{1-40}$ sample showed a typical appearance of amyloid fibrils, shown as a dense network of fibrils extending several microns in length. In contrast, $A\beta_{1-40}$ /AAMP mixtures reveal disassembly of $A\beta_{1-40}$ fibrils yielding particles with different morphologies.

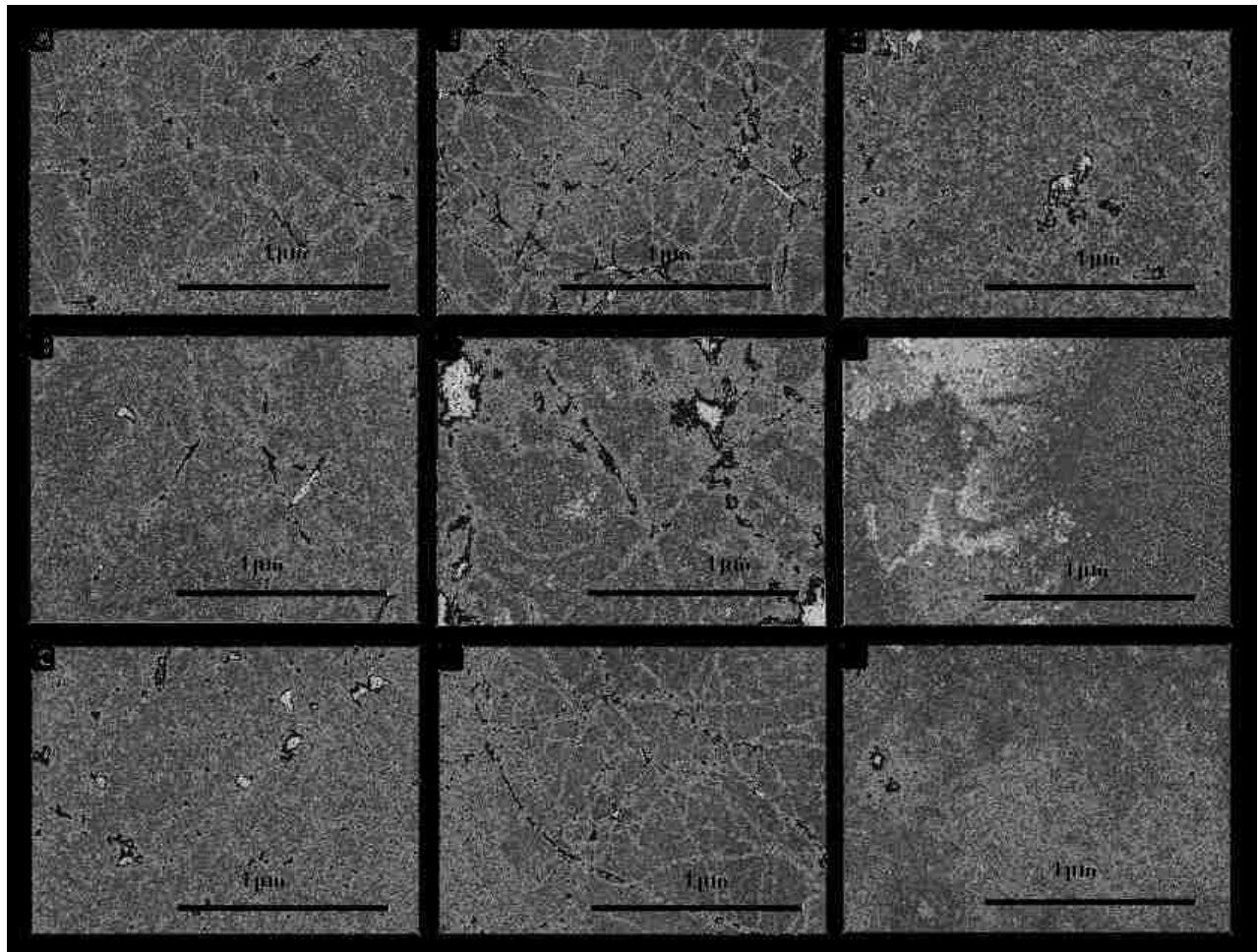


Figure 4.15 Disassembly of $\text{A}\beta_{1-40}$ preformed fibrils. [A] $\text{A}\beta_{1-40}$ preformed fibrils; [B]; $\text{A}\beta_{1-40}$ preformed fibrils different view; [C] Fibrils disassembly by AAMP-11; [D] isolated fibrils formed from disassembly by AAMP-12; [E] Fibrils formed from disassembly by AAMP-13; [F] isolated fibrils formed from disassembly by AAMP-14; [G] Non fibrillar structures observed from disassembly by AAMP-15; [H] Fibrils formed from disassembly by AAMP-16; [I] Non fibrillar structures formed from disassembly by AAMP-17.

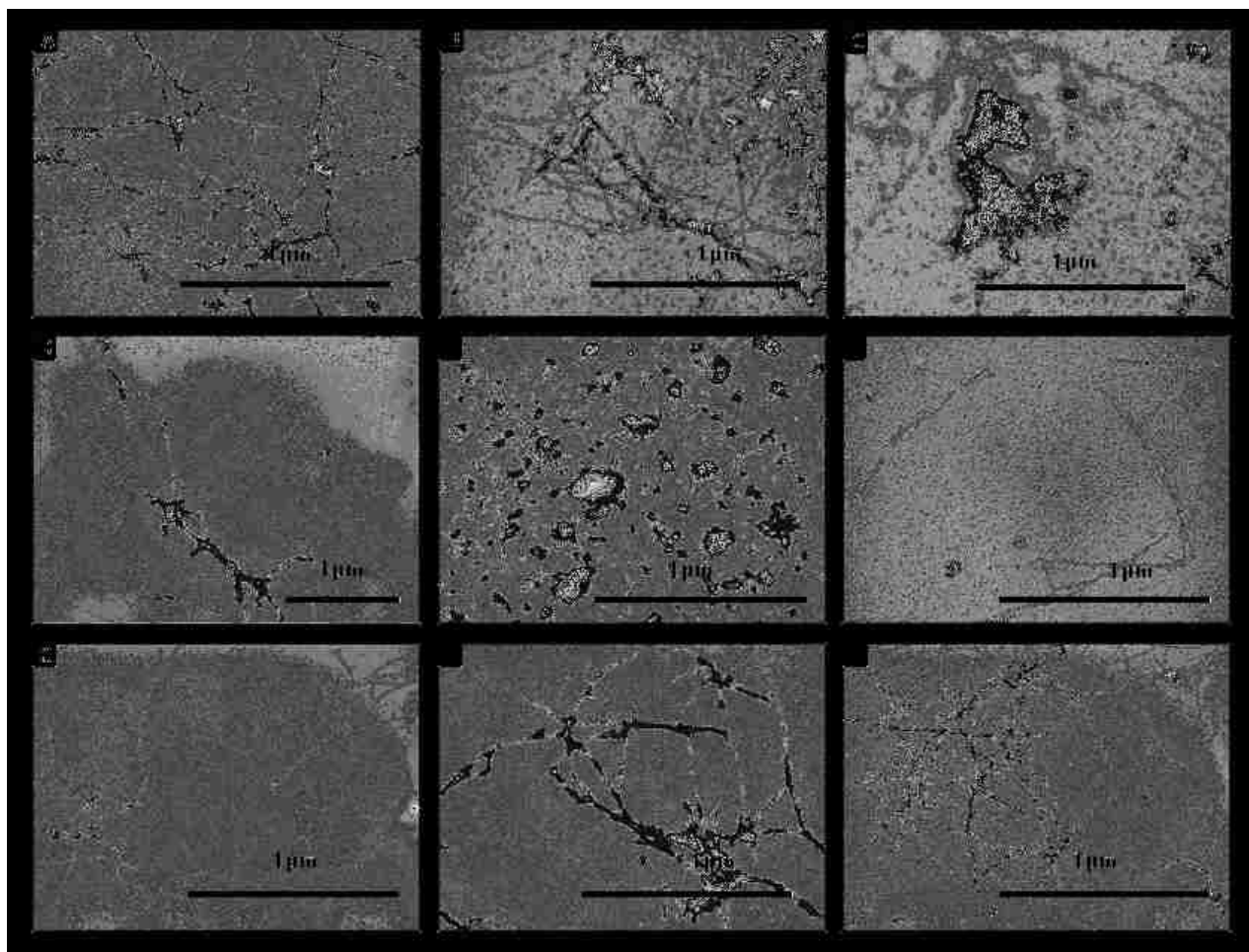


Figure 4.16 Disassembly of $\text{A}\beta_{1-40}$ preformed fibrils. [A] Fibrils observed from disassembly by AAMP-18; [B]; Fibrillar structures observed from disassembly by AAMP-19; [C] Fibrils disassembly by AAMP-20; [D] Isolated fibrils formed from disassembly by AAMP-21; [E] Spherical aggregates formed from disassembly by AAMP-22; [F] Isolated fibrils formed from disassembly by AAMP-23; [G] Isolated fibrils formed from disassembly by AAMP-24; [H] Fibrils formed from disassembly by AAMP-25; [I] Fibrillar structures from disassembly by $\text{A}\beta_{16-22m}$;

4.4 Conclusions

This study demonstrates that terminal modifications of the mitigator core sequence (KLVFF) with different polar groups altered A β fibrillization yielding particles with different morphologies and sizes. They also disrupt pre-formed fibrils to produce prefibrillar assemblies, suggesting that an equilibrium exists between fibrils and prefibrillar aggregates. Different results were obtained with modification of only the *C*-terminus as compared to changes for both *N*- and *C*-termini. In the process, a mitigator AAMP-16 with the *C*-terminal modified with Arg was found to potent disrupter of A β_{1-40} fibril assembly, forming spherical aggregates. This is consistent with the previously reported use of Arg to solubilize inhibitors of A β_{1-42} ⁴² and α -synuclein⁴³ fibrillogenesis, and protects differentiated SHSY-5Y neuroblastoma cells against A β toxicity. Also, AAMPs with a MiniPEG group were found to disrupt A β_{1-40} fibril formation. This is important because it can be used as a replacement for charged polar groups to improve systemic bioavailability of a drug during in vivo studies, and hence reduce toxicity as previously shown for Lys-containing AAMP-1. Smaller-sized spherical particles were observed for disruption by AAMP-17 as compared to AAMP-14, with *C*-terminus or *C*- and *N*-terminus modified with MiniPEG, respectively. This indicates that the *N*-terminal modification enhances aggregation to form larger assemblies. We have previously reported similar results where large sizes of particles formed with *N*-terminal modification of $\alpha\alpha\text{AA-KLVFF}$ compared to *C*-terminal modification using six oligolysine chains.²² The particle size difference is closely associated with disruption of the hydrophobic *C*-terminal group⁴⁴ which has more impact on aggregation than the hydrophilic *N*-terminal.⁴⁵

The different morphologies of particles formed with AAMP-19 (fibrils) and AAMP-16 (spherical aggregates) are attributable of the *N*-terminal and *C*-terminal, respectively. Through

SPR binding studies, Murphy and coworkers have shown that AAMPs with positively charged polar groups placed on the *N*-terminus have a 3-fold lower affinity for immobilized A β ₁₀₋₃₅ than the ones placed on the *C*-terminus.²⁵ From SPR and our AFM studies, it can be concluded that mitigators with a higher affinity for the target A β ₁₋₄₀ are better disrupters of A β fibrillization. Higher binding affinities for AAMPs with polar groups added to the *C*-terminus as compared to *N*-terminus are due to Coulombic interactions between positively charged polar groups in the AAMP (Lys, Arg) and negatively charged residues (E22 and D23) in A β . Coulombic interactions can also occur for AAMPs with polar groups added to the *N*-terminus, but the AAMP has to align in an antiparallel manner to align the two appositively charged groups in A β and AAMP. Even with antiparallel orientation, SPR studies have demonstrated lower binding affinities as compared to the parallel orientation.²⁵

The AAMPs incorporating $\alpha\alpha$ AAs were better disrupters of A β fibrillization as compared to AAMPs without $\alpha\alpha$ AAs. For instance, linear structures and fibrils were formed from incubation of A β ₁₋₄₀ in the presence of $\alpha\alpha$ AA-containing AAMP-20 and AAMP-18 respectively. This is because incorporating $\alpha\alpha$ AAs in the AAMP core forces the peptide to adopt an extended conformation that is ideal for interacting with A β ₁₋₄₀ through side chain-side chain hydrophobic interactions. Also, incorporation of $\alpha\alpha$ AAs into the mitigator core increases its hydrophobic character and in essence, impacts A β ₁₋₄₀ assembly since the initial aggregation is controlled by hydrophobic interactions. Mitigator AAMP-22 incorporating two $\alpha\alpha$ AAs in the KLVFF motif and containing three lysines on the *C*-terminus was found to have similar disruptive properties as compared to AAMP-3 (Chapter 3) with six lysines.²² This shows that the number of lysines can be reduced without affecting solubility and disruptive properties of the mitigator.

Topographic AFM data of the disassembly of pre-formed fibrils show agreement with data from ThT fluorescence. The lower percent ThT fluorescence exhibited by AAMP/ $\text{A}\beta_{1-40}$ mixtures is consistent with the observations of lower surface coverage of fibrils. Peptides, which have their termini modified with Lys, Arg, Glu and glycol chains have been shown to be effective at disrupting fibril formation as well as to protect against neuronal toxicity.^{14, 18, 26, 46} Fibrils/protofibrils were observed in AAMPs without $\alpha\alpha$ AAs as with AFM and TEM data. Mitigators, AAMP-21, AAMP-22, AAMP-23 induced disassembly of pre-formed fibrils to a similar degree to *N*-methylated peptide, $\text{A}\beta16-22\text{m}$ which was previously shown to disassemble pre-formed fibrils.¹⁴ The *N*-methylated, $\text{A}\beta16-22\text{m}$ as disassembled pre-formed fibrils, yielded large spherical aggregates with mean heights of 35.6 nm. In contrast, smaller aggregates were observed with $\alpha\alpha$ AA-AAMPs. The difference in the height of assemblies that formed can only be attributable to the added polar groups. Thus, polar groups play a role in determining the size of assemblies formed. We hypothesize that substitution of hydrogen atom on α -carbon of certain amino acids in the critical KLVFF region with an alkyl substituent yields a more hydrophobic peptide. Initial assembly of $\text{A}\beta$ oligomers is controlled by the hydrophobic side-chains. Thus, increasing the hydrophobicity of this region should also enhance interactions between $\text{A}\beta$ and the mitigator, leading to both disruption of $\text{A}\beta$ assembly into fibrils as well as the disassembly of pre-formed fibrils.

Also, because of terminal modifications with different polar groups, potent mitigators of $\text{A}\beta_{1-40}$ fibrillization were found, where the most interesting are the ones with neutral MiniPEG polar groups. Previous designs mostly used positively charged amino acids such as Lys or Arg, which makes peptide delivery through the brain barrier difficult. Thus, this study serves as a foundation for future design of more effective peptides with increased systemic bioavailability

and for optimal use in vivo. In addition, there is increasing evidence that an equilibrium exists between fibrils and monomers.^{41, 47, 48} Mitigator KLVFFK₆ was previously shown by Murphy and coworkers to alter the A β ₁₋₄₀ fibrillization process, forming fibrils with different morphologies that were protective against A β cytotoxicity. The non-toxic nature of these fibrils is believed to be because they are stable to the equilibrium change unlike A β fibrils which are in constant equilibrium with the more toxic oligomeric assemblies.¹² Thus, future cytotoxicity experiments on mitigators that form fibrils with different morphology as those of A β ₁₋₄₀ fibrils will further provide a basis for design of mitigators that result in fibrils that are stable and protect against neurotoxicity. Also, we designed mitigators that induced partial disassembly of pre-formed fibrils. The mechanism of disassembly is believed to occur by mitigator monomers binding to the end of fibrils and shifting equilibrium towards prefibrillar assemblies. Thus, this study can guide future designs of dissolution agents. Lastly, it is possible now to introduce unnatural amino acids into a given protein selectively in a cell; therefore, $\alpha\alpha$ AAs would be valuable for studying the structural elements responsible for A β toxicity in animal models of AD.

4.5 References

1. Selkoe, D. J., The molecular pathology of Alzheimers-Disease. *Neuron* **1991**, *6* (4), 487-498.
2. Selkoe, D. J., Folding proteins in fatal ways. *Nature* **2003**, *426* (6968), 900-904.
3. Tycko, R., Insights into the amyloid folding problem from solid-state NMR. *Biochemistry* **2003**, *42* (11), 3151-3159.
4. Baglioni, S.; Casamenti, F.; Bucciantini, M.; Luheshi, L. M.; Taddei, N.; Chiti, F.; Dobson, C. M.; Stefani, M., Prefibrillar amyloid aggregates could be generic toxins in higher organisms. *J. Neurosci.* **2006**, *26* (31), 8160-8167.
5. Chromy, B. A.; Nowak, R. J.; Lambert, M. P.; Viola, K. L.; Chang, L.; Velasco, P. T.; Jones, B. W.; Fernandez, S. J.; Lacor, P. N.; Horowitz, P.; Finch, C. E.; Krafft, G. A.; Klein, W.

L., Self-assembly of A beta(1-42) into globular neurotoxins. *Biochemistry* **2003**, *42* (44), 12749-12760.

6. Hardy, J.; Selkoe, D. J., Medicine - The amyloid hypothesis of Alzheimer's disease: Progress and problems on the road to therapeutics. *Science* **2002**, *297* (5580), 353-356.
7. Walsh, D. M.; Selkoe, D. J., Oligomers in the brain: The emerging role of soluble protein aggregates in neurodegeneration. *Protein Peptide Lett.* **2004**, *11* (3), 213-228.
8. Walsh, D. M.; Selkoe, D. J., A beta Oligomers - a decade of discovery. *J. Neurochem.* **2007**, *101* (5), 1172-1184.
9. Kemsley, J., Analyzing protein Drugs. *Chem. Eng. News* **2009**, 20-23.
10. Tjernberg, L. O.; Lilliehook, C.; Callaway, D. J. E.; Naslund, J.; Hahne, S.; Thyberg, J.; Terenius, L.; Nordstedt, C., Controlling amyloid beta-peptide fibril formation with protease-stable ligands. *J. Biol. Chem.* **1997**, *272* (19), 12601-12605.
11. Tjernberg, L. O.; Naslund, J.; Lindqvist, F.; Johansson, J.; Karlstrom, A. R.; Thyberg, J.; Terenius, L.; Nordstedt, C., Arrest of beta-amyloid fibril formation by a pentapeptide ligand. *J. Biol. Chem.* **1996**, *271* (15), 8545-8.
12. Ghanta, J.; Shen, C.-L.; Kiessling, L. L.; Murphy, R. M., A strategy for designing inhibitors of b-amyloid toxicity. *J. Biol. Chem.* **1996**, *271* (47), 29525-29528.
13. Etienne, M. A.; Aucoin, J. P.; Fu, Y.; McCarley, R. L.; Hammer, R. P., Stoichiometric Inhibition of Amyloid beta -Protein Aggregation with Peptides Containing Alternating alpha ,alpha -Disubstituted Amino Acids. *J. Am. Chem. Soc.* **2006**, *128* (11), 3522-3523.
14. Gordon, D. J.; Sciarretta, K. L.; Meredith, S. C., Inhibition of β-Amyloid(40) Fibrillogenesis and Disassembly of β-Amyloid(40) Fibrils by Short β-Amyloid Congeners Containing N-Methyl Amino Acids at Alternate Residues. *Biochemistry* **2001**, *40* (28), 8237-8245.
15. Sciarretta, K. L.; Gordon, D. J.; Meredith, S. C., Peptide-based inhibitors of amyloid assembly. In *Amyloid, Prions, and Other Protein Aggregates, Pt C*, 2006; Vol. 413, pp 273-312.
16. Pallitto, M. M.; Ghanta, J.; Heinzelman, P.; Kiessling, L. L.; Murphy, R. M., Recognition sequence design for peptidyl modulators of beta-amyloid aggregation and toxicity. *Biochemistry* **1999**, *38* (12), 3570-3578.
17. Gordon, D. J.; Tappe, R.; Meredith, S. C., Design and characterization of a membrane permeable N-methyl amino acid-containing peptide that inhibits A.bet.1-40 fibrillogenesis. *J. Pept. Res.* **2002**, *60* (1), 37-55.
18. Gordon, D. J.; Meredith, S. C., Probing the role of backbone hydrogen bonding in beta-amyloid fibrils with inhibitor peptides containing ester bonds at alternate positions. *Biochemistry* **2003**, *42* (2), 475-485.

19. Fu, Y. W.; Gao, J. M.; Bieschke, J.; Dendle, M. A.; Kelly, J. W., Amide-to-E-olefin versus amide-to-ester backbone H-bond perturbations: Evaluating the O-O repulsion for extracting H-bond energies. *J. Am. Chem. Soc.* **2006**, *128* (50), 15948-15949.
20. Bieschke, J.; Siegel, S. J.; Fu, Y. W.; Kelly, J. W., Alzheimer's A beta peptides containing an isostructural backbone mutation afford distinct aggregate morphologies but analogous cytotoxicity. Evidence for a common low-abundance toxic Structure(s). *Biochemistry* **2008**, *47* (1), 50-59.
21. Soto, C.; Sigurdsson, E. M.; Morelli, L.; Kumar, R. A.; Castano, E. M.; Frangione, B., beta-sheet breaker peptides inhibit fibrillogenesis in a rat brain model of amyloidosis: Implications for Alzheimer's therapy. *Nat. Med.* **1998**, *4* (7), 822-826.
22. Etienne, M. A.; Aucoin, J. P.; Fu, Y. W.; McCarley, R. L.; Hammer, R. P., Stoichiometric inhibition of amyloid beta-protein aggregation with peptides containing alternating alpha,alpha-disubstituted amino acids. *J. Am. Chem. Soc.* **2006**, *128* (11), 3522-3523.
23. Formaggio, F.; Bettio, A.; Moretto, V.; Crisma, M.; Toniolo, C.; Broxterman, Q. B., Disruption of the beta-sheet structure of a protected pentapeptide, related to the beta-amyloid sequence 17-21, induced by a single, helicogenic C-alpha-tetrasubstituted alpha-amino acid. *J. Pept. Sci.* **2003**, *9* (7), 461-466.
24. Gilead, S.; Gazit, E., Inhibition of amyloid fibril formation by peptide analogues modified with alpha-aminoisobutyric acid. *Angewandte Chemie-International Edition* **2004**, *43* (31), 4041-4044.
25. Cairo, C. W.; Strzelec, A.; Murphy, R. M.; Kiessling, L. L., Affinity-Based Inhibition of beta-Amyloid Toxicity. *Biochemistry* **2002**, *41* (27), 8620-8629.
26. Austen, B. M.; Paleologou, K. E.; Ali, S. A. E.; Qureshi, M. M.; Allsop, D.; El-Agnaf, O. M. A., Designing peptide inhibitors for oligomerization and toxicity of Alzheimer's beta-amyloid peptide. *Biochemistry* **2008**, *47* (7), 1984-1992.
27. Li, Q.; Gordon, M.; Etienne Marcus, A.; Hammer Robert, P.; Morgan, D., Contrasting in vivo effects of two peptide-based amyloid-beta protein aggregation inhibitors in a transgenic mouse model of amyloid deposition. *Cell Transplant* **2008**, *17* (4), 397-408.
28. Krebs, M. R. H.; Bromley, E. H. C.; Donald, A. M., The binding of thioflavin-T to amyloid fibrils: localisation and implications. *Journal of Structural Biology* **2005**, *149* (1), 30-37.
29. Levine, H., Thioflavine-t interaction with synthetic alzheimers-disease beta-amyloid peptides - detection of amyloid aggregation in solution *Protein Sci.* **1993**, *2* (3), 404-410.
30. LeVine, H., III, Thioflavine T interaction with amyloid beta -sheet structures. *Amyloid* **1995**, *2* (1), 1-6.

31. Nilsson, M. R., Techniques to study amyloid fibril formation in vitro. *Methods* **2004**, *34* (1), 151-160.
32. Lee, S.; Fernandez, E. J.; Good, T. A., Role of aggregation conditions in structure, stability, and toxicity of intermediates in the A beta fibril formation pathway. *Protein Sci.* **2007**, *16* (4), 723-732.
33. Bieschke, J.; Zhang, Q. H.; Powers, E. T.; Lerner, R. A.; Kelly, J. W., Oxidative metabolites accelerate Alzheimer's amyloidogenesis by a two-step mechanism, eliminating the requirement for nucleation. *Biochemistry* **2005**, *44* (13), 4977-4983.
34. Laczkó, I.; Vass, E.; Soos, K.; Fulop, L.; Zarandi, M.; Penke, B., Aggregation of A beta(1-42) in the presence of short peptides: conformational studies. *J. Pept. Sci.* **2008**, *14* (6), 731-741.
35. Gazit, E., Mechanisms of amyloid fibril self-assembly and inhibition. *FEBS J.* **2005**, *272* (23), 5971-5978.
36. Wogulis, M.; Wright, S.; Cunningham, D.; Chilcote, T.; Powell, K.; Rydel, R. E., Nucleation-dependent polymerization is an essential component of amyloid-mediated neuronal cell death. *J. Neurosci.* **2005**, *25* (5), 1071-1080.
37. Kad, N. M.; Myers, S. L.; Smith, D. P.; Smith, D. A.; Radford, S. E.; Thomson, N. H., Hierarchical assembly of beta(2)-microglobulin amyloid in vitro revealed by atomic force microscopy. *J. Mol. Biol.* **2003**, *330* (4), 785-797.
38. Paravastu, A. K.; Petkova, A. T.; Tycko, R., Polymorphic fibril formation by residues 10-40 of the Alzheimer's beta-amyloid peptide. *Biophys. J.* **2006**, *90* (12), 4618-4629.
39. Jarrett, J. T.; Berger, E. P.; Lansbury, P. T., The Carboxy Terminus of The Beta-Amyloid Protein is critical for the Seeding of Amyloid Formation- Implications for the Pathogenesis of Alzheimers-Disease. *Biochemistry* **1993**, *32* (18), 4693-4697.
40. Soto, P.; Griffin Mary, A.; Shea, J.-E., New insights into the mechanism of Alzheimer amyloid-beta fibrillogenesis inhibition by N-methylated peptides. *Biophys J* **2007**, *93* (9), 3015-25.
41. Carulla, N.; Caddy, G. L.; Hall, D. R.; Zurdo, J.; Gairi, M.; Feliz, M.; Giralt, E.; Robinson, C. V.; Dobson, C. M., Molecular recycling within amyloid fibrils. *Nature* **2005**, *436* (7050), 554-558.
42. Fulop, L.; Zarandi, M.; Datki, Z.; Soos, K.; Penke, B., beta-amyloid-derived pentapeptide RIIGL(a) inhibits A beta(1-42) aggregation and toxicity. *Biochem. Biophys. Res. Commun.* **2004**, *324* (1), 64-69.
43. El-Agnaf, O. M. A.; Paleologou, K. E.; Greer, B.; Abogrein, A. M.; King, J. E.; Salem, S. A.; Fullwood, N. J.; Benson, F. E.; Hewitt, R.; Ford, K. J.; Martin, F. L.; Harriot, P.; Cookson, M. R.; Allsop, D., A strategy for designing inhibitors of alpha-synuclein aggregation and toxicity

as a novel treatment for Parkinson's disease and related disorders. *FASEB J.* **2004**, *18* (9), 1315-+.

44. Schmechel, A.; Zentgraf, H.; Scheuermann, S.; Fritz, G.; Pipkorn, R. D.; Reed, J.; Beyreuther, K.; Bayer, T. A.; Multhaup, G., Alzheimer beta-amyloid homodimers facilitate A beta fibrillization and the generation of conformational antibodies. *J. Biol. Chem.* **2003**, *278* (37), 35317-35324.
45. Morimoto, A.; Irie, K.; Murakami, K.; Masuda, Y.; Ohigashi, H.; Nagao, M.; Fukuda, H.; Shimizu, T.; Shirasawa, T., Analysis of the secondary structure of beta-amyloid (A beta 42) fibrils by systematic proline replacement. *J. Biol. Chem.* **2004**, *279* (50), 52781-52788.
46. Gordon, D. J.; Tappe, R.; Meredith, S. C., Design and characterization of a membrane permeable N-methyl amino acid-containing peptide that inhibits A β 1-40 fibrillogenesis,. *The Journal of Peptide Research* **2002**, *60* (1), 37-55.
47. Sato, T.; Kienlen-Campard, P.; Ahmed, M.; Liu, W.; Li, H. L.; Elliott, J. I.; Aimoto, S.; Constantinescu, S. N.; Octave, J. N.; Smith, S. O., Inhibitors of amyloid toxicity based on beta-sheet packing of A beta 40 and A beta 42. *Biochemistry* **2006**, *45* (17), 5503-5516.
48. O'Nuallain, B.; Shivaprasad, S.; Kheterpal, I.; Wetzel, R., Thermodynamics of A β (1 \sim 40) Amyloid Fibril Elongationâ€ Biochemistry **2005**, *44* (38), 12709-12718.

CHAPTER 5

SUMMARY

5.1 Discussion

This dissertation focused on design and synthesis of short model peptides that incorporate $\alpha\alpha$ AAs in the core sequence. $\alpha\alpha$ AAs are known to induce extended peptide conformation (two hydrogen bonding face) in a model peptide such that one face is blocked by $\alpha\alpha$ AAs and the other is available for interaction with A β via side-chain, side-chain hydrophobic interactions.^{1, 2} Thus, a series of $\alpha\alpha$ AA-containing AAMPs were designed.

Chapter 2 of this dissertation describes the synthesis of $\alpha\alpha$ AAs and incorporation into a short model peptides. Dipropylglycine (Dpg) and Diisobutylglycine (Dibg) were easily synthesized following Fu protocols.³⁻⁵ Procedural adjustments especially in the reaction workup resulted in increased yields. Dpg was also synthesized in high yields via palladium catalyzed alkylation reaction. Dibenzylglycine (Dbg) was difficult to synthesize in large amounts such that it was enough for peptide synthesis. This was because the dialkylated ester was unstable to rotary evaporation and distilled out with the solvent into the waste flask. With the increasing success of microwave irradiation to hydrolyze sterically hindered hydantoins,^{6, 7} I hypothesize that Dbg hydantoin too can be successfully hydrolyzed using microwave irradiation such that it can easily be synthesize in high yields using Bucherer-Bergs method,⁸ the most common way of synthesizing $\alpha\alpha$ AAs. Acylation of N-terminus of $\alpha\alpha$ AAs during peptide synthesis was found to be difficult as shown by the very low coupling yields. Coupling yields were also improved using microwave irradiation and a library of AAMPs designed was successfully synthesized.

Chapter 3 describes solution analysis of the various AAMPs for their ability to disrupt properties against A β fibrillization. AAMP-1, which has three $\alpha\alpha$ AAs incorporated in the core

sequence, was shown previously to disrupt A β fibril formation yielding non-fibrillar assemblies that were still stable after 4.5 months.⁹ In this Chapter, the role of individual $\alpha\alpha$ AAs was investigated for their effects on the resulting A β -AAMP aggregate size and morphology. The number and position of $\alpha\alpha$ AAs relative to the KLVFF core was shown to be crucial for the AAMP to disrupt A β fibrillization. Also, for the first time $\alpha\alpha$ AA-containing AAMPs were found to induce fibril disassembly. These $\alpha\alpha$ AA-AAMPs disassemble fibrils by binding to A β fibril and because of their bulky side chains, it hinders both β -sheet extension and lateral association into layers¹⁰

Chapter 4 describes terminal modifications of AAMPs derived from A β central hydrophobic core with differently charged polar residues. Terminal modifications of peptides derived from A β central hydrophobic core have been shown previously to affect the A β -AAMP binding affinity or aggregate size and morphology. For instance Murphy and Coworkers showed that polar groups added to C-terminus have more affinity for immobilized A β 10-35 than polar groups added to the N-terminus.¹¹ Also, Fu et al showed that AMY-2 with six lysines added to N-terminus aggregated faster forming large assemblies as compared to AMY-1 with six lysine's added to C-terminus.^{12, 13} Thus, in this chapter terminal modifications using polar residues with different charged led to several potent mitigators of A β assembly, majority of which incorporate polar groups to the C-terminus. More importantly, AAMPs incorporating miniPEG polar groups were found to be effective against A β fibrillization. It is imperative to design mitigators that can easily be delivered through the brain barrier to their targets. Thus, future design of mitigators should include uncharged polar groups such as miniPEG. Also, the number of both Lys and $\alpha\alpha$ AAs was reduced without changing the ability of the AAMP to

disrupt fibril formation. This is important because our original goal of reducing the charge and size of the AAMP was achieved.^{12, 13}

Currently collaborative work with Dr. Keller at LSU Pennington is ongoing to test the assemblies formed from A β mitigation by these AAMPs on primary neurons.

5.2 References

1. Toniolo, C.; Crisma, M.; Formaggio, F.; Peggion, C., Control of peptide conformation by the Thorpe-Ingold effect (C-alpha-tetrasubstitution). *Biopolymers* **2001**, *60* (6), 396-419.
2. Tanaka, M., Design and synthesis of chiral alpha ,alpha -disubstituted amino acids and conformational study of their oligopeptides. *Chem. Pharm. Bull. (Tokyo)* **2007**, *55* (3), 349-358.
3. Fu, Y.; Etienne, M. A.; Hammer, R. P., Facile Synthesis of α,α -Diisobutylglycine and Anchoring its Derivatives onto PAL-PEG-PS Resin. *J. Org. Chem.* **2003**, *68* (25), 9854-9857.
4. Fu, Y.; Hammarstroem, L. G. J.; Miller, T. J.; Fronczek, F. R.; McLaughlin, M. L.; Hammer, R. P., Sterically Hindered C α,α -Disubstituted α -Amino Acids: Synthesis from α -Nitroacetate and Incorporation into Peptides. *J. Org. Chem.* **2001**, *66* (21), 7118-7124.
5. Fu, Y. W.; Hammer, R. P., Efficient acylation of the N-terminus of highly hindered C-alpha,C-alpha-disubstituted amino acids via amino acid symmetrical anhydrides. *Org. Lett.* **2002**, *4* (2), 237-240.
6. Colacino, E.; Lamaty, F.; Martinez, J.; Parrot, I., Microwave-assisted solid-phase synthesis of hydantoin derivatives. *Tetrahedron Lett.* **2007**, *48* (30), 5317-5320.
7. Ware, E., The Chemistry of the Hydantoins. *Chem. Rev.* **1950**, *46* (3), 403-470.
8. Dyker, G., Amino Acid Derivatives by Multicomponent Reactions. *Angew. Chem. Int. Ed.* **1997**, *36*, 1700-1702.
9. Etienne, M. A.; Aucoin, J. P.; Fu, Y.; McCarley, R. L.; Hammer, R. P., Stoichiometric Inhibition of Amyloid beta -Protein Aggregation with Peptides Containing Alternating alpha ,alpha -Disubstituted Amino Acids. *J. Am. Chem. Soc.* **2006**, *128* (11), 3522-3523.

10. Chebaro, Y.; Derreumaux, P., Targeting the early steps of Abeta 16-22 protofibril disassembly by N-methylated inhibitors: a numerical study. *Proteins: Struct., Funct., Bioinf.* **2009**, *75* (2), 442-452.
11. Ghanta, J.; Shen, C.-L.; Kiessling, L. L.; Murphy, R. M., A strategy for designing inhibitors of b-amyloid toxicity. *J. Biol. Chem.* **1996**, *271* (47), 29525-29528.
12. Cairo, C. W.; Strzelec, A.; Murphy, R. M.; Kiessling, L. L., Affinity-Based Inhibition of β -Amyloid Toxicity. *Biochemistry* **2002**, *41* (27), 8620-8629.
13. Etienne, M. A.; Aucoin, J. P.; Fu, Y. W.; McCarley, R. L.; Hammer, R. P., Stoichiometric inhibition of amyloid beta-protein aggregation with peptides containing alternating alpha,disubstituted amino acids. *J. Am. Chem. Soc.* **2006**, *128* (11), 3522-3523.

VITA

Cyrus K Bett was born in Eldama Ravine, Kenya, and is a graduate of Nakuru High School. He graduated with a bachelor of science degree in chemistry from Moi University in December 1999. After graduation, he taught briefly high school chemistry and math before enrolling for a master's degree in analytical chemistry in 2001. His research was to screen herbal medicine as possible therapeutic agents. He won an internship award to go finish his research work at Rothamsted Research laboratories in the UK. Cyrus went on to pursue his doctoral degree at Louisiana State University where he will graduate in Fall 2009